Measurement of Surface and Interfacial Energies between Solid Materials Using an Elastica Loop

Jia Qi

Thesis submitted to the faculty of the
Virginia Polytechnic Institute and State University
in partial fulfillment of the requirements for the degree of

Master of Science
in
Engineering Mechanics

APPROVED BY:

David A. Dillard, Chairman
Raymond H. Plaut
John G. Dillard

September 11, 2000
Blacksburg, Virginia

Keywords: Interfacial Energy, Surface Energy, Work of Adhesion, Contact Mechanics, Elastica, JKR technique

Measurement of Surface and Interfacial Energies between Solid Materials Using an Elastica Loop

(ABSTRACT)

The measurement of the work of adhesion is of significant technical interest in a variety of applications, ranging from a basic understanding of material behavior to the practical aspects associated with making strong, durable adhesive bonds. The objective of this thesis is to investigate a novel technique using an elastica loop to measure the work of adhesion between solid materials. Considering the range and resolution of the measured parameters, a specially designed apparatus with a precise displacement control system, an analytical balance, an optical system, and a computer control and data acquisition interface is constructed. An elastica loop made of poly(dimethylsiloxane) [PDMS] is attached directly to a stepper motor in the apparatus. To perform the measurement, the loop is brought into contact with various substrates as controlled by the computer interface, and information including the contact patterns, contact lengths, and contact forces is obtained. Experimental results indicate that due to anticlastic bending, the contact first occurs at the edges of the loop, and then spreads across the width as the displacement continues to increase. The patterns observed show that the loop is eventually flattened in the contact region and the effect of anticlastic bending of the loop is reduced. Compared to the contact diameters observed in the classical JKR tests, the contact length obtained using this elastica loop technique is, in general, larger, which provides potential for applications of this technique in measuring interfacial energies between solid materials with high moduli. The contact procedure is also simulated to investigate the anticlastic bending effect using finite element analysis with ABAQUS. The numerical simulation is conducted using a special geometrically nonlinear, elastic, contact mechanics algorithm with appropriate displacement increments. Comparisons of the numerical simulation results, experimental data, and the analytical solution are made.

ACKNOWLEDGEMENTS

I would like to thank Dr. David A. Dillard for acting as my advisor, giving me this opportunity to go deep in this project and providing his guidance throughout my research and writing efforts. I would also like to thank Dr. Raymond H. Plaut of the Civil and Environmental Engineering Department and Dr. John G. Dillard of the Chemistry Department for serving as my committee members.

Additionally, I appreciate the assistance from Prof. M. Chaudhury and his student Hongquan She of Lehigh University, Bob Simonds, as well as all the members in the Adhesion Mechanics Lab. Furthermore, I would like to acknowledge the support of the National Science Foundation under grant CMS-9713949, and the Center for Adhesive and Sealant Science of Virginia Tech.

I would like to take this opportunity to thank my parents for continually supplying me with their love and support throughout my life. Finally, I would like to thank my husband, Dr. Buo Chen, for his endless supply of love, advice, and understanding.

Table of Contents

List of Figures

List of Tables

CHAPTER 1 Introduction

1.1 Adhesion and role of the interface

Adhesion is a phenomenon by which two materials in contact form a region of adhesive bond that is able to sustain and transmit stresses. The formation of adhesive bonds is governed by molecular interactions occurring at the interface of the adhering materials. As discussed in Kinloch [1], scientists have recognized for many years that intimate molecular contact and active interactions are necessary, though sometimes insufficient, requirements to form strong adhesive bonds. As summarized by Mangipudi and Tirrell [2], these interactions include: i) van der Waals or other non-covalent interactions that form bonds across the interface; ii) interdiffusion of polymer chains across the interface and coupling of the interfacial chains with the bulk polymer; and iii) formation of primary chemical bonds between chains or molecules at or across the interface.

The van der Waals and other non-covalent interactions at the interface are macroscopic intrinsic material characteristics, and they are quantified as the surface and interfacial energies. Defined as the energy required to create a unit area of surface of a material in a thermodynamically reversible manner, the surface energy of a material, γ, and the interfacial energy between two materials in contact, γ_{12}, determine the work of cohesion, $W_{coh,}$ for two identical surfaces, or the work of adhesion, $W_{adh,}$ for two dissimilar surfaces in contact [3]. For two identical surfaces in contact, W_{coh} is given by

$$W_{coh} = 2\gamma \tag{1}$$

For two dissimilar surfaces in contact, W_{adh} is given by

$$W_{adh} = \gamma_1 + \gamma_2 - \gamma_{12} \tag{2}$$

where γ_1 and γ_2 are the surface energies of materials 1 and 2, respectively, γ_{12} is the interfacial energy between materials 1 and 2.

Although the practical fracture toughness of an adhesive bond, which is usually quantified as the critical strain energy release rate G_c, is in general several orders of magnitude larger than the thermodynamic work of adhesion W_{adh}, sufficient evidence in the literature has shown that the strength or fracture toughness of adhesive bonds is directly associated with the work of adhesion [[4], [5], [6]]. As indicated in Figure 1.1, Wightman *et al.* [6] showed that the peel strength of a pressure sensitive tape increases significantly as the work of adhesion increases. Other examples can be found in references [4] and [5]. Gent and Schultz [4] proposed that the fracture toughness, $G_{c,}$ and work of adhesion, $W_{adh,}$ follow the relationship

$$G_c = W_{adh}\left[1 + \Phi(v, T)\right] \tag{3}$$

where Φ represents the viscoelastic energy dissipation associated with the debonding process, and is a function of the debonding rate v and testing temperature T.

Although equation (3) is obtained directly based on experimental observations, the equation underlines the importance of the thermodynamic work of adhesion to a strong and durable adhesive joint. Consequently, measurement of surface and interfacial energies is of significant technical importance in aspects such as obtaining a basic understanding of material behavior and manufacturing durable adhesive bonds.

1.2 Contact mechanics and measurement of surface energies

The measurement of surface energies of solids has been a difficult task [7]. This is due to the fact that the moduli of solids in general are relatively high (as compared to liquids and vapors), and the deformation due to the surface energy is usually insufficient to be measured. Historically, estimates of the surface energies of solids have been obtained through measuring the surface energy of the melt and assuming that the energetics of the solid and liquid are similar. However, since the surface energy of a material is closely related to the surface temperature, results obtained using this melting technique contain significant errors [3]. Moreover, this technique is very difficult to

apply to high-molecular-weight polymers, which are very viscous even in the melt. In addition, this technique cannot be applied to cross-linked polymers, because cross-linked polymers cannot be melted.

Currently, the most widely used technique to estimate surface energies of solids is the wetting method [3]. The basis of this technique is Young's wetting equation, which is given by

$$\gamma_{lv} \cos\theta = \gamma_{sv} + \gamma_{sl} \tag{4}$$

where, as shown in Figure 1.2, subscripts *s*, *l*, and *v* denote the solid, liquid, and vapor phases, and γ_{lv}, γ_{sv}, and γ_{sl} are the interfacial energies between the various phases. In practice, a serie of liquid droplets with different liquid-vapor interfacial energies is used as probes to measure contact angles θ with a solid surface. If the solid-liquid interfacial energy is assumed to be small, an estimate of the solid-vapor interfacial energy γ_{sv} can then be obtained by extrapolating the results to $\theta = 0$, which is also referred as the critical surface tension γ_c. This wetting procedure was first introduced by Zisman, and is relatively easy to perform [3]. However, the solid-liquid interactions are essentially ignored in the method, which reduces the accuracy of the results significantly in some cases. More importantly, especially for the purpose of adhesion, this technique cannot be extended to the measurement of interfacial energies between two solids.

Another useful quantity for characterizing the interactions between two materials is the work of adhesion, $W_{adh,}$ [3]. After the contact angle of a droplet is measured, the work of adhesion between the substrate and the liquid of the droplet can be obtained as

$$W_{adh} = \gamma_{lv}(1+\cos\theta) \tag{4}$$

By knowing the work of adhesion between various solids and liquids, interactions between two solids can be estimated. However, some critical assumptions are often required and consequently errors are introduced, which in some cases may not be negligible.

Of significant recent interest has been the use of contact mechanics to study interfacial interactions. The seminal study of contact mechanics was conducted by Hertz [8], who analyzed the deflection, contact area, and stress distributions of two elastic spheres in contact, and obtained relationships between the contact radius, contact force, and deflection as

$$a_0^3 = \frac{PR}{K} \tag{5}$$

$$\delta = \frac{P^2 R}{K} = \frac{a_0^2}{R} \tag{6}$$

$$\frac{1}{R} = \frac{1}{R_1} + \frac{1}{R_2} \tag{7}$$

$$\frac{1}{K} = \frac{3}{4}\left[\frac{1-\nu_1^2}{E_1} + \frac{1-\nu_2^2}{E_2}\right] \tag{8}$$

In equations (5)-(8), as shown in Figure 1.3, a_0 is the contact radius, δ is the deflection, P is the contact force, and R_1, R_2, E_1, E_2, ν_1, and ν_2 are the radii, moduli, and Poisson's ratios for the two spheres in contact, respectively. In Hertz's theory, the materials are linearly elastic; contact surfaces are frictionless; and the interfacial attractive forces between the spheres are ignored. Consequently, if the contact force decreases to zero, this theory predicts that the contact area is also zero as indicated in equation (5). Lee and Radok [9], Graham [10], and Yang [11] later investigated the contact problem between viscoelastic solids. However, none of these treatments accounts for the influence of the interfacial interactions.

Johnson, Kendall, and Roberts [12] showed that if one of the spheres in contact is elastomeric, the contact area measured is larger than what Hertz predicted. In addition, they also showed that the contact area at zero contact loads has a finite size and requires a small tensile force to separate the spheres. They recognized that this additional deformation is due to the interfacial energy between these two spheres, and extended

Hertzian theory to include the influence of surface energies in their analysis, which is now known as the JKR theory.

In developing the JKR theory, Johnson *et al.* [12] considered two similar, solid, homogeneous, linearly elastic spheres with frictionless surfaces in contact with each other under a normal applied load P as shown in Figure 1.3. The shear tractions acting on the contact surfaces are identically zero. The deformation of the spheres is assumed to be small so that linear continuum mechanics theory can be used. In particular, small strains are required so that there is no distinction between the deformed and undeformed configurations of the bodies as far as equilibrium is concerned. In addition, the bonding and debonding process at the interface is assumed to be reversible and the energy available for debonding is independent of the local failure process.

According to the JKR theory, the contact radius, a, resulting from the combined influences of the interfacial interactions and the external force, P, is given by

$$a^3 = \frac{R}{K}\sqrt{P + 3\pi W_{adh} R + [6\pi W_{adh} RP + (3\pi W_{adh} R)^2]} \tag{9}$$

where W_{adh} is the work of adhesion between the two spheres and the rest of the symbols are as stated before. Based on equation (9), the work of adhesion W_{adh} can be calculated from knowledge of the contact radius, the applied load, and the material properties of the spheres. Equation (9) also indicates that due to the interfacial interactions, the resultant contact radius a is larger than the contact radius a_0 predicted by equation (5), which represents the Hertzian theory. In addition, equation (9) also predicts that when the contact force is zero, the contact area will not be zero, and a tensile load is required to separate the two spheres.

The JKR theory provided a new experimental technique to directly measure the work of adhesion between two solids and consequently the surface and interfacial energies. A variety of experimental tools such as the JKR apparatus and the surface

force apparatus (SFA) also have been developed. All of the apparatuses are based on the JKR theory and measure the same quantities, i.e., the contact area (by means of contact radius or contact length) and the applied load. Using these tools, many research investigations in various areas have been conducted.

Tabor [13] examined the effects of surface roughness and material ductility on the adhesion of solids. The results indicated that the adhesion between two surfaces decreases as the roughness of the surface increases. However, the rate of decrease depends on the moduli of the materials in contact. Chaudhury and Whitesides [14] tested the surface energies of poly(dimethylsiloxane) [PDMS] in air and in mixtures of water and methanol. The results showed that the interfacial interactions decrease in the mixtures of water and methanol as the methanol content increases. However, a small interaction persists, even in pure methanol. In both the Tabor [13] and Chaudhury and Whitesides' [14] experiments, the probes used were hemispherical elastomeric lenses.

After the success in measuring the interfacial energy between elastomeric materials, efforts have been made to measure the interfacial energy between glassy polymers. Using their surface force apparatus (SFA), Mangipudi *et al.* [15] obtained the thermodynamic work of cohesion and adhesion between poly(ethylene terephthalate) [PET] and polyethylene thin films. The surface energy of PET determined by the direct force measurement is higher than the critical surface tension of wetting. They later applied the surface force apparatus (SFA) to measure the surface energies of polyethylene films modified with corona treatment [16]. Comparing the results with those obtained using the contact angle measurement technique, they also believed that the contact angle measurement technique is not sensitive to small changes in surface composition, and SFA can directly measure the true surface energy of polymer films.

Tirrell [17] discussed the applications of JKR theory for glassy or semi-crystalline polymers. In his experiments, high modulus materials were coated on the

elastomer lenses and contacted with flat surfaces coated with the same polymer. He also compared the results with those obtained using contact angle measurements, and obtained similar conclusions as Mangipudi *et al* [15] that the results obtained using the contact JKR method are larger than those obtained using the contact angle technique. Tirrell [17] attributed the difference to the rearrangement of the polymer functionality group on the surface. For polar materials, high-energy functional groups on the surface may be buried when in contact with air, but might rearrange to expose themselves when in contact with a polar polymer surface.

Mangipudi *et al.* [18] further expanded the applicability of the classical JKR experiment to allow measurements of the work of adhesion between glassy polymers using a novel method to prepare samples, and they measured the surface energies of polystyrene [PS] and poly(methyl methacrylate) [PMMA]. In these experiments, the spherical cap was made of O_2-plasma modified cross-linked PDMS, and the glassy polymer was coated on the PDMS cap as a thin layer about 0.1 μm thick by solvent casting. Detailed experimental procedures are presented in their paper. During their experiments, contact hysteresis was observed in PMMA-PMMA and PS-PS interfaces. Similar to Tirrell [17], they also concluded that contact hysteresis is due to contact induced rearrangements of the interface since no contact hysteresis was observed in PDMS-PS and PDMS-PMMA interfaces. Ahn and Shull [19] investigated the work of adhesion between a lightly cross-linked poly(n-butyl acrylate) [PNBA] hemispherical lens and a PMMA flat surface, and contact hysteresis was observed at all accessible rates of unloading. More contact hysteresis work will be discussed later in this section. Other work worth mentioning is Shull *et al.* [20], who investigated nonlinear elasticity effects and extended the small contact radius assumption used in the JKR theory by using a correction factor.

Besides the spherical geometry, other sample geometries have also been used to study interfacial interactions. Using SFA and adhering thin mica sheets to two

cylindrical glass lenses, Horn *et al.* [21] investigated the contact between two solids. In their study, the axes of the two cylinders were perpendicular to each other, and the separation distance between the mica layers was measured using an optical interferometer through a layer of silver coating between the mica sheets and the glass lenses. The SFA apparatus was either filled with a KCL solution or N_2 during the experiments in order to achieve different interfacial interactions. For the tests involving KCL solution, which represents non-adhesive contact, the contact radius increases with the load following the Hertzian theory. For the tests involving N_2, which represents the adhesive contact, results indicated that a greater contact area is observed under the same load, and a finite contact area exists under zero load conditions that can be analyzed using the JKR theory. However, due to the layered structure, Sridhar *et al.* [22] pointed out that there will be some errors using JKR theory to analyze the experiment, and they developed an extended JKR theory to analyze the layered structure by introducing an adhesion parameter $\alpha = \sqrt{\frac{2W_{adh}R^2}{E_1^* h_1^3}}$, layer thickness ratio, and the ratio of elastic moduli to characterize the interfacial interactions. In their paper, Sridhar *et al.* [22] also conducted a finite element analysis using ABAQUS to simulate the contact procedure and verify their analytical model.

In JKR theory, the interfacial forces are assumed to act only within the contact region, and consequently a stress singularity results at the contact edge. Derjaguin *et al.* [23] suggested that the attractive forces between two solids also exist in a small zone just outside of the contact region, and developed a new theory. In their analysis, deformation was assumed to follow Hertzian theory, and the attractive forces were modeled as van der Waals' force. However, Muller *et al*. [24] showed that more accuracy would be gained by using a Lennard-Jones potential to model the attractive forces. Errors in Derjaguin *et al.* [23] were corrected in Muller *et al.* [25] and Pashley [26], in which equilibrium conditions were obtained by balancing the elastic reaction forces with the

surface forces and the applied load. Due to the efforts of these researchers, this theory is now known as the DMT theory.

Because different approaches had been used to develop the theories, and results predicted were significantly different [27], there was controversy between the JKR and the DMT theories. However, the controversy has been satisfactorily resolved. According to Tabor [28], JKR theory should be used when the dimensionless parameter

$$\mu = \left(\frac{R W_{adh}^2}{K^2 z_0^2} \right)^{1/3} \tag{10}$$

is greater than five. In equation (10), R and K are as defined earlier in this chapter, W_{adh} is the work of adhesion, and z_0 is the equilibrium separation distance of the contact surface. Physically, the DMT theory is more appropriate to use for high modulus solids with low surface energy and small radius of curvature. On the other hand, JKR theory should be used for low modulus solids with high surface energy and large radius of curvature.

Using the Dugdale model for fracture mechanics, Maugis [29] treated the contact edge as a propagating crack in mode I and developed a general theory to form a link between the DMT and JKR theories. Similar to Tabor [28], the results again showed that the JKR theory is valid only for short-range interactions and/or for soft materials; in contrast, the DMT theory is applicable for long-range interactions and/or for hard materials. Maugis and Gauthier [30] showed a JKR-DMT transition in the presence of a liquid meniscus around the contact using a surface force apparatus. Baney and Hui [31] extended Maugis's work. They modeled a cohesive zone to describe the adhesion between long cylinders in contact and found the valid regions for the JKR and DMT theories, respectively.

As discussed earlier in this thesis, materials are assumed to be linearly elastic, isotropic, and homogeneous in the JKR theory, and the bonding and debonding processes

are assumed to be reversible. While this is true for some model systems, most systems exhibit some irreversibility. As a result, hysteresis appears during the loading and unloading process as discussed in Mangipudi *et al.* [18] and Ahn and Shull [19]. Due to the contact hysteresis, a lower compressive force is needed to obtain a given contact radius during the unloading phase than is required during the loading phase. Silerzan *et al.* [32] demonstrated that there is a large hysteresis between the loading and unloading regimes of siloxane elastomers, and proposed a generalized JKR model to explain the experimental data. Kim and his co-workers [33], [34] studied the adhesion and adhesion hysteresis using cross-linked PDMS hemispherical surfaces and a self-assembled model surface containing different chemical functional groups. Using the JKR method, they observed that the hysteresis resulting from a fast relaxation process is practically eliminated using stepwise loading and unloading protocols. The contact pressure-induced, interfacial hydrogen bonds were shown to make significant contributions to the contact hysteresis and were used to explain the phenomena observed. She *et al.* [35] used a rolling contact geometry to study the effects of dispersion forces and specific interactions on interfacial adhesion hysteresis. Hemi-cylindrical elastomers (both unmodified and plasma oxidized) were rolled on PDMS thin films bonded to silicon wafers. The results indicated that the adhesion hysteresis in the PDMS-plasma oxidized PDMS system depends significantly on the molecular weight of the grafted polymer, whereas the hysteresis is rather negligible for the pure unmodified PDMS system. These results are explained in terms of hydrogen bonding, and orientation and relaxation of polymer chains. Li and Tirrell [36] measured the surface energy of an acrylic pressure sensitive adhesive PSA-LN-NoAA and the hysteresis behavior under different loading/unloading speeds. They showed that 27% adhesion hysteresis exists between the equilibrium values from the curves of contact radius versus force in the loading and unloading procedures.

To investigate the work of adhesion, JKR theory has also been applied to the atomic force microscope (AFM), which provides a higher accuracy for the contact radius

and load measurement. Carpick *et al.* [37] used a platinum coated AFM tip in contact with the surface of mica in an ultrahigh vacuum, and determined the interfacial adhesion energy and shear stresses using the JKR theory. Gracias and Somorjai [38] modified the AFM using a tip with a large radius of curvature to reduce the pressure in the contact region. They then measured the surface energies of low-density polyethylene, high-density polyethylene, isotactic polypropylene, and atactic polypropylene. K. Takahashi *et al.* [39] studied the stiffness of the measurement system such as the AFM cantilever and the significant figures of measured displacement. They again confirmed the transition between JKR theory and DMT theory discussed by Maugis [29].

Contact mechanics has also been substantially used in investigations for the adhesion of particles to various substrates. Rimai *et al.* [40] measured the surface force-induced contact radii of 20 μm glass particles deposited on polyurethane substrates with a 5 μm thick thermoplastic layer. The results showed that the size of the deformations depends only on the coating and not on the modulus of the underlying substrate. Soltani *et al.* [41] studied the particle removal mechanism from rough surfaces due to an accelerating substrate. The rough surface was modeled by asperities of the same radius of curvature and with heights following a Gaussian distribution. The JKR theory and the theory of critical moment, sliding, and detachment were used to analyze particle pull-off forces, and to evaluate the critical substrate accelerations for particle removal. Reasonable agreement between the model prediction and experimental data was obtained for aluminum and glass particles. Gady *et al.* [42] measured the force needed to remove micrometer-size polystyrene particles from elastomeric substrates with Young's moduli of 3.8 and 320 MPa using an atomic force technique. They found that the removal force differed by an order of magnitude between the two substrates. When the more compliant substrate was overcoated with a thin layer of the more rigid material, the removal force increased with increasing applied load, which is in conflict with the predictions by the JKR theory and can be explained by taking into account the roughness of the particle and the amount of embedment of the particle into the substrate.

In brief, contact mechanics technology has brought great success in the measurement of interfacial interactions. Recently, Mangipudi and Tirrell [2] gave a complete review of the recent developments in the theories of contact mechanics, and their applications in the design and interpretation of experimental measurement of molecular level adhesion between elastomers, glassy polymers and viscoelastic polymers. They also identified some potential applications in other fields, such as biomaterials.

Despite all the successes achieved so far in the measurement of surface and interfacial energies, techniques presently used are only applicable to certain types of materials. For example, the JKR apparatus requires a compliant, elastomeric lens. However, not all solid polymers of interest for interfacial energy measurement have bulk mechanical properties amenable to the JKR-type of analysis. In particular, many materials have a modulus higher than is convenient to measure a significant increase in contact radius in the linear contact mechanics regime. If the hemispherical lens is directly made of a stiffer material, such as an epoxy, the change of contact zone due to interfacial interactions is too small to be measured easily. Liechti *et al.* [43] reported pioneering investigations measuring the work of adhesion of the epoxy/glass interface and compared it with the work of adhesion obtained from contact angle measurement. If interfacial energies between two solid materials, neither of which is an elastomer, are desired, the lens must be coated with one of the materials of interest, which can be an inconvenience. In addition, not all materials can be deposited on such a lens. As an example, present testing methods cannot be used to determine the interfacial energy between aluminum and steel. Consequently, efforts have also been made to investigate other testing technologies, by which the surface energies for a broader range of materials can be measured directly.

Recently, Shanahan [44] published a mathematical model to measure interfacial energies using a spherical membrane or "balloon". In his model, a spherical membrane under slight internal pressure is brought into contact with a flat and rigid surface. The results of his analysis showed that the interfacial energy depends on the square of the contact radius rather than the cube of the contact radius as with the JKR theory. As a result, the potential inaccuracy induced from the measurement error of the contact radius can be significantly reduced. Additionally, Shanahan [44] also showed that the contact area observed using the balloon method is approximately 10 times larger than that observed in JKR tests under the same load. This greater contact area also provides greater convenience for the test. However, in practice, sample preparation for this method is very difficult, and no experimental data has yet been published.

Plaut *et al.* [45] modeled an elastica loop with a fixed separation distance pushed into contact with a flat surface. In their analysis, the surface energies of the materials were ignored, and the elastica was assumed to be thin, uniform, smooth, inextensible, and flexible in bending. Through the analysis, the conformations of an elastica loop for a given displacement of the loop as well as the contact length and the resultant contact force were obtained. Because the structure of the elastica loop is very compliant even though the modulus of the material is high, measurable deformations due to interfacial interactions when the loop is in contact with another surface may be obtained. The analysis of Plaut *et al*. [45] provides a potential method to measure the surface and interfacial energies between arbitrary material systems. In conjunction with this thesis, Dalrymple [46] extended the solution of Plaut *et al.* [45] and included surface energies in the analysis. The study [46] serves as the analytical background of this study.

In this study, a novel technique using “soft structures” instead of “soft materials” (i.e. elastomers) is proposed and investigated to measure surface and interfacial energies between solids. In practice, a probe is first constructed as a thin, uniform, smooth, and flexible-in-bending elastica loop using the material of interest. Then the elastica loop is

brought into contact with a flat rigid surface made of another material of interest. Because of the compliant structure, measurable changes in the deformation of the elastica due to interfacial interactions are obtained. Since the final conformation of the elastica is the result of the applied load and the interfacial attractive forces, the interfacial energy can be estimated by analyzing the relationship between the contact area and the applied load of the loop.

1.3 Outline of the study

This thesis is divided into five chapters. Chapter 1 gives the project background, the literature review, the objective of this research, and the outline of the study. Chapter 2 discusses the development of the testing method, the experimental procedure, and the results. Chapter 3 shows the numerical analysis of the contact procedure of the elastica loop in contact with a rigid flat surface using ABAQUS 5.8 [47]. The comparison and discussion among the experimental results, numerical simulation, and analytical results are presented in Chapter 4. Finally, in Chapter 5, the major conclusions are summarized as well as some suggestions related to this research work.

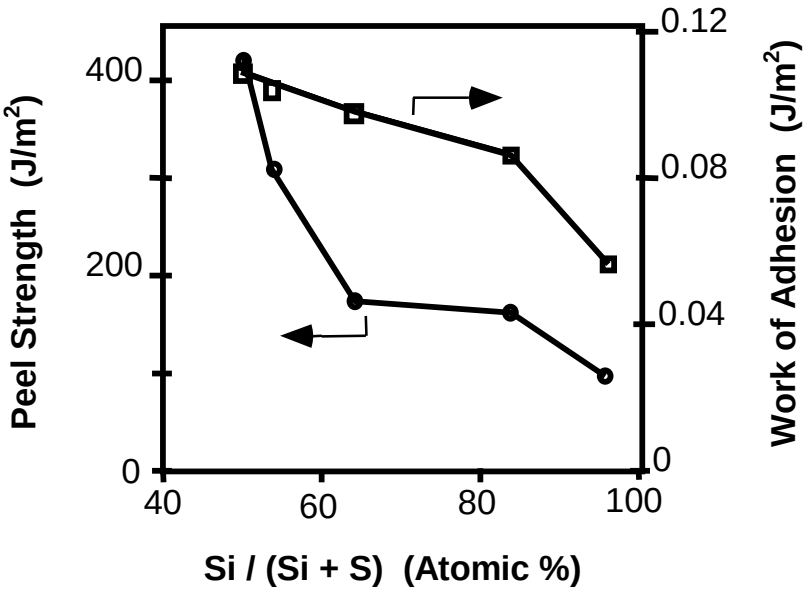

Figure 1.1 The relationship between the work of adhesion and peel strength. After reference 6.

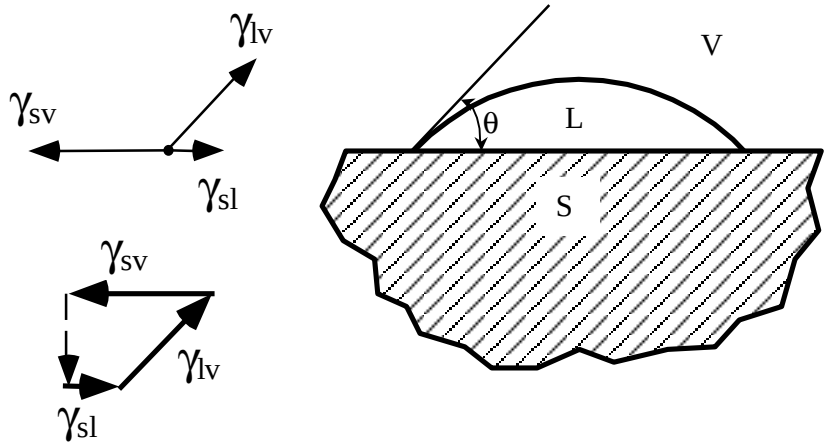

Figure 1.2 Contact angle measurement for a liquid drop on a solid surface and surrounded by a vapor.

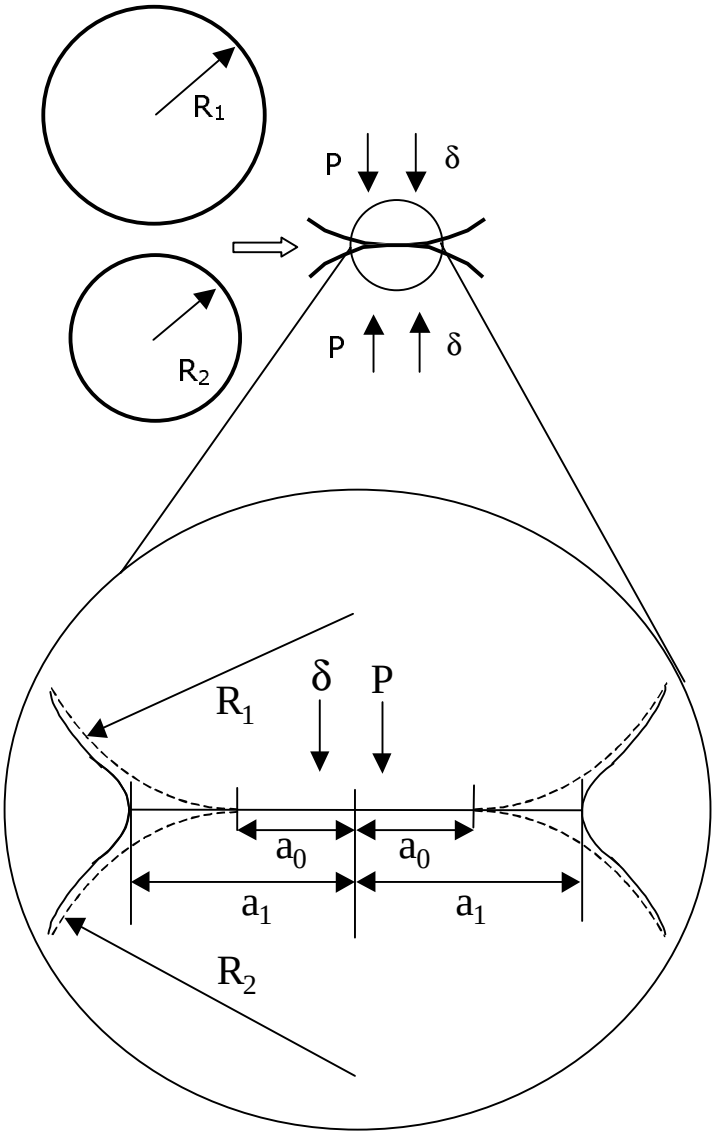

Figure 1.3 Interfacial energy's effect on the contact zone: the solid lines show the actual contact situation with contact radius a_1, and the dashed lines show the Hertzian contact solution with contact radius a_0. After reference 12.

CHAPTER 2 Experimental Study

2.1 Abstract

In the attempt to develop a method that can be used to measure surface and interfacial energies of solids for a broader range of material types, the use of a flexible structure has been proposed. An elastica loop was chosen for use in this research. In the apparatus, the elastica loop is directly attached to the shaft of a stepper motor that is controlled by a computer. When the elastica loop is brought into contact with a flat substrate, the interfacial attractive force produces a measurable change in contact area. The contact pattern is observed in the monitor through a Nikon macro lens with a magnification factor of 50x, and the contact length is measured. At the same time, the force F between the loop and flat substrate is also measured using an analytical balance.

Distinct contact patterns of the elastica loop made of poly(dimethylsiloxane) [PDMS] in contact with a variety of substrates are observed, and the effect of anticlastic bending is eliminated in the center of the contact area due to the flattening of the loop. As compared to the classical JKR tests, the force applied is smaller, the contact length is larger, and the displacement of the loop applied is also larger. Large contact hysteresis with a tail due to interfacial interactions has also been observed in the tests.

2.2 Construction of elastica loop

To directly measure surface and interfacial energies of solids for a broader range of materials compared to the JKR technique, an elastica loop probe with characteristics of a compliant structure is prepared using the material of interest. To achieve the desired structural compliance, the elastica strip is prepared to be thin, uniform, smooth, and flexible in bending. During the test, the elastica loop is brought into contact with a rigid, flat surface made of, or coated with another material of interest, and the compliant

structure permits measurable deformation due to small interfacial attractions. Through the analysis of the deformation, the interfacial energy between the two materials can be obtained. The analytical solution for an elastica in contact with a flat surface is given in Dalrymple's thesis [46].

The dimensions of the elastica and the forces acting on the system are defined as follows. The total length of the elastica strip is 2L, the width of the strip is W, the thickness is t, the bending stiffness is EI, and the distance between the two ends of the strip is 2C. The ends of the elastica are first lifted, bent, and then clamped vertically at an equal height with a specified distance apart. When the bent elastica strip is brought into contact with a flat substrate, the contact length is a result of the applied load and the interfacial attractive force. The total the contact length is defined as 2B, and the resulting reaction force is indicated as F in Figure 2.1.

2.3 Sample preparation and material property characterization

2.3.1 Sample preparation

In this study, the major material used for the elastica loop is SYLGARD 184 silicone elastomer (PDMS) provided by the Dow Corning Company because this material is very stable over a wide temperature range (-50°C to 200°C), and has a very low water absorption and very good radiation resistance. The choice of an elastomeric material for the elastica loop allows comparison of the results with findings obtained using the JKR method. This comparison is a necessary step to verify the methodology. The SYLGARD 184 silicone elastomer contains a silicone base and curing agents and is supplied in a two-part kit comprised of liquid components. The base and the curing agent were mixed in a ratio of 10 parts base to 1 part curing agent by weight with gentle stirring for about 10 minutes to minimize the amount of air introduced. The mixture then rested in air for 30 minutes to remove the air bubbles before use. The PDMS liquid

mixture was then poured on a glass plate cleaned with acetone, and a doctor's blade was used to spread the liquid and to control the thickness of the film to be 1.0 mm. SYLGARD 184 silicone elastomer offers a flexible cure temperature from 25°C to 150°C for various amounts of time, and requires no post-cure. In this study, after the PDMS liquid mixture was spread on the glass surface, the plate was then placed in a programmable oven. The curing process started from room temperature and the temperature was increased at a rate of 5°C/min until 100°C, where the temperature was maintained for 1 hour. Then the temperature was decreased to room temperature at a rate of 5°C/min. After curing, the film was peeled off from the glass plate. The product was a homogeneous, transparent, and flexible film with a final thickness about 0.2 mm, which varied slightly from batch to batch. Specimens were then cut from the film with appropriate dimensions for various mechanical tests.

Various substrates were selected to perform the measurement of surface energies. They were glass plates coated with PDMS, acetone-washed glass plates, polycarbonate [PC] plates, and a commercial cellulose acetate substrate (3M Scotch^{TM} Transparent Tape 600). The preparation of the substrates was relatively straightforward and after preparation, all the substrates, as well as the elastomer films, were stored in a desiccator at room temperature with relative humidity controlled at 30%RH.

2.3.2 Tensile tests

The Young's modulus of the elastica loop is directly related to the compliance of the loop and therefore is a very important factor in the analysis. The Young's modulus of the elastomer was determined via tensile tests conducted as part of this study using an Instron 4505 universal testing frame. The tests were performed at room temperature under a constant crosshead rate of 5 mm/min using a pair of pneumatic grips to clamp the sample. Because the films are very thin (about 0.25 mm) and the modulus of the material is relatively low, attachment of an extensometer to the film would significantly affect the results of the measurement. To resolve this problem, the sample geometry was chosen to

be a rectangular strip instead of the regular dog-bone shape, and the strain was calculated based on the ratio of the crosshead displacement to the sample's original length between grips. To reduce end effects, the ratio of the length to the width of the samples was controlled to be greater than 10.

A typical stress-strain curve in the test from a particular batch of the PDMS material is shown in Figure 2.2. The Young's modulus was obtained using a data fit algorithm of the linear portion of the curve. Figure 2.3, Figure 2.4, and Figure 2.5 show the modulus data for specimens from different batches. These figures indicate that the stress-strain curves are very repeatable within a given batch but differ slightly from one batch to another. Table 2.1 summarizes all the modulus data for all the different batches of the material tested. One possible reason for variations of the modulus among different batches is the lack of precise control of the ratio between the base material and the curing agent. As indicated by the data sheet provided by the Dow Corning Company, the content of the curing agent will have some effect on cure time and the physical properties of the final cured elastomer. Lowering the curing agent concentration will result in a softer and weaker elastomer; increasing the concentration of the curing agent too much will result in over-hardening of the cured elastomer and will tend to degrade the physical and thermal properties.

2.3.3 Orientation of the elastica loop

A narrow strip was first cut from the cured PDMS film prepared earlier. The ends of the strips were lifted, bent, and fixed vertically with a known separation distance. The specimen was then attached to a sample holder as shown in Figure 2.6. The angles of the PDMS strip at the fixed ends were 90°. The height of the loop, *h*, depended on the total length of the loop, 2L, and the distance between the clamped ends of the loop, 2C.

2.4 Apparatus

There are four major components in the experimental apparatus as indicated in Figure 2.7: 1) the displacement control device; 2) the force measurement device; 3) the optical system; and 4) the computer control and data acquisition system (not shown in the figure). The elastica loop is directly attached to the shaft of the stepper motor, which is a major part of the displacement device and is controlled by a computer. When the elastica loop is brought into contact with a flat substrate by the displacement device, the interfacial attractive force produces a measurable change in contact area. The contact zones are observed in the monitor through a Nikon macro lens using a magnification factor of 50x, and the contact length, 2B, can be measured directly from the monitor provided a careful calibration is performed before the test. At the same time, the contact force F between the loop and the flat substrate can be measured using an analytical balance mounted on the force measurement device. The whole contact sequence and data acquisition were controlled by the computer control and data acquisition system. In the following sections, detailed descriptions for each component of the apparatus are given.

2.4.1 Displacement control device

Based on the dimensions of the specimen and the deformation level of the loop induced by the interfacial interactions, a low speed, low vibration, and high-resolution displacement control system is required for the study. From a broad search of various positioning products, the IW-710 INCHWORM motor from Burleigh Instruments, Inc. was chosen as the major component for the high-resolution positioning system. This IW-710 INCHWORM motor uses compact piezoelectric ceramic actuators to achieve nanometer-scale positioning steps over several millimeters. This motor offers a range of motion for 6 mm and is featured with a mechanical resolution of approximately 4 nm over the entire range of motion with a maximum speed specified as 1.5 mm/sec. In addition, this motor has a very high lateral stability with a lateral shaft runout of $\pm 0.2\mu m$.

This instrument also provides a non-rotating shaft and forward and reverse limit switches, providing a convenient way to control the contact procedure. The motor can sustain a light load (less than 1000 grams), and consequently, the elastica loop was directly attached to the shaft in the tests. The position of the elastica loop is read through an integral encoder associated with the IW-710 motor. The resolution of the encoder is 0.5 μm with an accuracy up to ±1 μm. The motor and the encoder are controlled by the Burleigh 6200ULN closed-loop controller, which can be operated in either manual or computer control mode. In manual mode, the motor speed and the stop and start functions are all operated through the controller. In addition, the controller can actuate a moving procedure consisting of a series of predetermined increments with the size being as small as the resolution of the encoder. If the controller is operating under the computer control mode, the motor is controlled by the controller through the 671 interface with the computer in a bi-directional communication mode. The bi-directional interface has the following functions, which can be combined arbitrarily to perform a task: 1) load an absolute target displacement value; 2) load a step size; 3) set motor speed; 4) read current motor position; 5) read the current status of the motor and controller; 6) control position maintenance (On/Off); 7) perform motor stall test; 8) set zero reference and clear counter.

As the major component of the displacement device, the IW-710 motor is positioned in the apparatus as shown in Figure 2.8. The outer cylinder made of polycarbonate [PC] rests on the base of the analytical balance and is used to support the motor and reduce air circulation around the elastica loop. The inner PC cylinder has no connection with the motor and rests on the scale pan of the balance. The substrate is placed on the top of the inner cylinder with the surface of interest facing down. When the motor is controlled to move through the contact sequence, the elastica loop attached to the shaft is brought into contact with the substrate and then withdraws to separate the contact. The contact force is measured through the force measurement system, and simultaneously, the contact length is measured through the optical system.

2.4.2 Force measurement device

The attractive force between two solid bodies in this study is several milligrams, which requires a high-resolution force measurement device. To satisfy this requirement, an SA 210 analytical balance from Scientech, Inc. was chosen. This balance is equipped with a high standard of accuracy and has a resolution of 0.1 mg over the entire weight range of 210 grams. The balance is also equipped with a very reliable electronic filtering system, which helps to stabilize the weight reading when mechanical damping of the balance is insufficient. As a result, the display of the balance is prompt, clear, and reliable. In addition, the stability indicator in the balance will also show an "OK" sign when the reading is valid insuring reliable results. In the setup for this study, the analytical balance is placed on a vibration reduction table along with the optical system, and is connected to the computer through an RS-232 interface for the purpose of data acquisition.

2.4.3 Optical system and calibration

To measure the contact pattern and the contact length with adequate accuracy, an optical system is needed. In this study, the optical system mainly consists of a Nikon macro lens with up to 50X magnification, an FOI-150 fiber optic illuminator with two goosenecks, a TK-66 CCD Shutter camera from Micro-techica, Inc, a monitor, and a VCR as partially indicated in Figure 2.7. During the tests, the contact patterns are observed through the macro lens, and the FOI-150 provides uniform illumination in a focused area with white light. Through the digital video camera the entire contact procedure can be observed and can be recorded if necessary using the VCR. The support of the macro lens also rests on the vibration reduction table to enhance the visual observation.

The contact length or contact area is measured directly from the monitor. However, careful calibration is needed before any measurement is taken. To calibrate the readings from the monitor, a fine scale with 20μm resolution was set beside the

substrate underneath the micro lens and, once the system was in focus, readings of the scale were taken from the monitor. According to readings taken, a ruler was made and was directly attached to monitor, from which the contact length can be measured.

2.4.4 Computer control interface and data acquisition system

The computer control program used in this study was written in LabVIEW 5.0 from National Instruments [48]. LabVIEW is a graphic programming language, and is a very powerful tool in areas such as control, automated testing, and data acquisition. LabVIEW provides the flexibility and comprehensive functionality available in standard C programming languages. A LabVIEW virtual instrument (VI) consists of a front panel and a block diagram. The source code uses an intuitive block diagram approach that works much like schematics and flow charts to solve problems. In addition, LabVIEW is platform-independent, so the programs created on one platform can easily be exported to other platforms without any modification.

In this study, the control software written in LabVIEW 5.0 was used primarily to control the movement of the motor and collect the readings from the balance. The analytical balance is equipped with an RS-232 interface and a subVI was therefore written to set up a bi-directional communication between the balance and the computer serial port in order to tare the balance and start or stop collecting data. The INCHWORM stepper motor is supplied with a data acquisition board and a control subVI. Both the subVIs for the balance and for the motor were then imbedded into the main VI to form a complete control and data acquisition software. The final interface of the control software is shown in Figure 2.9.

2.5 Measurement using the JKR method

In order to compare and validate results obtained using the novel technique with those obtained using the JKR technique, measurements of the interfacial interactions using the JKR technique were taken using the apparatus discussed above. First,

hemispherical lenses and thin films using the SYLGARD 184 silicone elastomer (PDMS) were prepared. The hemispherical lenses were provided by Lehigh University and the thin films were then coated on glass substrates. The hemispherical lens was directly attached on top of the shaft of the step motor. A glass substrate was then set on the inner cylinder of the apparatus with the side of the surface coated with the same PDMS material facing down as shown in Figure 2.10.

When the test began, as controlled by the computer, the PDMS lens moved upward slowly until the lens was very close to the substrate, where the interfacial interactions are high enough and the surface of the lens "jumped" forward to be in contact with the substrate. Hence, a finite circular contact area resulted. The contact area increased as the stepper motor continued to move upward and then decreased as the unloading cycle started. The whole contact procedure and the contact pattern were recorded through the digital video camera and the VCR, and the bi-directional data acquisition system allowed the contact force to be monitored instantaneously. As the unloading continued, the contact force decreased. When the contact force decreased to zero, a finite contact still remained at the interface, which was clearly observed during all the tests. Consequently, a tensile force was required to separate the lens and the substrate, a well-known feature of the JKR technique.

Figure 2.11 shows a typical contact pattern resulting from the contact between the lens and the flat glass substrate coated with the PDMS. The result of the contact radius versus the contact force for both the loading and unloading cycle is shown in Figure 2.12. The positive values represent compressive contact forces between the PDMS lens and the substrate, and the negative values represent tensile forces, which were required to separate the contact. The data indicate that there is a small hysteresis between the loading and unloading cycles, similar to what She *et al.* [35] observed for similar material systems.

The data were then analyzed using the JKR theory and a numerical regression method as discussed in Appendix A was used to obtain W_{adh} and K. Figure 2.13 shows the fitting curves of the experimental data, where a^3 is plotted as a function of P. The calculation method is based on the work in reference [14]. The best fit between the experimental loading data and equation (9) yielded values W_{coh} = 45.8 mJ/m^2 and K = 1.73 MPa, which are consistent with the values measured by other researchers [[14], [17]]. However, the best fit between the experimental unloading data and equation (9) yielded W_{coh} = 60.2 mJ/m^2. The resultant high value for W_{coh} in unloading procedure is possibly due to energy loss or molecular interdiffusion across the interface during the loading and unloading cycle, which has not been taken into account in the JKR theory. The data from the loading cycle were therefore chosen to determine the surface and interfacial energies in this study. According to equation (1), the surface energy of the PDMS material is half of the work of cohesion in this case and thus γ = 22.9 mJ/m^2.

2.6 Measurement using elastica loop

In this test, the PDMS films coated on glass substrates were prepared in the same way as discussed in the previous section. The PDMS elastica loop was carefully attached to the shaft of the motor with a tight connection. Before the test started, a volume static eliminator VSE 3000 from Chapman Corp. was used to remove static charges through blowing both the loop and the substrate for 10 minutes. Following a similar control algorithm as in the JKR test, the loop moved upward and then contact occurred between the loop and the substrate as shown in Figure 2.14. The contact length increased as the loading cycle continued and then decreased when the unloading cycle started. Finally, separation occurred when a tensile force was applied on the loop. Considering the effects of the interfacial interactions acting on the system and the time needed to reach equilibrium, the loading speed was selected as 10.1 μm/sec for each step, and between any two steps during the loading cycle, the sample was allowed to dwell for an interval of 200 sec. For the unloading cycle, the dwelling interval was increased to 300 sec/step, because the thermodynamic equilibrium took more time to reach. The whole contact

procedure as well as the contact patterns and contact forces were again recorded and stored for future analysis.

2.6.1 Contact patterns

Similar to the situation in the JKR test, when the elastica loop was close enough to the substrate, the loop "jumped" forward to form a contact with the substrate because of the interfacial energy. However, in this case, due to the anticlastic bending caused by the Poisson's effect, a transverse curvature is resulted when the loop is bent as shown in Figure 2.15. Consequently, the contact first happened at the two edges of the loop as indicated in Figure 2.16. As the shaft continue to move toward the substrate, the contact zone spread across the width and propagated outward in the longitudinal direction toward the loop ends. However, the contact front still remained curved because of the anticlastic bending as shown in Figure 2.17. As the contact area continued to grow, the curved contact front is self-similar as shown by Figure 2.18, which represents a typical contact pattern resulting from the contact between a PDMS elastica loop and a flat substrate coated with the same material. Because of the arched contact front, the determination of the contact length was very difficult. In this study, as indicated in Figure 2.18, the contact length is either defined as the length of the longitudinal center line of the contact zone 2B, which is also the lower bound of the contact length, or the length between the outer edges of the contact fronts $2B_o$, which in fact is the upper bound of the contact length. When $2B>>2B_o$, the contact area at corner was no longer negligible. During the unloading cycle, a finite contact area remained even when the contact force was zero, and a tensile force was required to separate the contact. Because of the compliant structure, the contact force, F, detected in this test were in general smaller than those in the JKR experiment, but the contact lengths, 2B, were normally larger than the contact diameter, 2a, observed in the JKR test.

2.6.2 Experimental results and discussion

In the following, detailed experimental observations and discussions are given for the PDMS elastica loop in contact with different substrates.

1. PDMS loop to PDMS substrate

In this test, both the elastica loop and substrate surface were made of the PDMS elastomer. The substrate consists of a piece of glass and a layer of the PDMS film about 0.2 mm thick. The film was coated using the same method discussed earlier. The glass was cleaned with acetone and de-ionized water before coating. The dimensions of the elastica strip were 14.7 mm $\times$ 0.96 mm $\times$ 0.17 mm. The distance between the two ends of the loop, 2C, was 6.38 mm and the modulus of the loop was 1.81 MPa.

A plot of contact length versus the contact force was obtained in the test and is shown in Figure 2.19. In the figure, a negative force value indicates a tensile force between the elastica loop and the substrate, and a positive force value indicates a compressive force. The diamond and square data are the loading and unloading curves corresponding to the inner contact lengths, 2B, which are the lower bounds of the contact length; and the triangle and circle data are the loading and unloading curves corresponding to the outer contact lengths, $2B_o$, which are the upper bounds of the contact length. Figure 2.19 indicates that the geometry of the contact front does not change during the test because the difference between the inner contact curve and outer contact curve remains almost the same. More specifically, in the test,

$$2B_o=2B+0.35\pm0.04 \text{ mm} \tag{10}$$

The result indicates that the contact spread occurred in a self-similar manner. Because the analytical solution, which will be discussed later, was developed based on beam theory and the effect of anticlastic bending was ignored, the choice of location to determine the contact length will influence the comparison between the experimental results and analytical predictions.

Both the unloading curves in Figure 2.19 indicate that a finite contact area still existed even when the contact force was zero and a tensile force was required to separate the contact.

Figure 2.19 also indicates that at the beginning of the loading cycle, the forces increased with the displacement at a relatively low rate. When the contact length increased to about 40% of the loop width (specified by the dashed line), the slope of the curve increased, suggesting that the contact area started to spread at a relatively high rate. The occurrence of this contact spreading transition is due to the effects of the main bending of the loop in longitudinal direction and the anticlastic bending in transverse direction. As the contact started, the loop first needed to overcome the anticlastic bending curvature. When the contact length exceeded about 40% of the loop width, the loop was flattened, the anticlastic bending effect was already eliminated, and the compliance of the loop substantially increased. In fact, the transition was difficult to capture but could be easily observed in unloading procedure, so the transition was determined using the unloading data. Consequently, the contact area started to spread at a relatively high rate. The contact forces detected in this test were in general smaller than those observed in the JKR test and the contact lengths (both the lower and upper bounds) were larger than the contact diameter observed in the JKR test because of the compliant structure of the loop. A plot of the contact force versus the displacement of the loop of this test is shown in Figure 2.20, which indicates that a small hysteresis loop exists in the loading and unloading curve, which will be discussed later.

2. PDMS loop to glass substrate

In this test, the substrate was changed to a piece of glass cleaned with acetone and de-ionized water. The dimensions of the elastica loop were 15.8 mm $\times$ 0.94 mm $\times$ 0.17 mm with a modulus of 1.81 MPa, and the distance between the two ends of the loop was 6.38 mm. A plot of contact length versus contact force is shown in Figure 2.21, and a

plot of contact force versus the displacement of the loop is shown in Figure 2.22. As same as the previous experiment, the spread transition was clarified using the unloading data. Figure 2.21 shows that in the beginning of the loading cycle, the forces increased slowly with the contact length until the contact length was about one-third of the loop width, where the slope of the curve increased and the contact started to spread rapidly. As compared to the case of PDMS loop in contact with PDMS substrate, the loading and unloading curve shapes are very different, i.e., the hysteresis increased with the decreased unloading force, which indicats a very different interfacial interaction between the PDMS loop and glass substrate. The reason may be stronger interdiffusion between the two materials or larger attractive force between the molecules on the two contact surfaces was occurred. Small hysteresis was observed in the contact force versus the displacement of the loop curve as shown in Figure 2.22.

3. PDMS loop to polycarbonate [PC] plate

In this test, a PC plate cleaned with soap water and DI water was selected as the substrate, and the surface of the PC plate is very smooth. The dimensions of the elastica strip were 15.3 mm $\times$ 0.61 mm $\times$ 0.21 mm, with a modulus of 2.00 MPa, and the distance between the two ends of the loop was 6.55 mm. A plot of contact length versus contact force and a plot of contact force versus displacement of the loop are shown in Figure 2.23 and Figure 2.24, respectively, similar to the experiments of PDMS loop in contact with the glass substrate, the contact spread transition in this case occurred when the contact length was about half of the loop width, and hysteresis existed between the loading and unloading curves.

4. PDMS loop to commercial cellulose acetate substrate

Following the same contact procedure, the measurement between the PDMS elastica loop and a commercial cellulose acetate tape (3M Scotch^{TM} Transparent Tape 600) was taken. The tape was adhered to a glass substrate to conduct the test. The

dimensions of the elastica strip were 16.8 mm × 0.84 mm × 0.17 mm with a modulus of 1.81 MPa, and the distance between the two ends of the loop was 6.38 mm. A plot of contact length versus contact force and of contact force versus the displacement of the loop are shown in Figure 2.25 and Figure 2.26, respectively, the contact spread transition in this test was observed when the contact length was about half of the loop width. A hysteresis loop was also observed.

2.6.3 Hysteresis

In the elastica loop tests, a large hysteresis with a tail was observed between the loading and the unloading curve for every test. To investigate the hysteresis, the creep and the hysteresis properties of the PDMS elastomeric material were characterized. Creep tests at room temperature were conducted on a TA Instruments Dynamic Mechanical Analyzer (DMA) 2980, and the creep time used was 8 hours, which corresponds to the longest running time ever experienced during the elastica loop tests. The hysteresis was characterized using tensile tests conducted on the screw-driven Instron 4505 machine and the tensile hysteresis tests were conducted for about three loading and unloading cycles at a rate of 5mm/min with maximum strain around 40%.

A typical creep test result is shown in Figure 2.27. The results indicate that only a negligible amount of creep occurred. The hysteresis tensile test data are shown in Figure 2.28. This figure shows that the PDMS material has a very low hysteresis since the loading and unloading curves were almost on top of each other.

The creep and hysteresis test results indicate that the viscoelastic properties of the PDMS material give a very limited contribution to the hysteresis observed in the contact of the PDMS elastica loop with various substrates. The hysteresis is believed to be primarily due to the interfacial interactions between the two surfaces at the interface.

To further investigate the hysteresis problem, the PDMS elastica loop versus PDMS substrate contact tests were conducted again. However, in this experiment, the loading and unloading cycles were performed in a cyclic fashion for three cycles. The loading rate was still 10.1 μm/sec for each step, and between any two steps during the loading cycle, the sample was allowed to dwell for an interval of 200 sec. For the unloading cycle, the dwelling interval was increased to 300 sec/step, because it took more time to reach the thermodynamic equilibrium. The experimental results for contact radius versus contact force in Figure 2.29 clearly show that the hysteresis increased significantly with the contact cycle since the area enclosed by the loading and unloading curves increased from the first contact cycle to the third contact cycle. This increase of hysteresis with the contact cycle is possibly due to the molecular inter-diffusion between the two surfaces occurred when they were in contact, which altered the interfacial interactions between these two surfaces.

The effect of contact rate on the contact hysteresis was also investigated in this study using the same testing procedure. In the tests, the loading and unloading cycles were performed continuously using constant testing rates with zero dwell time between any two steps, and two testing rates were evaluated in this study.

Plots of contact radius versus contact force obtained in the tests are shown in Figure 2.30. A testing rate of 5.1 μm/sec was the highest rate that could be achieved with the current apparatus. Figure 2.30 shows that although not significant, the contact hysteresis increases with the testing rate, which again indicates that the interfacial interaction is a time-dependent phenomenon.

Table 2.1 Young's modulus of the tensile specimens from different batches.

Batch No.	1	2	3	4	5
Number of Samples	8	3	3	4	4
Modulus (MPa)	2.28	1.55	1.64	2.00	2.50
Standard Deviation (MPa)	0.06	0.14	0.03	0.07	0.08

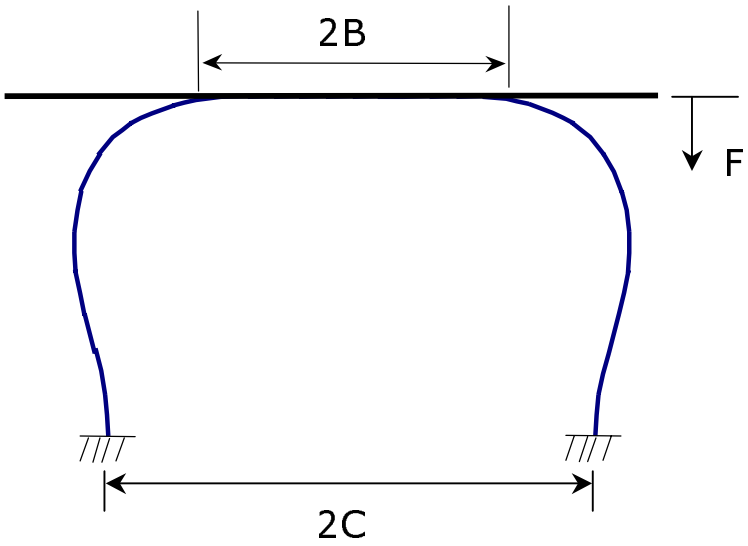

Figure 2.1 Elastica loop configuration

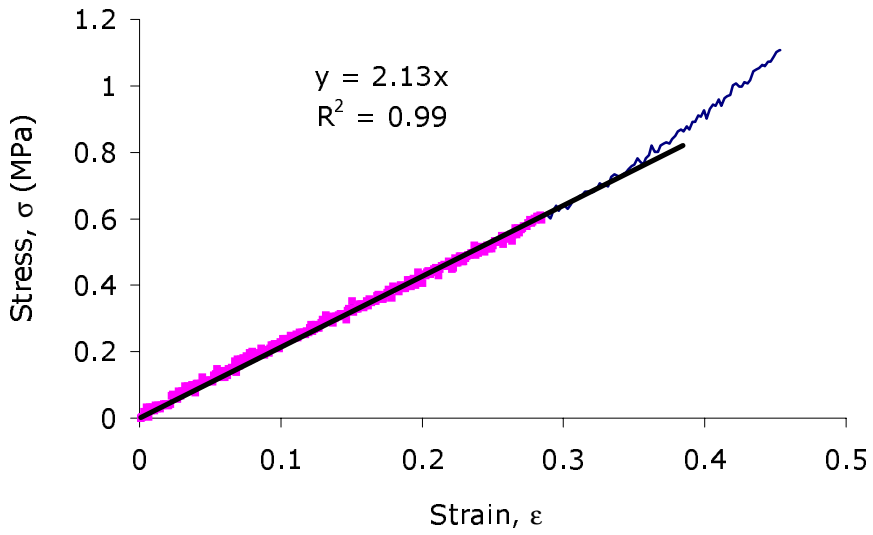

Figure 2.2 A typical stress-strain plot for a PDMS strip.

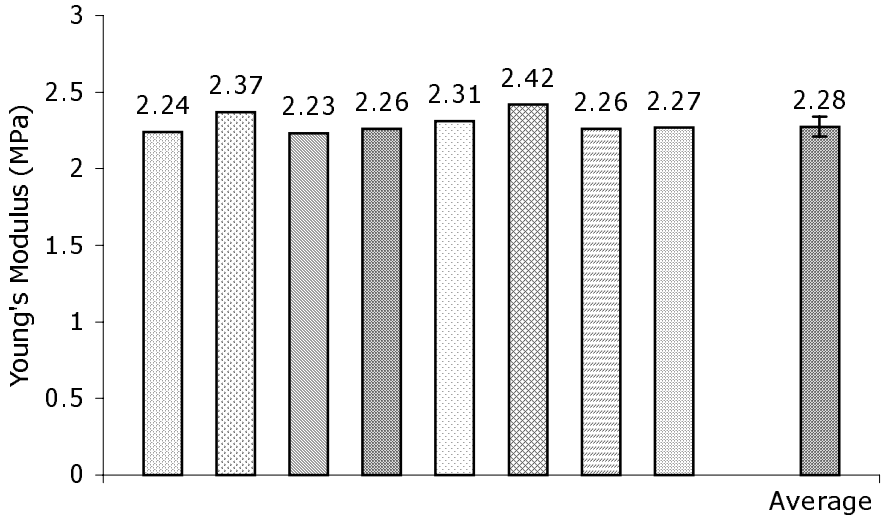

Figure 2.3 Young's moduli for eight PDMS samples of the first batch and their average. The error bar represents ±one standard deviation.

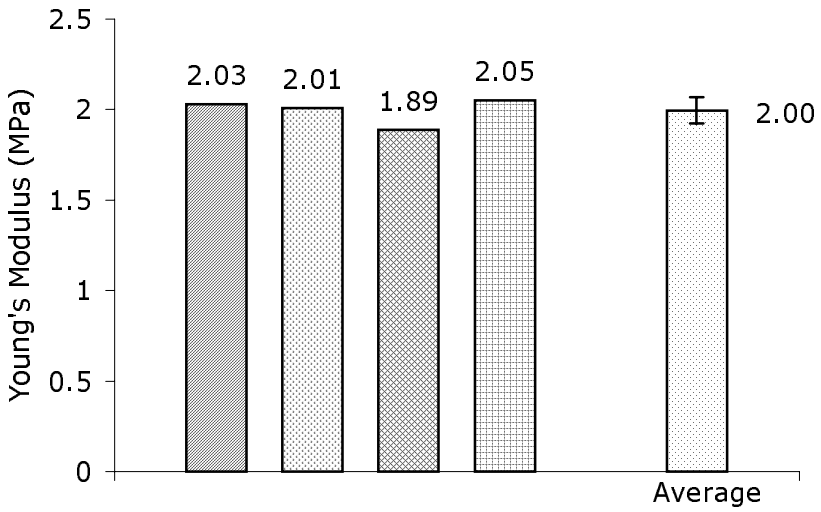

Figure 2.4 Young's moduli for four PDMS samples of the second batch and their average. The error bar represents ±one standard deviation.

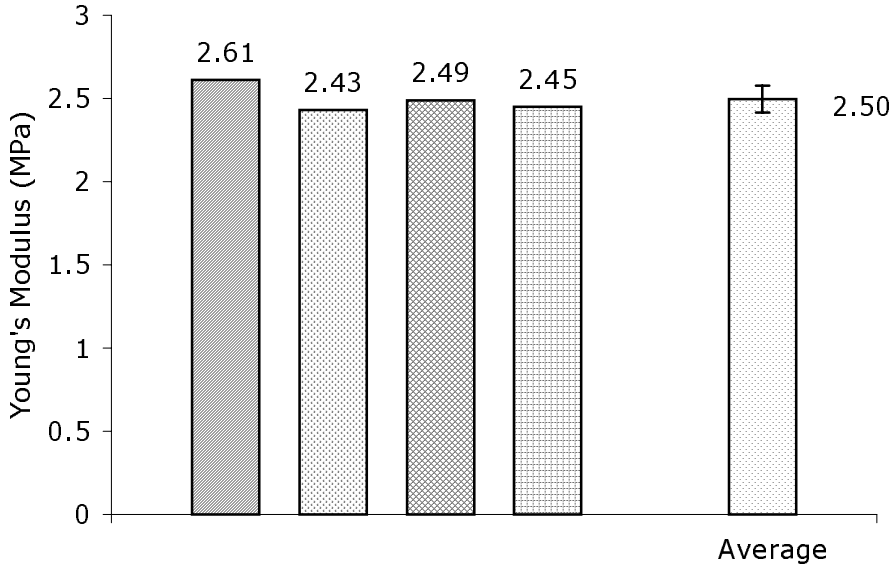

Figure 2.5 Young's moduli for four PDMS samples of the third batch and their average. The error bar represents ±one standard deviation.

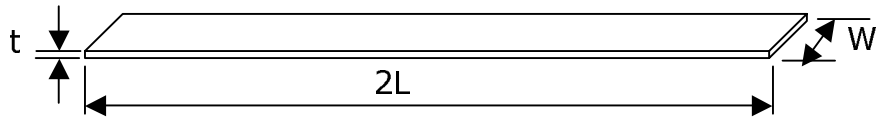

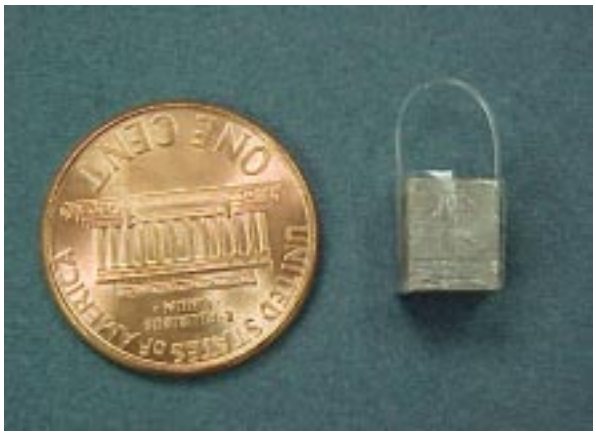

Figure 2.6 Geometry of an elatica loop probe

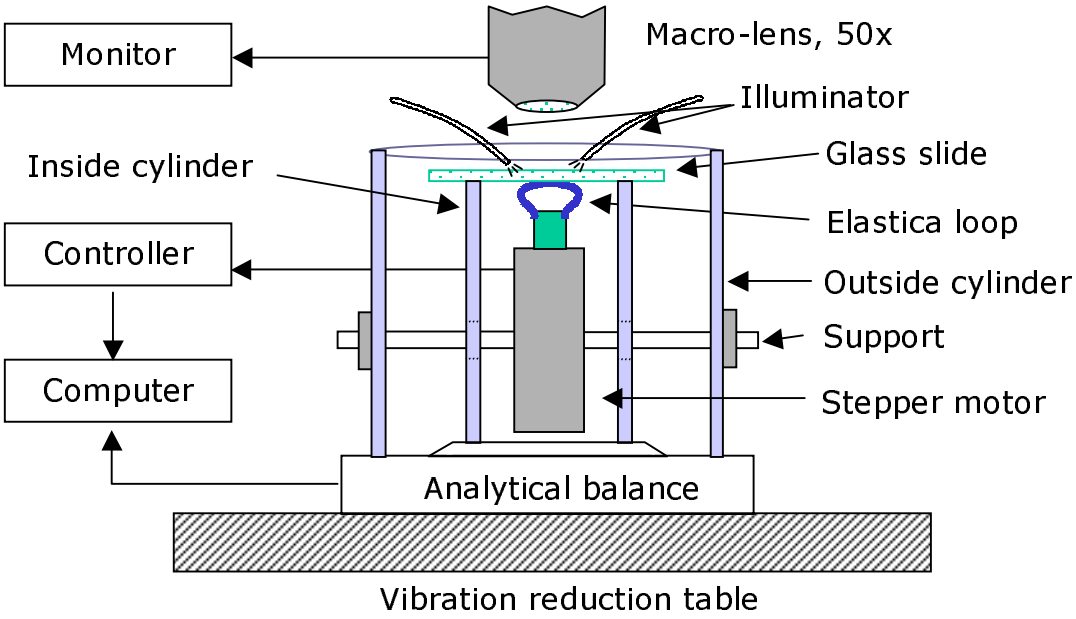

Figure 2.7 Schematic of apparatus

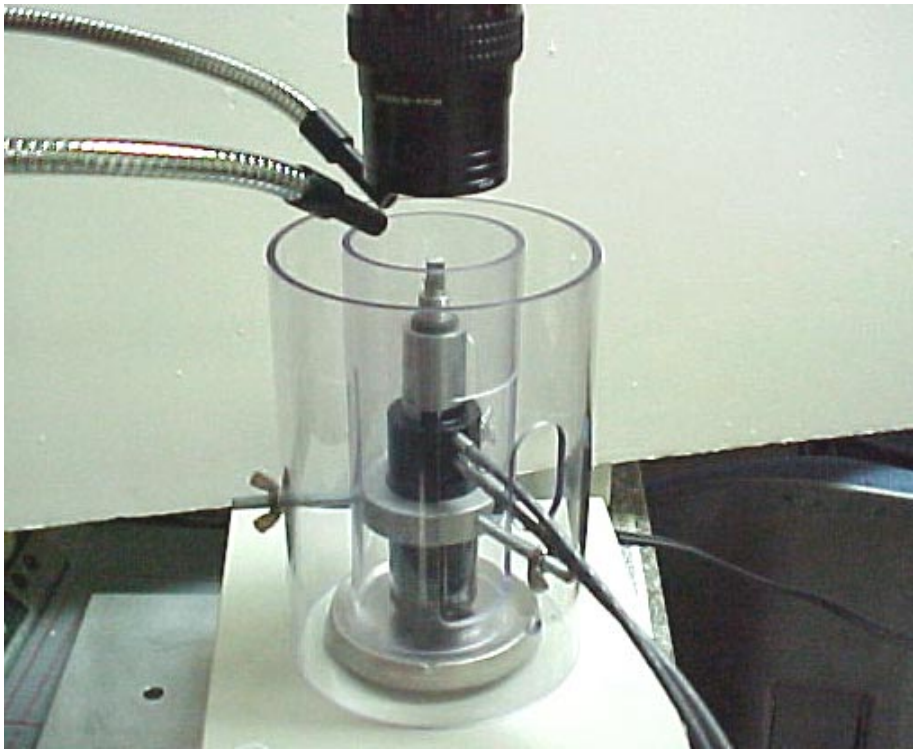

Figure 2.8 Photograph of the apparatus

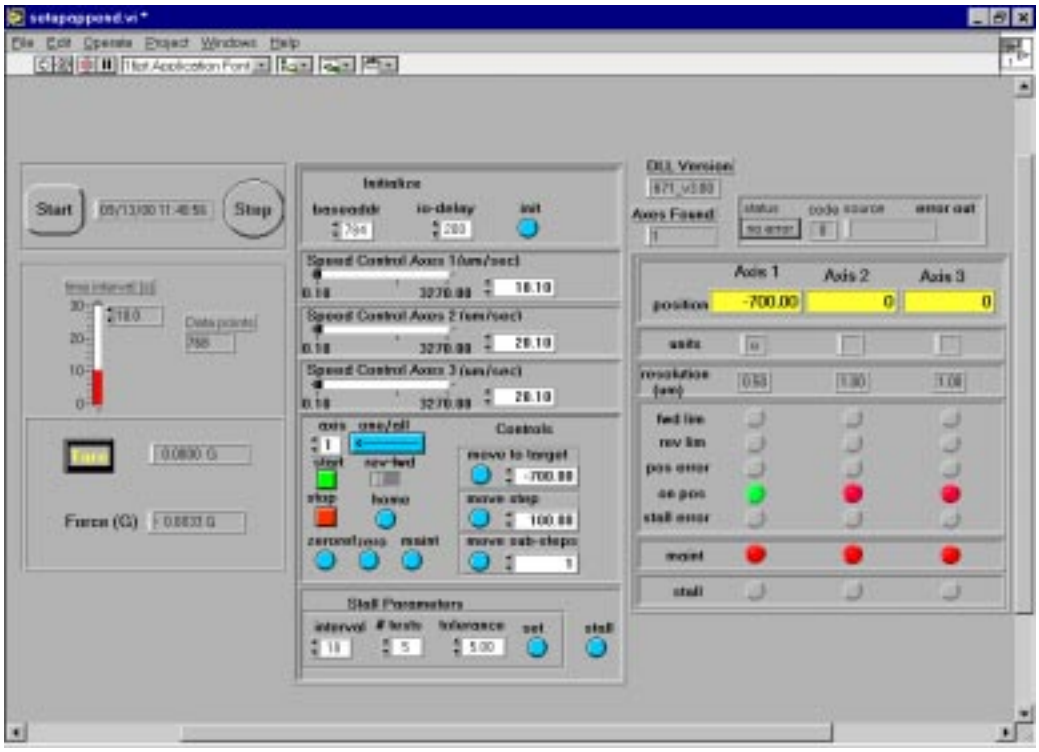

Figure 2.9 Front panel of LabVIEW VI created for the computer acquisition system.

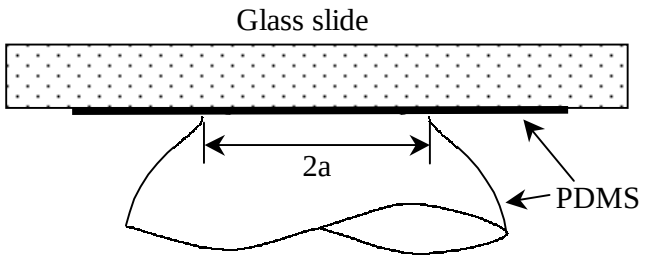

Figure 2.10 Interaction between a PDMS lens in contact with a PDMS film coated on a glass substrate. The dimensions of the figure are not to scale.

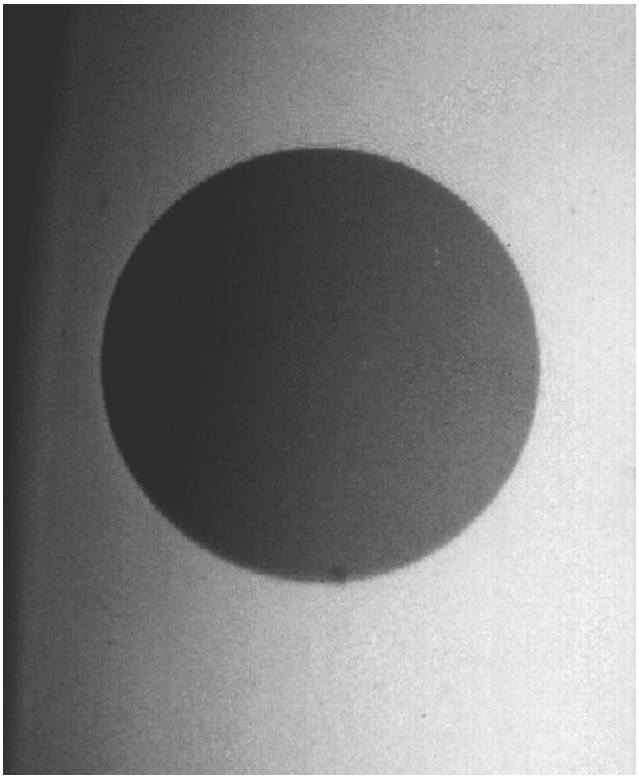

Figure 2.11 Typical contact pattern of a PDMS lens in contact with a PDMS film coated on a glass substrate.

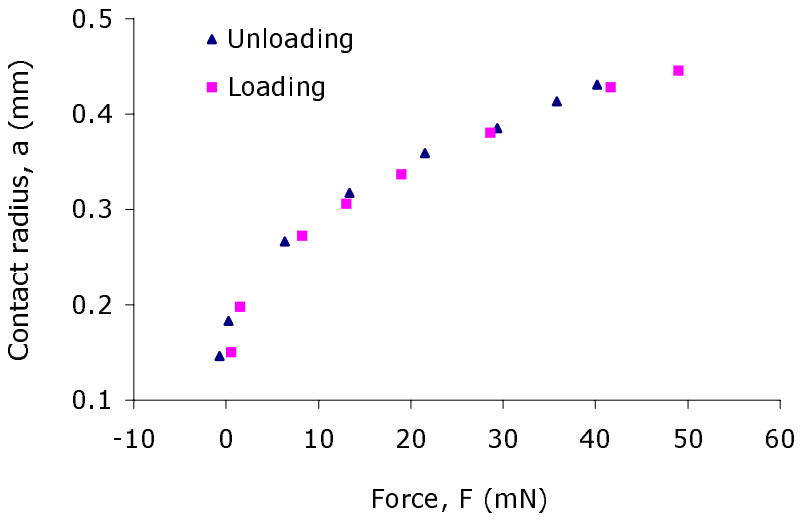

Figure 2.12 Plot of contact radius, a, vs. force, F, in JKR testing: a PDMS lens in contact with a PDMS film coated on a glass substrate.

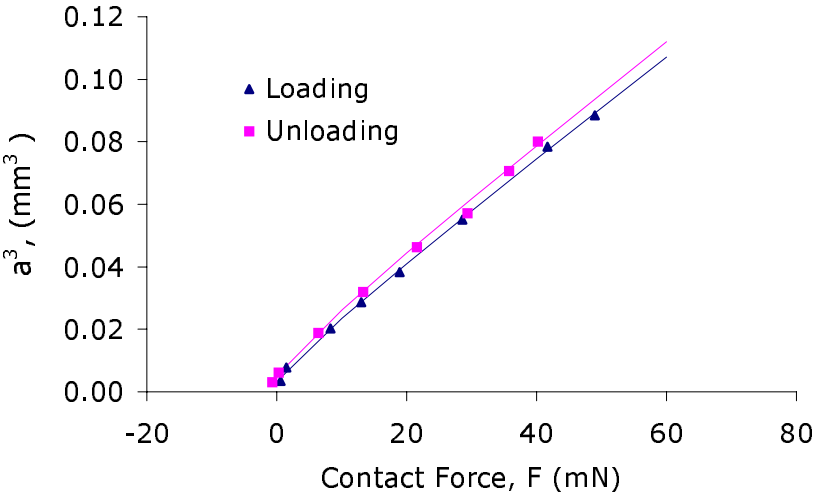

Figure 2.13 Plot of cube of contact radius vs. contact force: the dots represent loading and unloading experimental data and the solid lines represent fitting curves obtained using a numerical regression method.

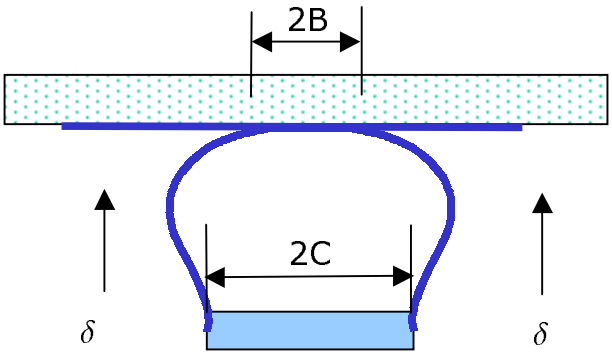

Figure 2.14 Interaction between a PDMS loop in contact with a PDMS film coated on a glass substrate.

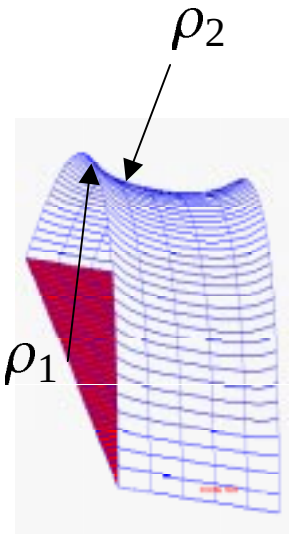

$$\rho_2 = -\frac{\rho_1}{\nu}$$

ν: Poisson's Ratio

Figure 2.15 Anticlastic bending of an elastica loop.

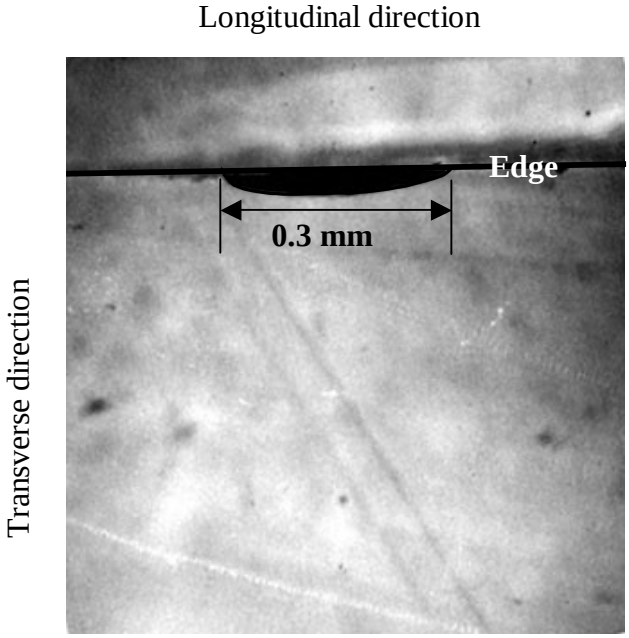

Figure 2.16 Initial contact zone of a PDMS elastic loop in contact with a PDMS coating on a glass substrate, and about two-thirds of the loop width is shown.

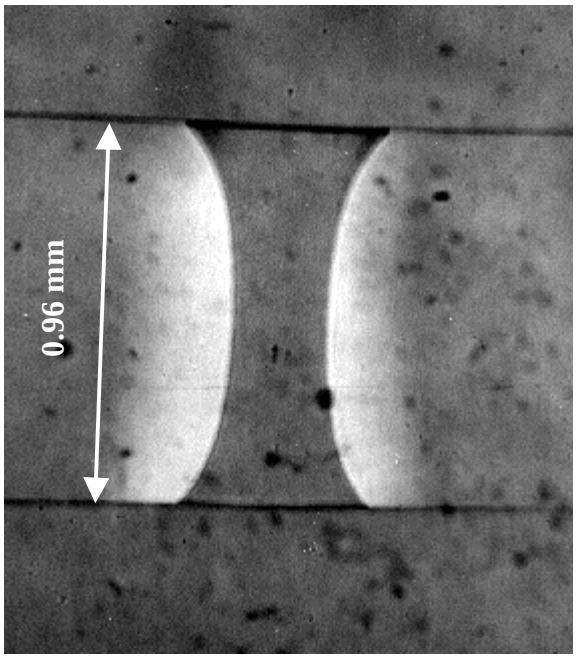

Figure 2.17 Further contact zone of a PDMS elastic loop in contact with a PDMS coating on a glass substrate, but the contact length is smaller than one third of the elastica loop width.

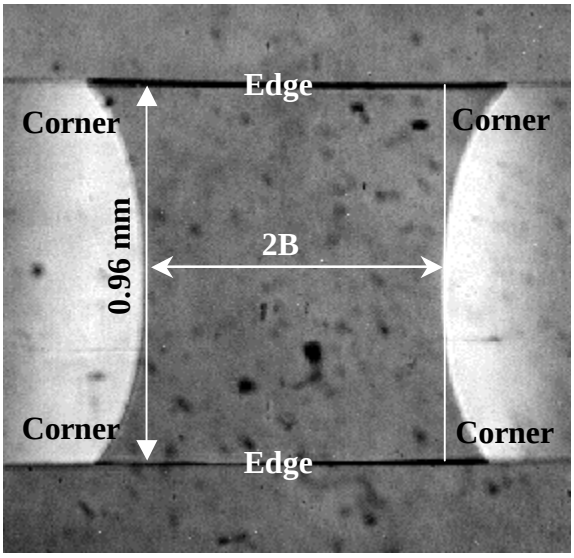

Figure 2.18 A typical contact zone of a PDMS elastica loop in contact with a PDMS coating on a glass substrate.

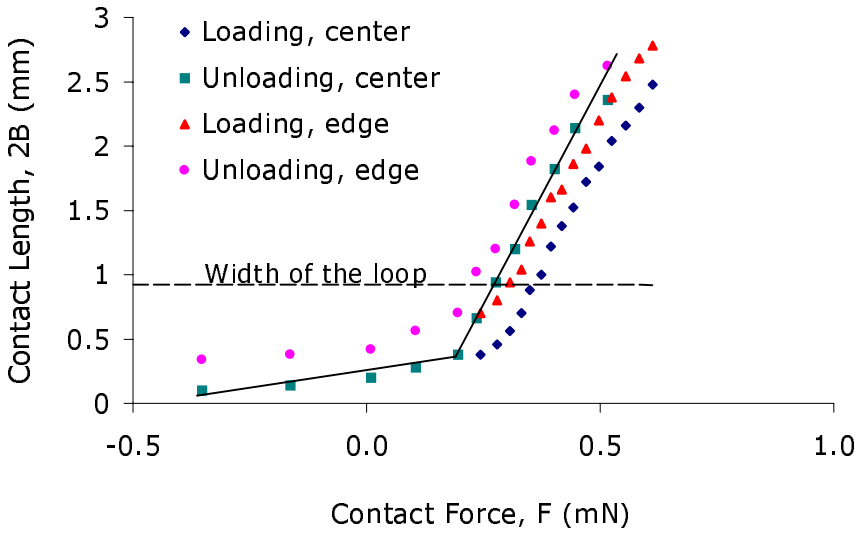

Figure 2.19 Plot of contact length, 2B vs. contact force, F: a PDMS loop in contact with PDMS coating on a glass plate. The solid lines represent the fits of data within the two different regions, which indicate that each region has a different contact spreading rate.

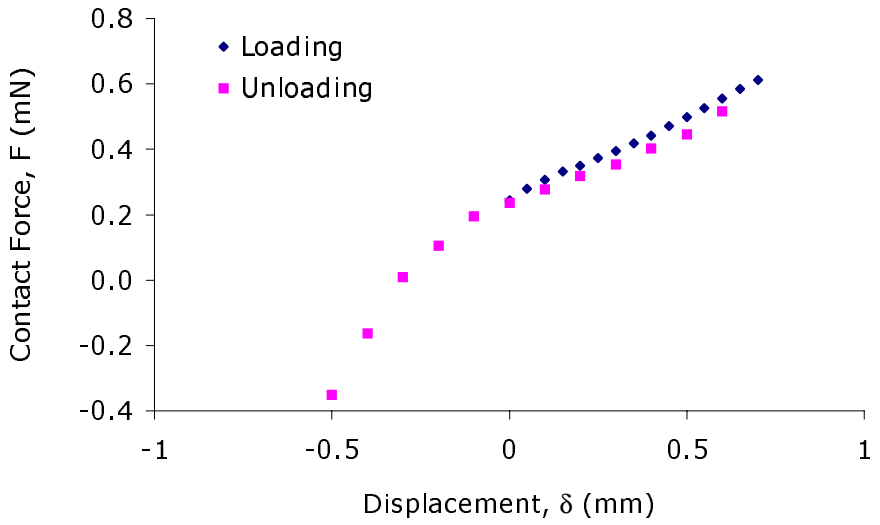

Figure 2.20 Plot of contact force vs. the displacement of the loop: PDMS loop in contact with PDMS substrate.

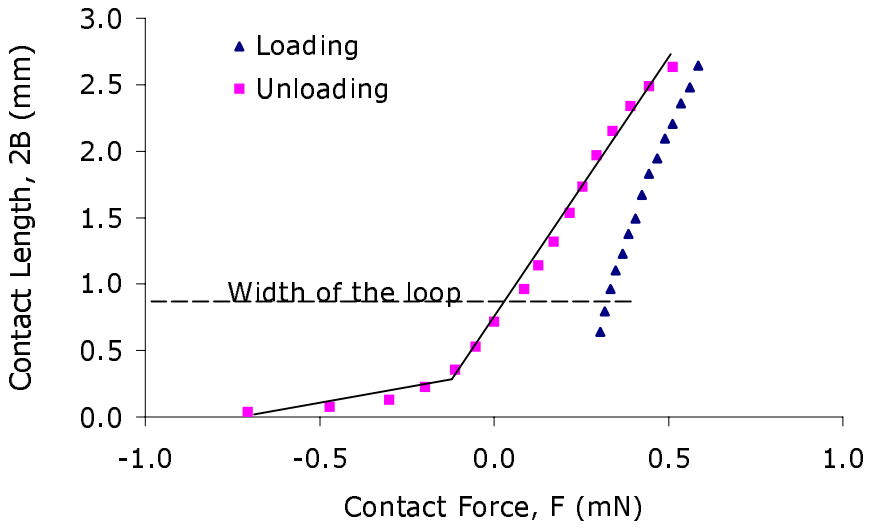

Figure 2.21 Plot of contact length, 2B vs. contact force, F: PDMS loop in contact with a glass plate. The solid lines represent the fits of data within the two different regions, which indicate that each region has a different contact spreading rate.

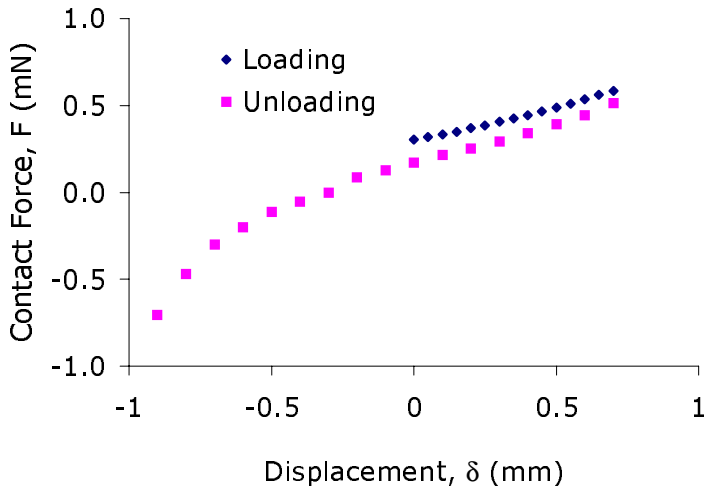

Figure 2.22 Plot of contact force vs. displacement of the loop: PDMS loop in contact with a glass plate.

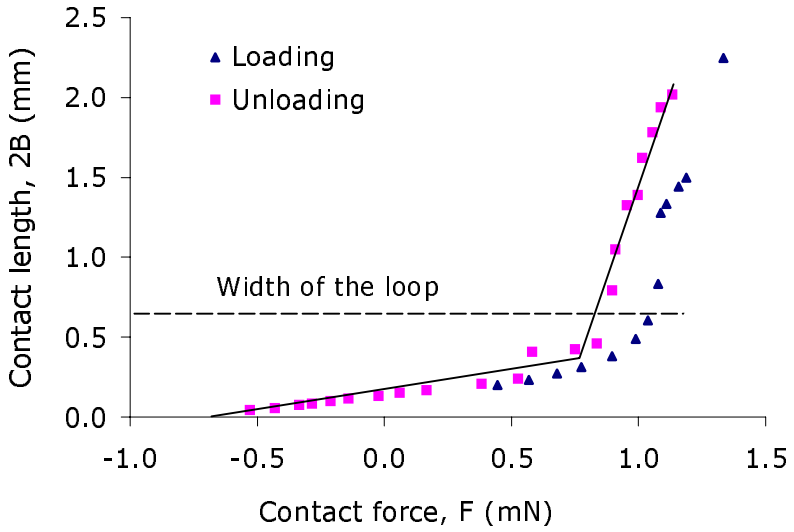

Figure 2.23 Plot of contact length, 2B vs. contact force, F: PDMS loop in contact with a PC plate. The solid lines represent the fits of data within the two different regions, which indicate that each region has a different contact spreading rate.

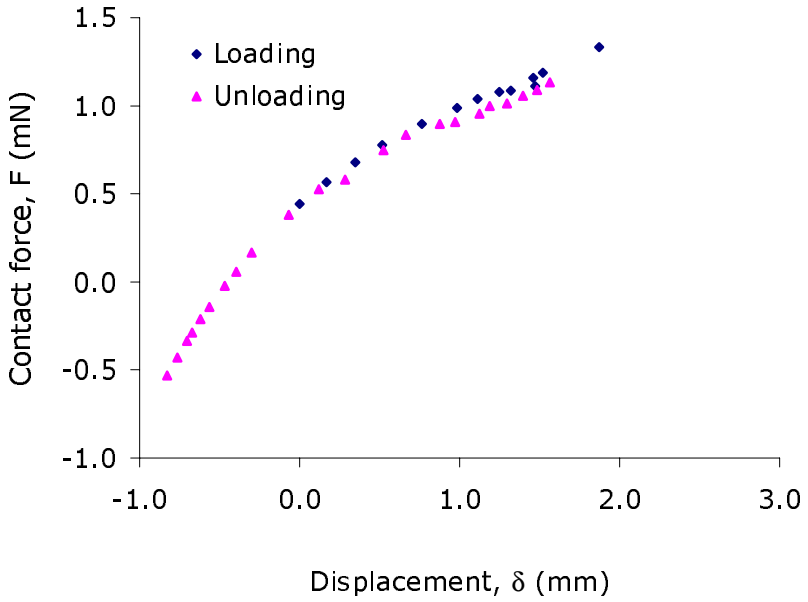

Figure 2.24 Plot of contact force vs. the displacement of the loop: PDMS loop in contact with a PC plate.

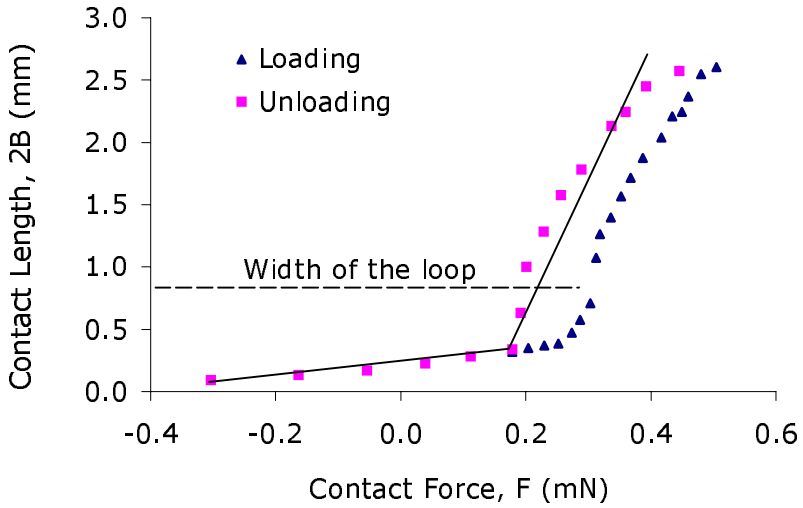

Figure 2.25 Plot of contact length, 2B, vs. contact force, F: PDMS loop in contact with backing of commercial cellulose acetate substrate (3M Scotch^{TM} Transparent Tape 600). The solid lines represent the fits of data within the two different regions, which indicate that each region has a different contact spreading rate.

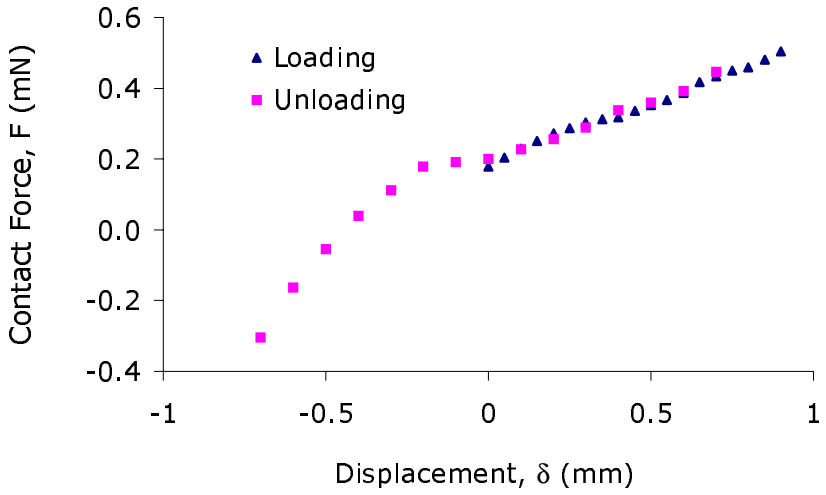

Figure 2.26 Plot of contact force vs. the displacement of the loop: PDMS loop in contact with backing of commercial cellulose acetate substrate (3M Scotch^{TM} Transparent Tape 600).

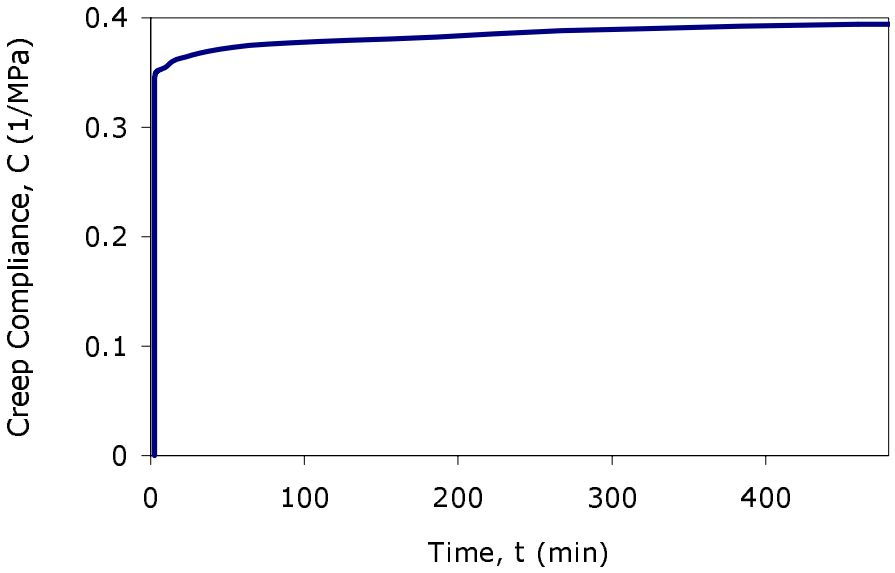

Figure 2.27 DMA creep test results using a rectangular PDMS strip at room temperature with a 0.2 MPa stress.

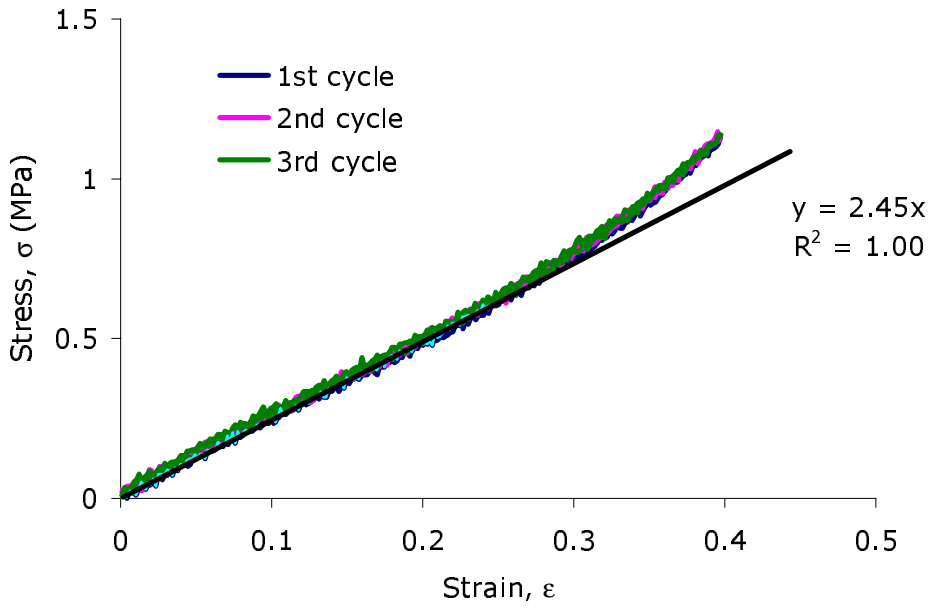

Figure 2.28 Room temperature stress-strain curves of PDMS for three loading-unloading cycles. The loading and unloading rate used in the tests was 5mm/min.

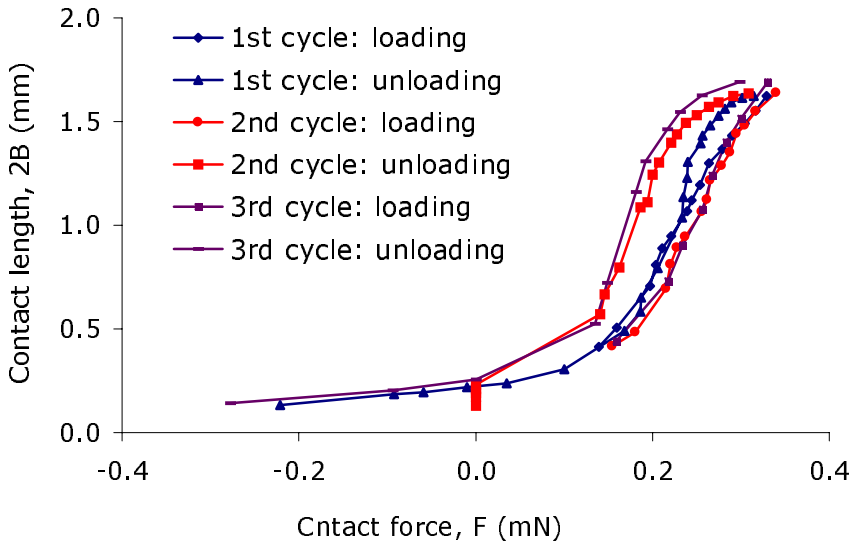

Figure 2.29 Plots of contact length, 2B vs. contact force, F for three loading-unloading cycles: PDMS loop in contact with PDMS substrate.

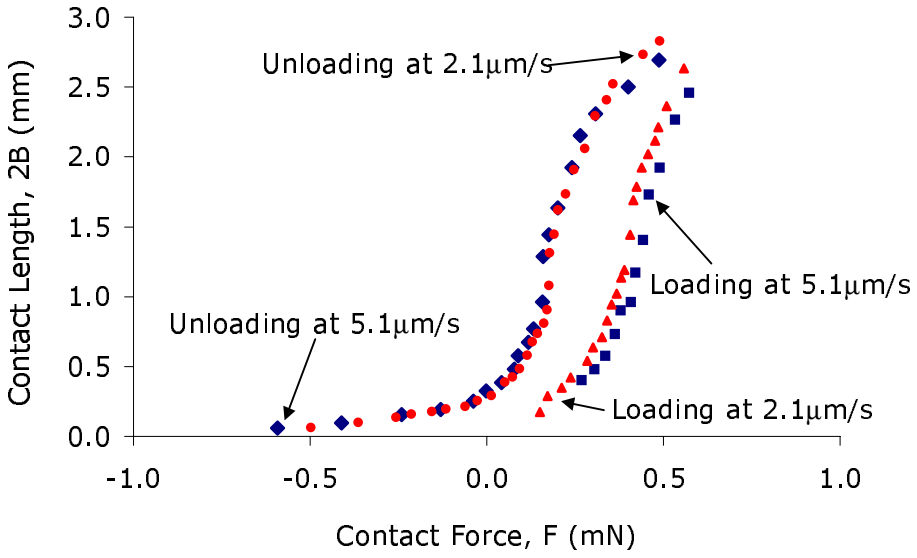

Figure 2.30 Plots of contact length, 2B, vs. contact force, F, for two constant loading-unloading rates with zero dwell intervals: PDMS loop in contact with PDMS substrate.

CHAPTER 3 Numerical Analysis

3.1 Abstract

3-D finite element analyses using ABAQUS 5.8 [47] are conducted to calculate the effect of anticlastic bending of the elastica loop and simulate the contact process between the loop and a flat rigid surface. The finite element model constructed is a geometrically nonlinear elastic contact mechanics model, and the analysis used appropriate mesh, element size, and step increments to simulate the contact procedure. The effect of Poisson's ratio on the contact behavior is given in this chapter.

3.2 Meshes and boundary conditions

To understand the mechanical behavior of the contact procedure at a quantitative level and to verify the analytical 2-D solution by Plaut *et al.* [45], numerical simulations of an elastica loop in contact with a flat rigid surface were conducted using the finite element method. The finite element package used was ABAQUS 5.8, which provides a very powerful tool to deal with general nonlinear and large-deformation problems. In the numerical analyses, the interfacial interactions were ignored due to the limitation of the ABAQUS codes.

The numerical simulation scheme started with a straight elastica strip and a flat surface. The dimensions of the elastica strip were taken from the actual specimens. The Young's modulus of the strip was taken from the tensile experimental data in Chapter 2, and the Poisson's ratio was chosen as ν=0.49, which represents a typical value for elastomeric materials. The flat surface was modeled as a rigid surface. Making use of symmetry, only one half of the strip was modeled. The elements used to model the elastic strip were the S4R four-node shell elements since this is a geometric nonlinear contact mechanics problem. In the central area of the strip, where the contact initiates, a

fine mesh with minimum element size about 0.05 mm × 0.05 mm was used. Moving toward the end of the loop, the mesh became coarser. Shown in Figure 3.1 is a typical mesh used in this study for the elastica strip. When the specimen size changed, the element sizes would also change but the density of the mesh would remain about the same. The constraint for the fixed end of the loop was modeled as a built-in constraint.

3.3 Simulation of the loop formation

Numerically the elastica loop was formed from a straight strip in several steps. The end of the straight strip was rotated 90° clockwise and moved toward the center for a certain distance as indicated in Figure 3.2. In the analysis by Plaut *et al.* [45], the loop was assumed to be an inextensible beam and the analysis was two-dimensional. However, the actual specimen used in the test was a three-dimensional object with a relatively low modulus. Once the loop was formed, there was anticlastic bending in the loop due to the Poisson's ratio effect. The relationship between the curvatures of the longitudinal bending and anticlastic bending is given by $\rho_2 = -\rho_1/\nu$ as indicated in

Figure 2.15, where ρ_1 and ρ_2 are the curvatures of the longitudinal and anticlastic bending, and ν is the Poisson's ratio of the loop. Because of the effect of anticlastic bending, the strain state in the elastica loop is more complex than the 2-D solution discussed by Plaut *et al.* [45]. As indicated by the finite element analysis results shown in Figure 3.3 and Figure 3.4, where the longitudinal and transverse strain on the concave side along the loop are shown, respectively, the maximum absolute value of the longitudinal strain (3.4%) occurred in the center of the loop, where the longitudinal curvature reached the maximum value. The minimum longitudinal strain (zero) occurred at the end of the loop. Similarly, the maximum absolute transverse strain (1.5%) occurred in the center of the loop because this was the location with maximum transverse curvature. The minimum transverse strain (zero) occurred at the fixed end. Although the strains along the loop were not zero, their level was quite low, which supported the

inextensible elastica loop assumption made by Plaut *et al.* [45] in developing the analytical solution for an elastica in contact with a flat rigid surface.

3.4 Contact simulation

3.4.1 Contact principle

When two solid bodies are in contact, stresses are transmitted across the interface. If the interface is frictionless, only the stresses normal to the interface will be transmitted. On the other hand, if friction is present at the interface, shear stresses will also be transmitted. Contact problems normally involve material property discontinuities and severe stress discontinuities across the interface, which sometimes causes serious numerical convergence problems. If large deformations also need to be considered, finite sliding at the interface between the two solids has to be taken into account and the numerical increments have to be very small. Consequently, the modeling usually requires a lot of computing time.

To model a contact problem, surfaces in contact are defined as master and slave surfaces in ABAQUS. The choice for master and slave surfaces is strict and each surface has different requirements for the mesh. In general, the slave surface requires a finer mesh since only the slave surface allows penetration, and if possible, the surface with a lower modulus material is usually chosen as the slave surface. In addition, the orientation of the master surface needs to be properly defined. The slave surface always has to be on the same side as the outward normal of the master surface. Otherwise, ABAQUS may detect severe overclosure and fail to converge. ABAQUS determines the overclosure, *h,* through calculating the relative distances between the integration points on the contact surfaces as indicated in Figure 3.5. The contact behavior is determined through *c*, *h*, and contact pressure *p*. In this study, the surface of the elastica loop was defined as the slave surface, named as SURF, and the rigid surface was defined as the master surface, named as RIGID. Because of the compliant structure of the loop, a

geometrically nonlinear finite element simulation scheme was used. At the interface, finite sliding conditions were applied to be compatible with the geometrically nonlinear model. According to suggestions in the ABAQUS manuals and after a series of trial calculations, the following contact simulation algorithm was chosen to simulate the contact procedure.

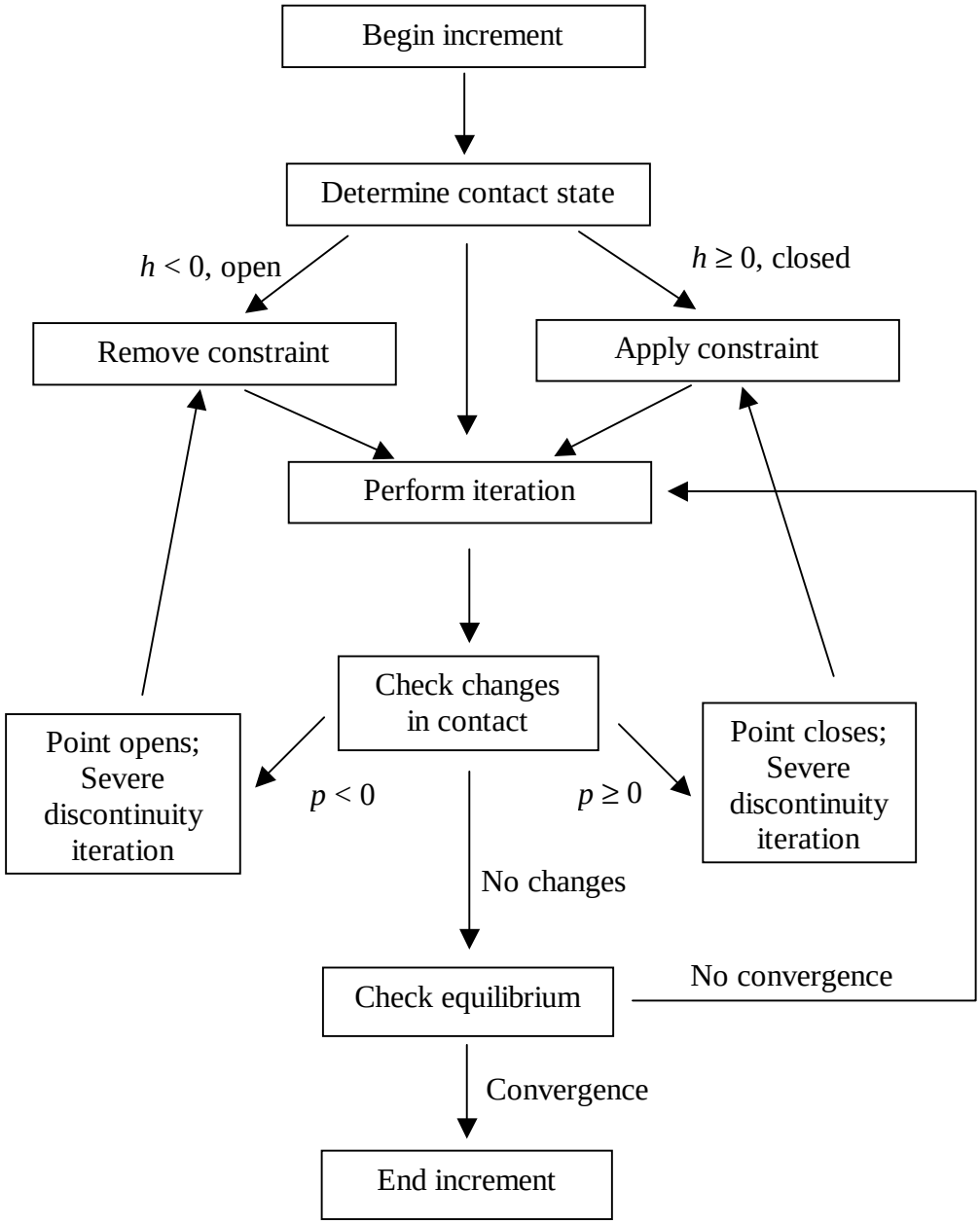
Begin increment
Determine contact state
$h < 0$, open
$h \geq 0$, closed
Remove constraint
Apply constraint
Perform iteration
Check changes in contact
Point opens; Severe discontinuity iteration
$p < 0$
$p \geq 0$
Point closes; Severe discontinuity iteration
No changes
Check equilibrium
No convergence
Convergence
End increment

3.4.2 Contact procedure

As the contact simulation started, the elastica loop was first formed through bending the strip, and the end was moved toward the center for a certain distance, which was taken from the actual sample geometry. Then the flat substrate, which was defined as a rigid surface, was moved toward the loop, and finally they were in contact with each other as shown schematically in Figure 3.6. The displacement increments and the initiation time were selected differently in different steps in order to deal with the nonlinear problem properly. Contact patterns, normal contact stresses, strain distribution, and displacement profiles were obtained during the analysis.

3.4.3 Contact patterns

Through the finite element analysis, the whole contact procedure was simulated. When the rigid plate was brought into contact with the loop, the contact first initiated at the edge of the loop because of the anticlastic curvature, as shown in Figure 3.7. The maximum normal contact stress was located in the center of the contact zone along the edge, as shown in Figure 3.8. As compared to the experimental observation of the contact zone as shown in the insert of Figure 3.7, the contact shape predicted by the finite element modeling in Figure 3.8 appears to be consistent. However, difference in contact shape has been noticed between the finite element result shown in Figure 3.7 and the experimental observation, which was possibly caused by the computer display error itself or the calculation error due to the use of symmetry at center line. As the displacement increased, the compressive force also increased, and the contact zone spread across the width and propagated outward longitudinally toward the loop end. The curved contact front, which was also due to the anticlastic bending, was clearly observed as shown in Figure 3.9. This result was also consistent with the experimental observations as shown in the insert of Figure 3.9.

The results also show that the maximum normal contact stresses always started at the edge of the loop, which was where contact initiates, and moved toward the end of the loop along the edge as the contact area increases, as indicated in Figure 3.10. Because the attractive interfacial forces could not be taken into account within current ABAQUS program, the contact stresses within the contact zone were zero. This is as would be expected for a portion of the loop that has returned to its original, stress free, and flat shape.

3.4.4 Strain of the elastica loop after contact

Once the elastica loop was in contact with the flat surface, the shape of the loop changed, and so did the locations of the maximum strain in both the longitudinal and transverse directions on the concave side of the loop. As discussed earlier, the maximum longitudinal strain along the loop before contact was about -3.4% and this occurred at the center of the loop as shown in Figure 3.3. However, as shown in Figure 3.11, the maximum value for the longitudinal strain was about -5.1% after contact occurred, and the location moved toward the end of the loop because at this moment, that was the location with the maximum longitudinal curvature. Due to the curvature change, the minimum strain reduced to zero at the contact region, where the curvature was infinite. Similarly, the transverse maximum stain was about 1.5% in the center of the loop before contact. After contact, as shown in Figure 3.12, the maximum transverse strain was about 2.1% and was located at the same location as the maximum longitudinal strain. The minimum transverse strain was again zero, which occurred in the contact region.

3.4.5 Contact force and contact area

The relationship between the contact length and the contact force obtained in the finite element analysis (FEA) is shown in Figure 3.13, where the contact length was measured from the center point of the contact front. The shape of the curve is very similar to the experimental data shown in Figure 2.21. As the loading cycle started, the forces increased with the contact length at a relatively slow rate until the contact length

reached a certain value, where the contact started to spread rapidly. In the experimental data shown in Figure 2.21, this contact rate transition occurred when the contact length was about 40% of the loop width. On the other hand, in the FEA result shown in Figure 3.13, this transition occurred when the contact length was a very small value. These results indicate that the transition in the experiment with the elastica loop is primarily due to the combined effects of the main bending along the longitudinal direction, the anticlastic bending and the interfacial energies. The difference between the experiment data and numerical result is the effects of interfacial energies between the loop and substrate.

Because of the curved contact front, the determination of the contact length is ambiguous. In this numerical study, the contact lengths measured from three different locations have been taken as indicated in Figure 3.14: 1) the outer edge point on the contact front; 2) the point with maximum pressure; or 3) the center point on the contact front. Figure 3.14 also shows the relationship between the contact forces and the contact lengths measured at different locations. This result indicates that if the attractive interfacial energy is not present, the curvature of the contact front remains constant as the contact length increases, since the relative distance among these three curves remains almost the same. This conclusion is consistent with the experimental observation discussed in Chapter 2, where the final curvature of the contact front resulted from the combined effects of the longitudinal main bending, the anticlastic bending and the interfacial interactions.

3.4.6 Poisson's ratio effects

In the analysis by Plaut *et al.* [45], the elastica loop was analyzed using beam theory. As a result, the Poisson's ratio, ν, of the loop has no effect on the solution because the width effects, including anticlastic bending, were not modeled. In the finite element analysis in this study, the elastica loop was treated as a three-dimensional object, and the results showed that the anticlastic bending affected the contact pattern, contact

length, and normal contact stress distribution. A sensitivity study of the effect of the Poisson's ratio was therefore conducted in order to understand the effect of the anticlastic bending. In the analysis, the contact procedure was simulated for loops with a series of Poisson's ratios of 0, 0.1, 0.2, 0.3, 0.4 and 0.49.

Figure 3.15 shows the changes of the contact front as the Poisson's ratio increased from 0 to 0.3 and 0.49. If the Poisson's ratio was set to zero in the finite element analysis, anticlastic bending was eliminated and the contact front was a straight line across the width. As the Poisson's ratio increased, the effect of anticlastic bending became more and more significant; as a result, the curvature of the contact front increased and so did the maximum contact pressure, which is located at the outer edges of the loop.

Figure 3.16, Figure 3.17, and Figure 3.18 show the effect of Poisson's ratio on the relationship between the contact length and the contact force. In Figure 3.16, the contact length was taken from the center of the contact front; in Figure 3.17, the contact length was taken from the point with maximum pressure; and in Figure 3.18, the contact length was taken from the outer edge of the contact front. In each figure, the contact length versus the contact force curves for Poisson's ratios of zero, 0.1, 0.2, 0.3, 0.4 and 0.49 are shown. If the contact length is measured either from the center of the contact front or from the point with maximum pressure, Figure 3.16 and Figure 3.17 show that the contact length increases as the Poisson's ratio decreases under a constant contact force. On the other hand, if the contact length is measured from the outer edge of the contact front, Figure 3.18 shows that the contact length decreases as the Poisson's ratio decreases. More importantly, Figure 3.16 shows that the transition occurs at a lower contact length as the Poisson's ratio increases if the contact length is measured from the center point of the contact front. On the other hand, as shown in Figure 3.18, the transition occurs at a higher contact length as the Poisson's ratio increases if the contact length is measured from the outer edge of the contact front. Figure 3.14 has already

demonstrated the effect of the measuring position of the contact length on the contact transition for the case of $\nu = 0.49$. These results provide valuable insights into how the interfacial energy measurements with an elastica loop ought to be performed to obtain the most sensitive observation of the effect of the interfacial interactions. More specifically a good understanding of the Poisson ratio's effects obtained in the FEA analyses can help us determine the proper measuring point of the contact length. For example, for the case of the PDMS loop used in this study, the proper point to measure the contact length is the central point of the contact front, because the FEA results and the experimental data have shown that the effect of the interfacial interactions on the contact spread transition were most clearly observed for this case.

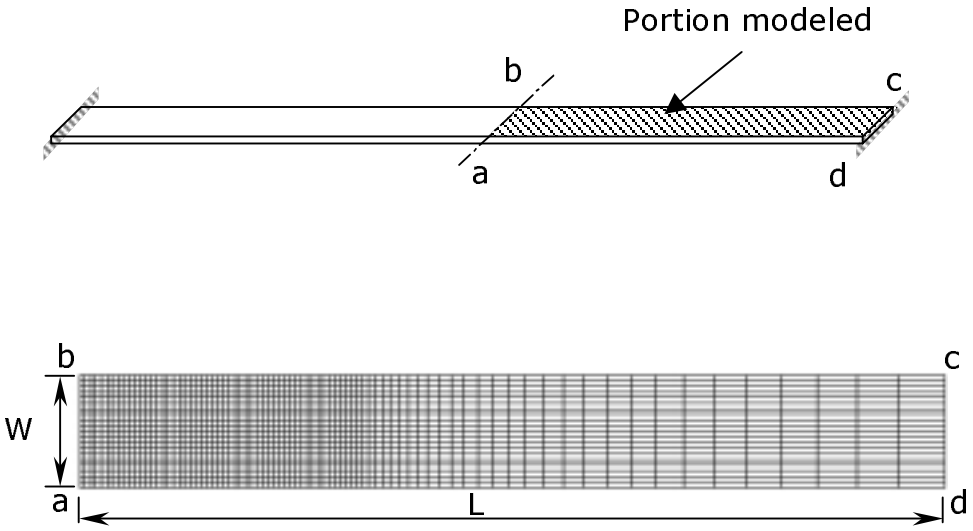

Figure 3.1 FEA mesh of elastica loop with dimensions 14.71 mm × 0.956 mm × 0.165 mm, modulus 1.81 MPa, and a series of Poisson's ratios of 0, 0.1, 0.2, 0.3, 0.4, 0.49.

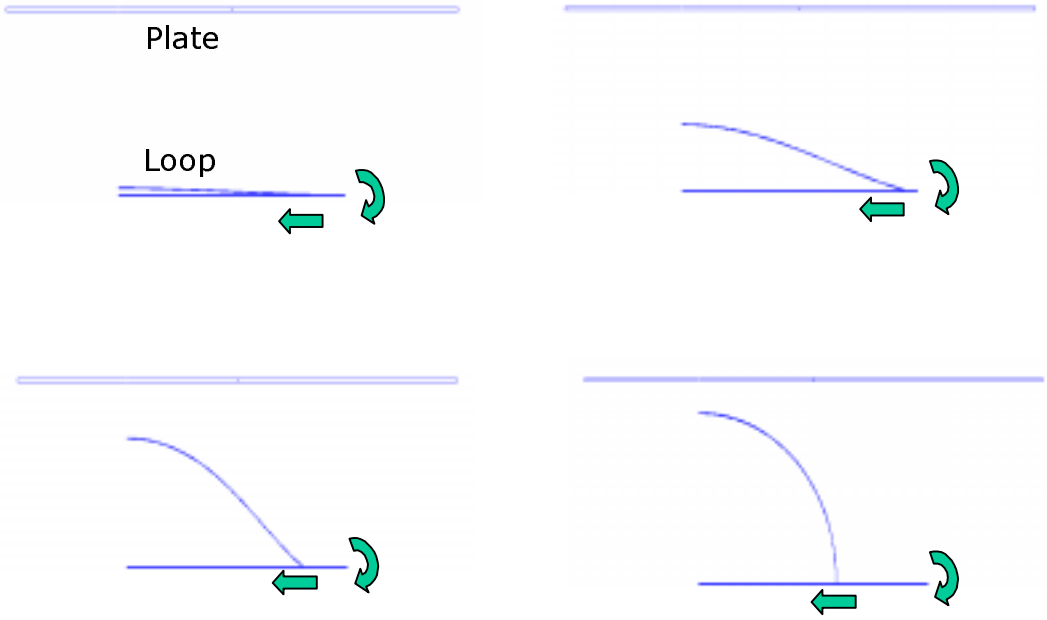

Figure 3.2 Simulating formation of the elastica loop.

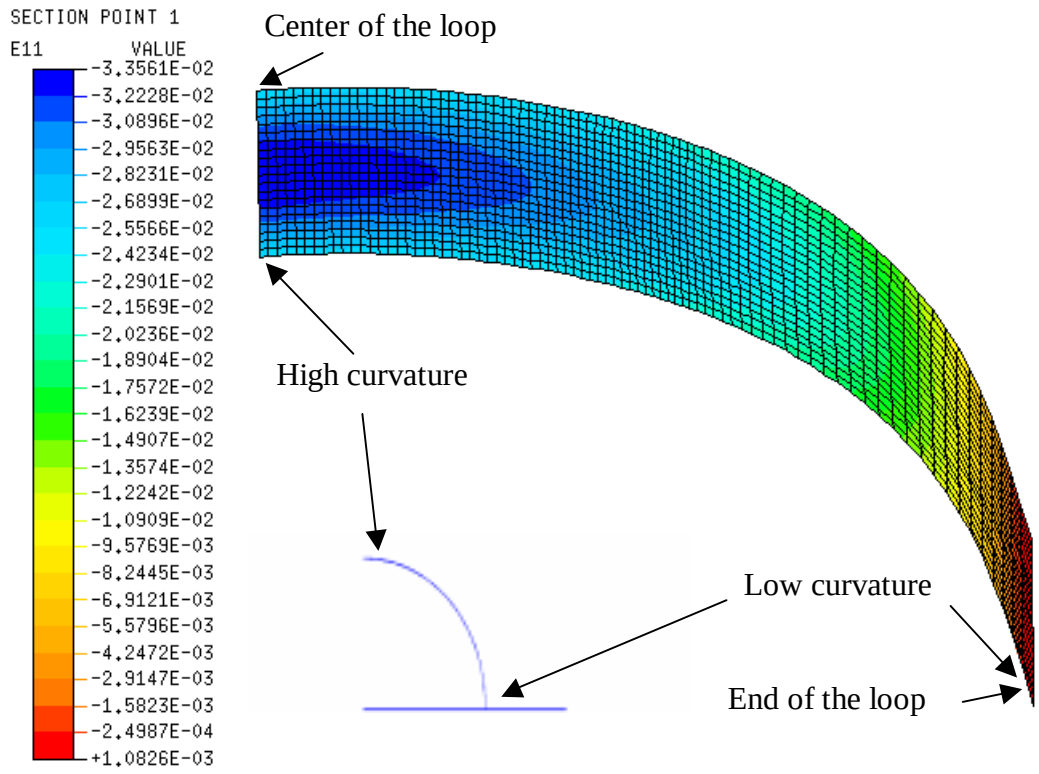

Figure 3.3 Longitudinal strains on the concave side of the loop before contact.

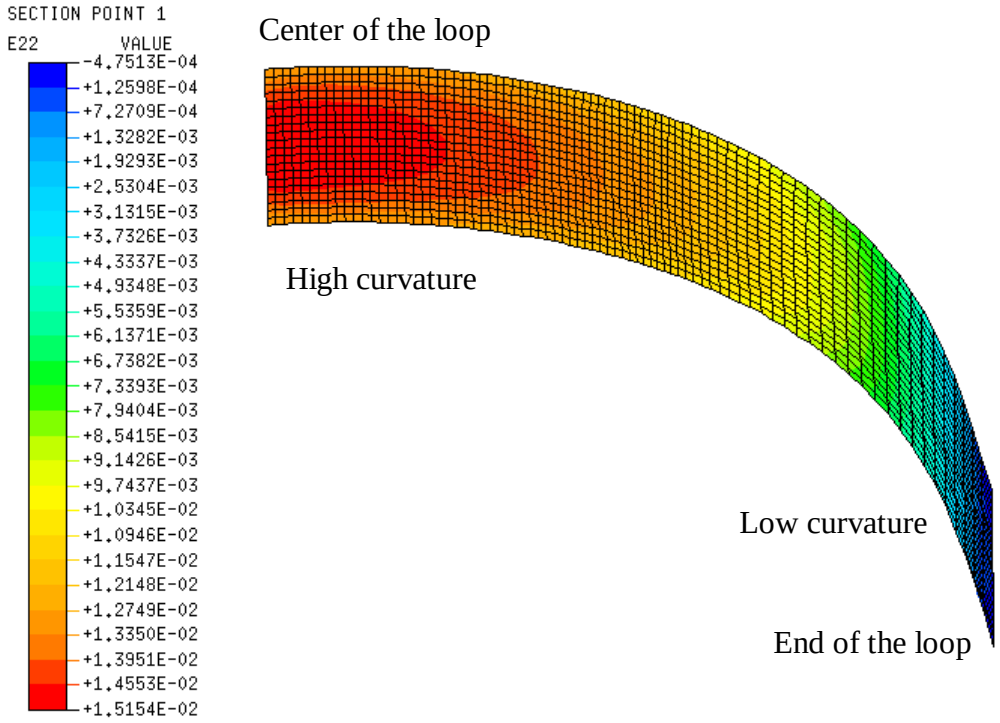

Figure 3.4 Transverse strains of the loop on the concave side before contact.

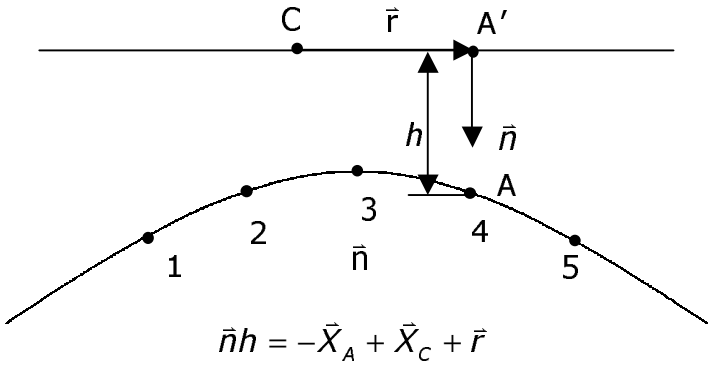

Figure 3.5 Contact schemes.

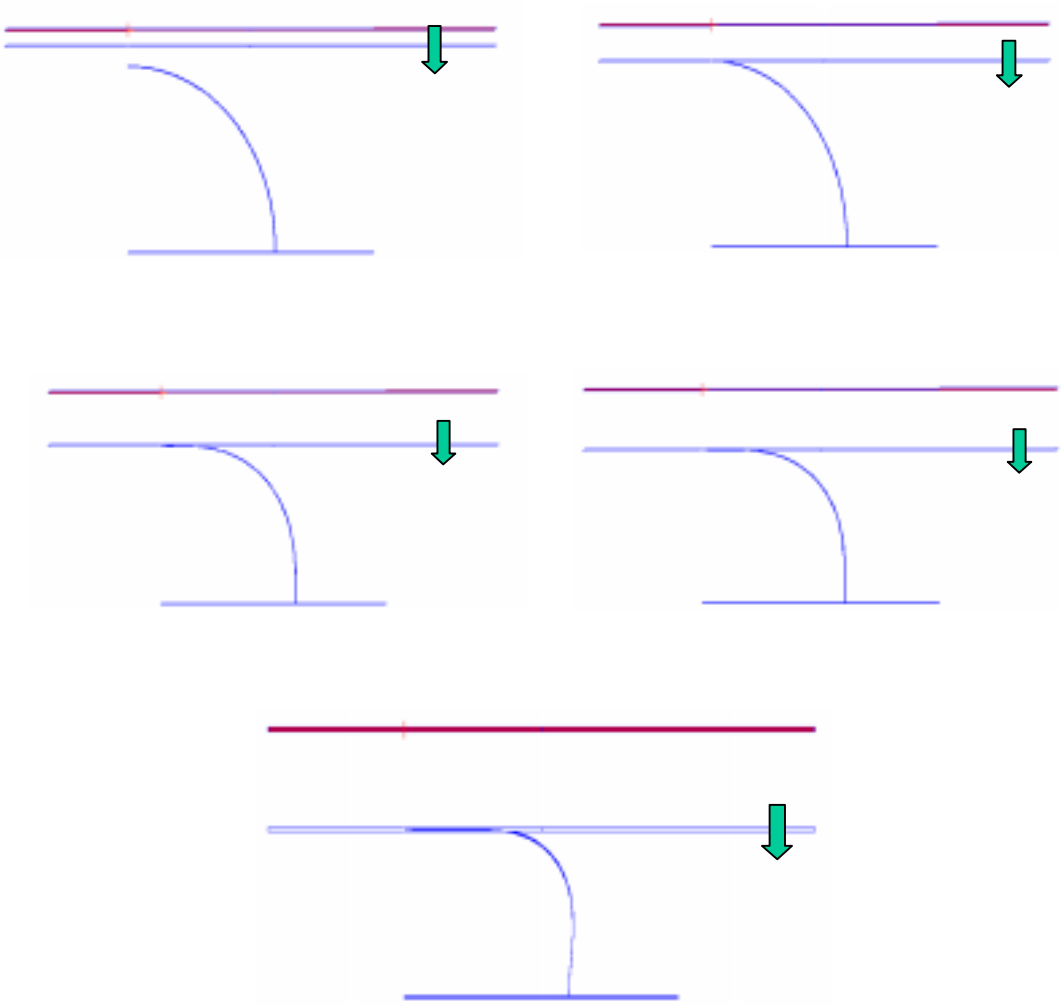

Figure 3.6 Contact actions simulated in FEA.

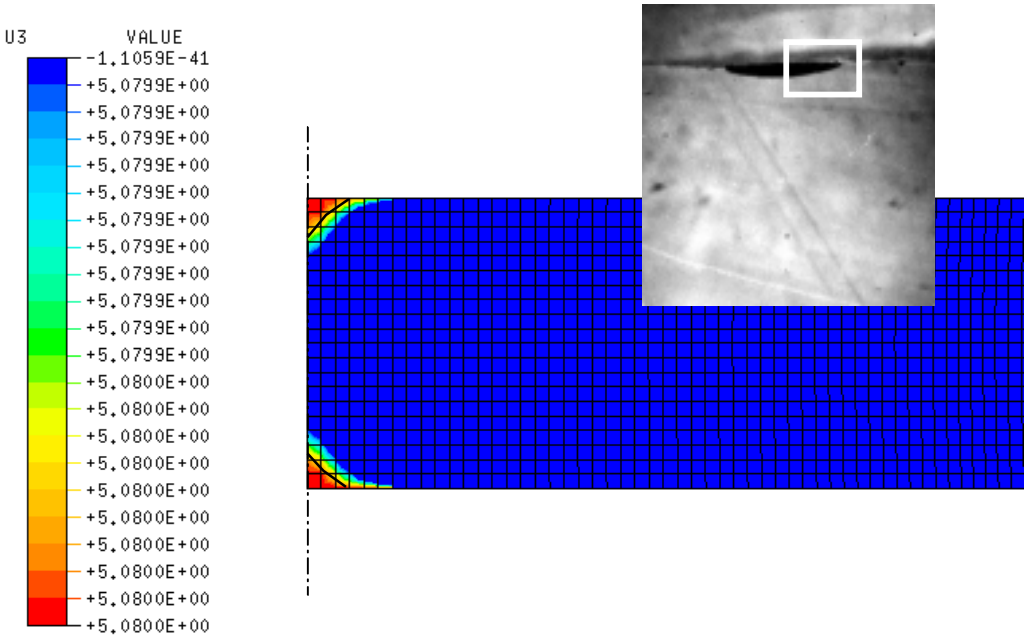

Figure 3.7 Contours of displacement of initial contact at edges with insert showing corresponding experimental results.

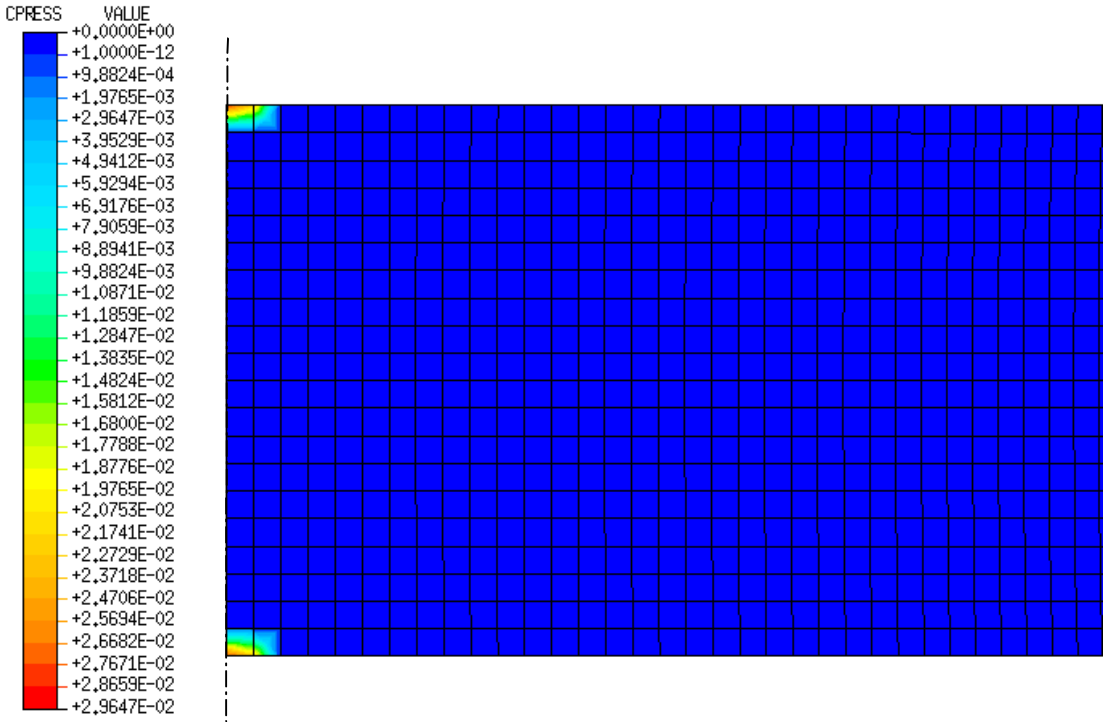

Figure 3.8 Compressive stress distribution on the upper loop suface of initial contact at edges.

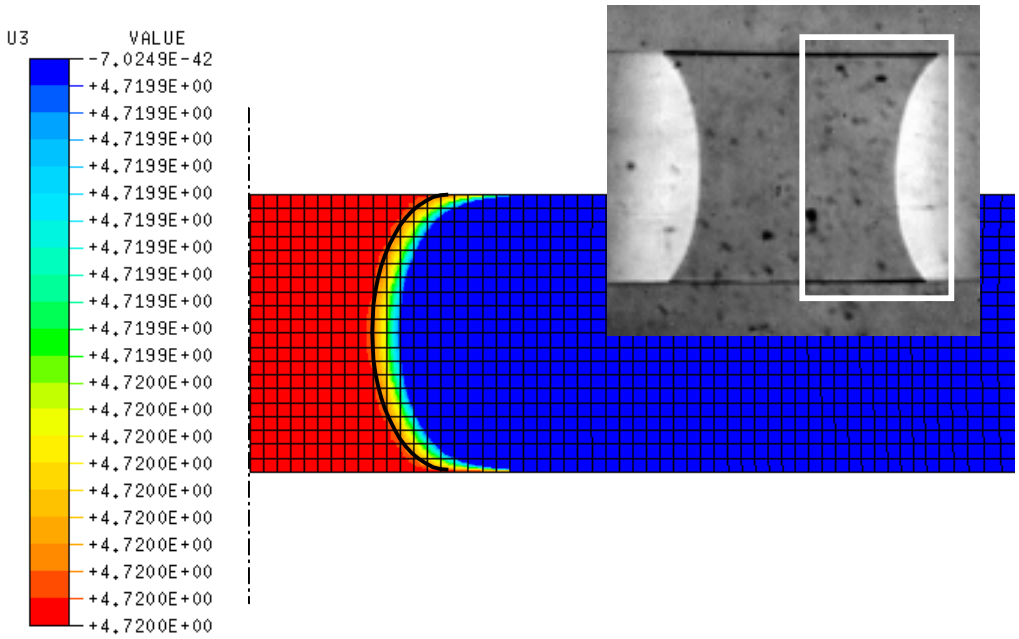

Figure 3.9 Contours of displacement after contact area spreading with insert showing corresponding experimental result.

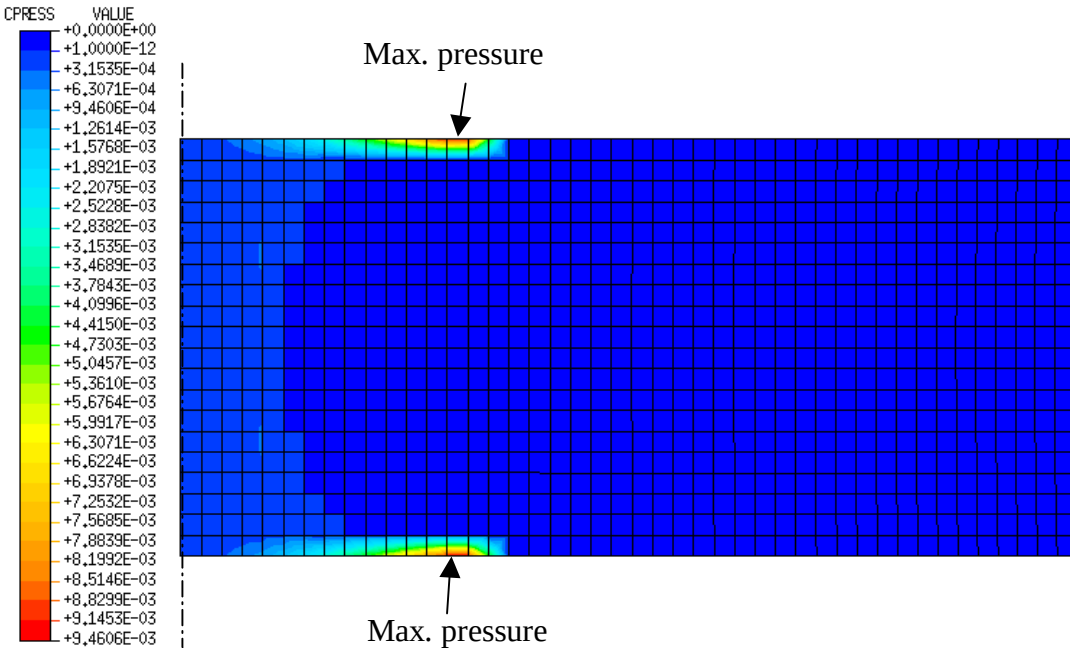

Figure 3.10 Contours of contact pressure on the upper loop surface after contact area spreading.

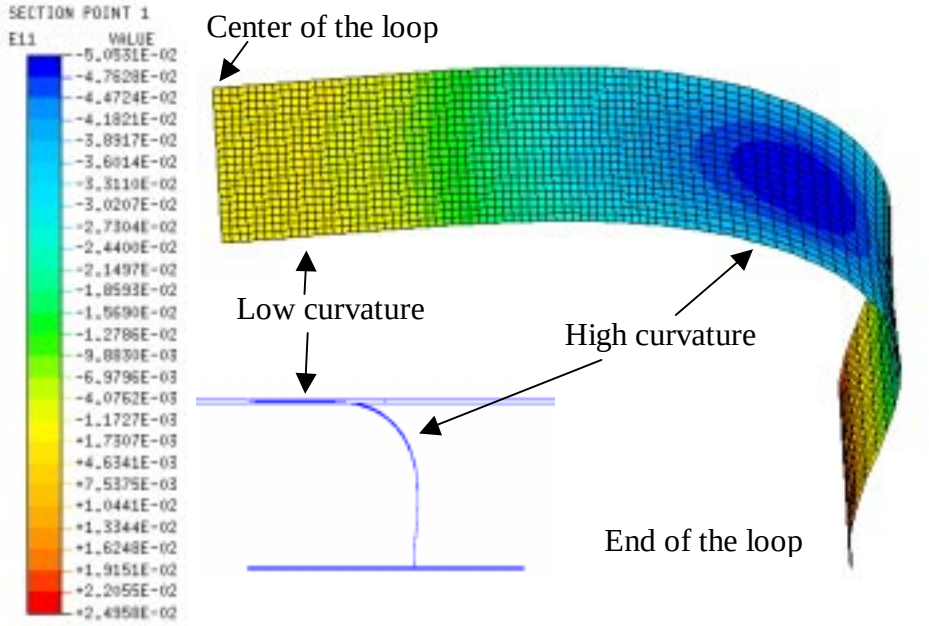

Figure 3.11 Longitudinal strain on the concave side of the loop after contact.

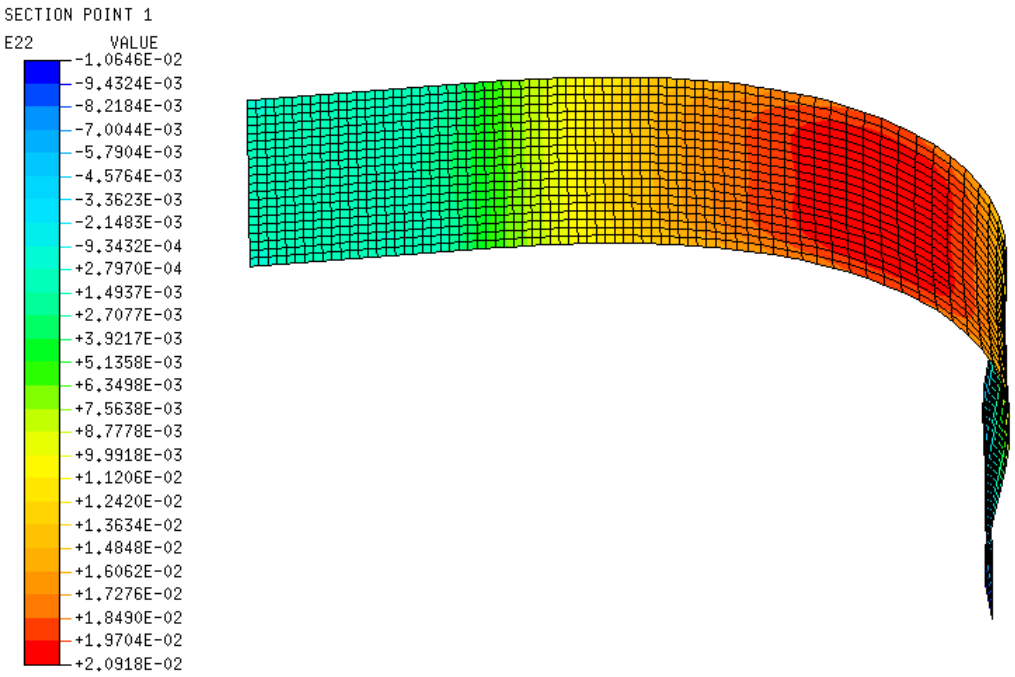

Figure 3.12 Transverse strain on the concave side of the loop after contact.

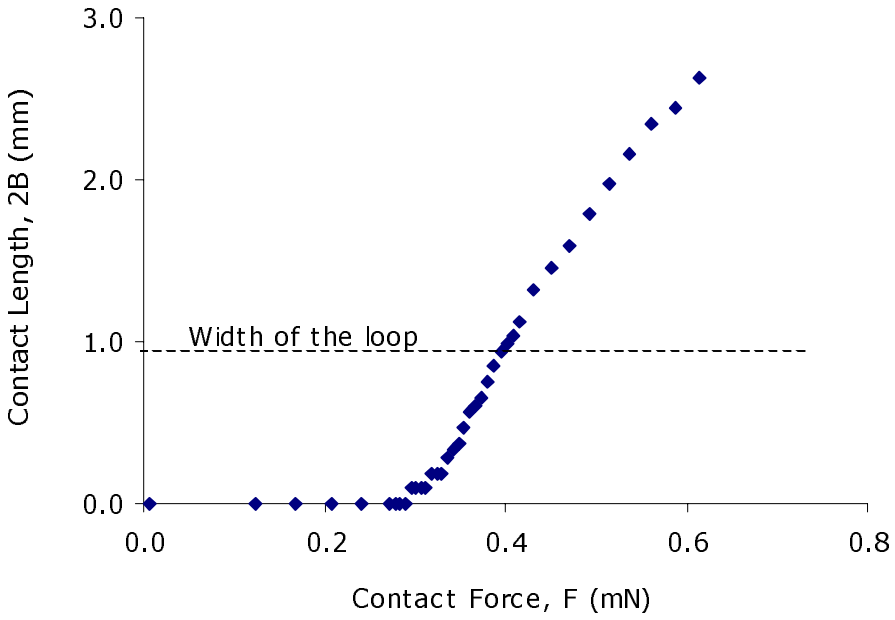

Figure 3.13 Plot of contact length vs. contact force: the contact lengths were measured at the center point of the contact front.

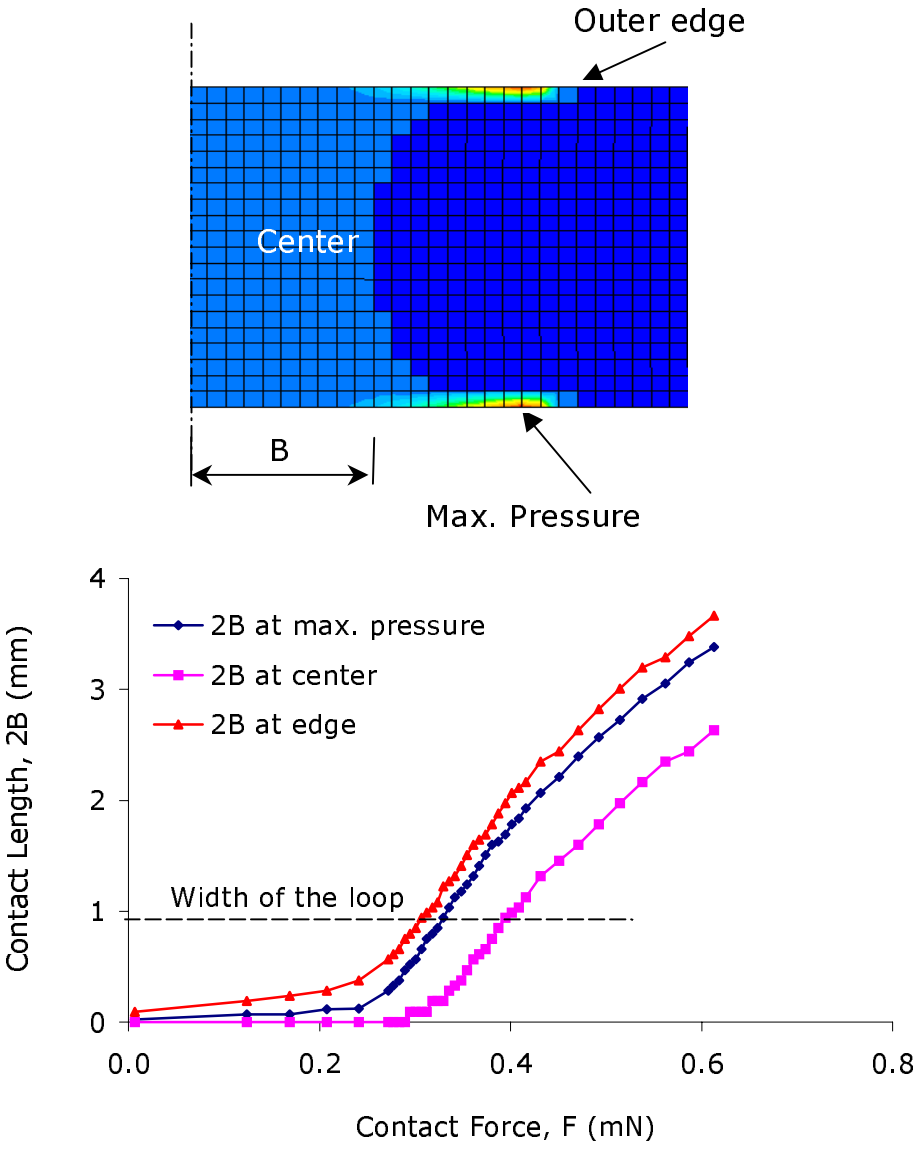

Figure 3.14 The effects of the measurement position on contact length: the dimensions of the elastica strip are 14.7 mm × 0.96 mm × 0.17 mm, E= 1.81 MPa, ν = 0.49, and 2C = 6.38 mm.

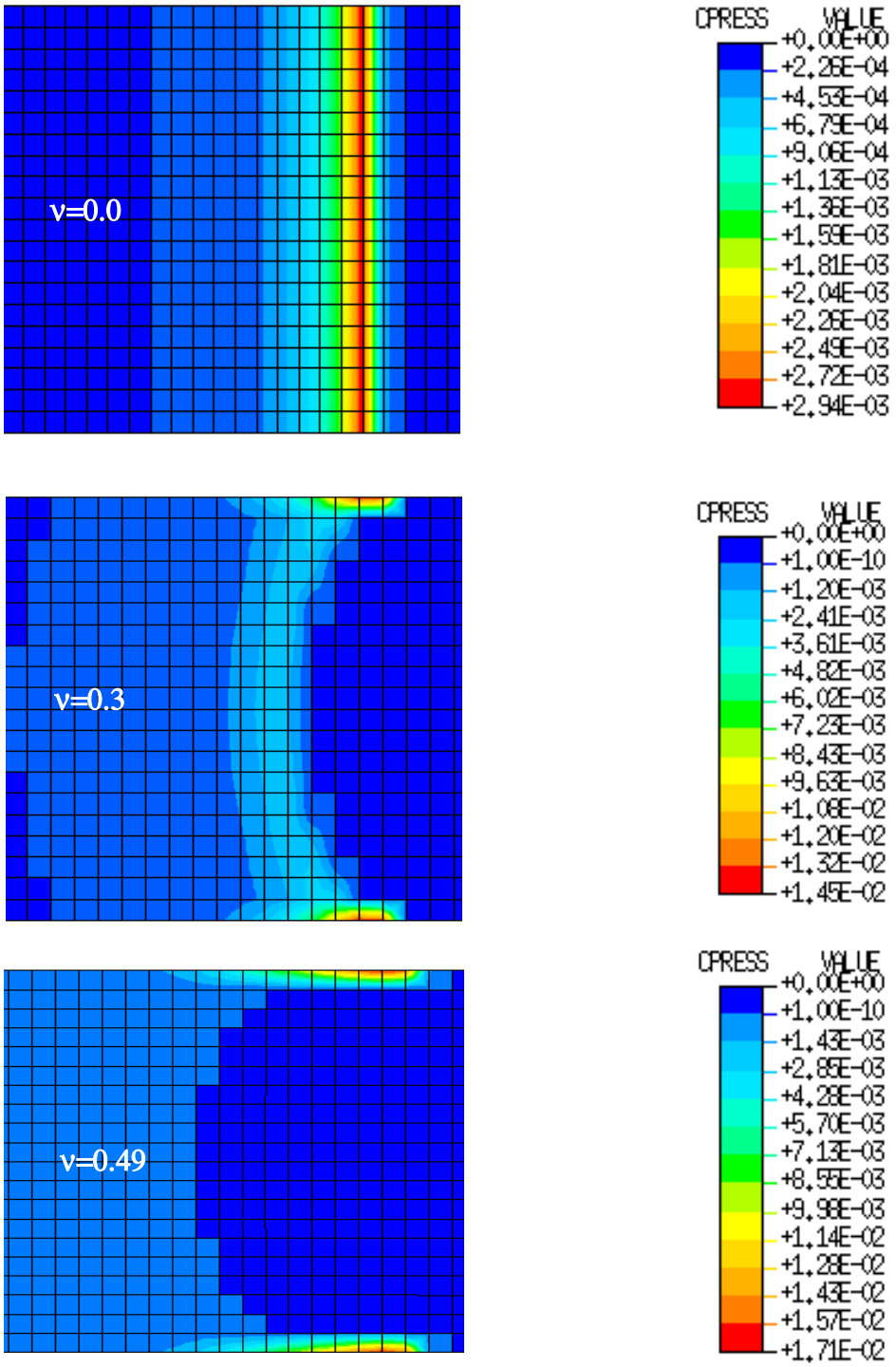

Figure 3.15 Effects of Poisson's ratio on the contact patterns with full width of the modeled elastica loop.

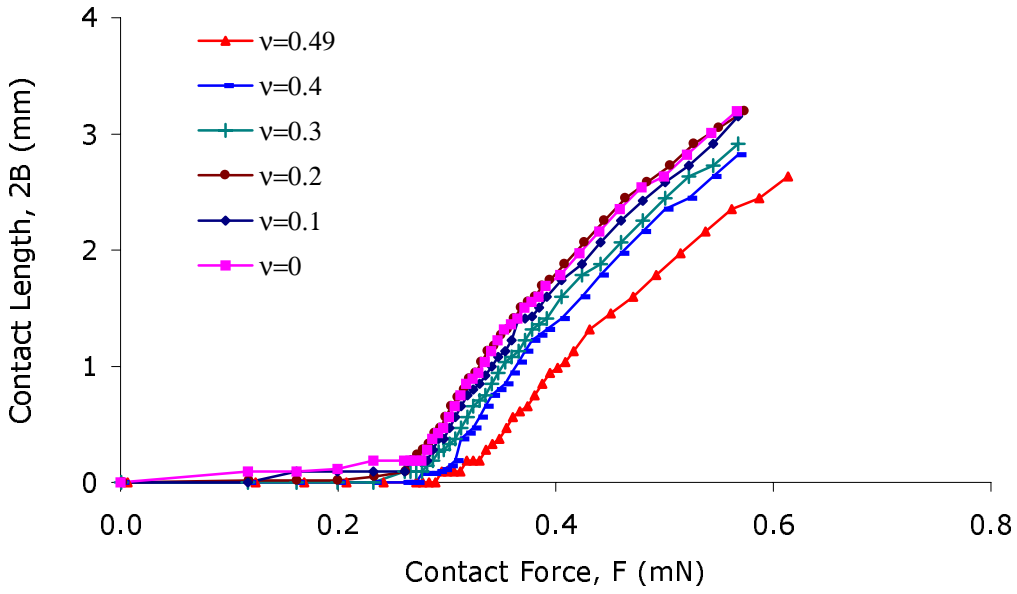

Figure 3.16 The relationship between contact length and contact force. The contact length was taken as the center of the contact front.

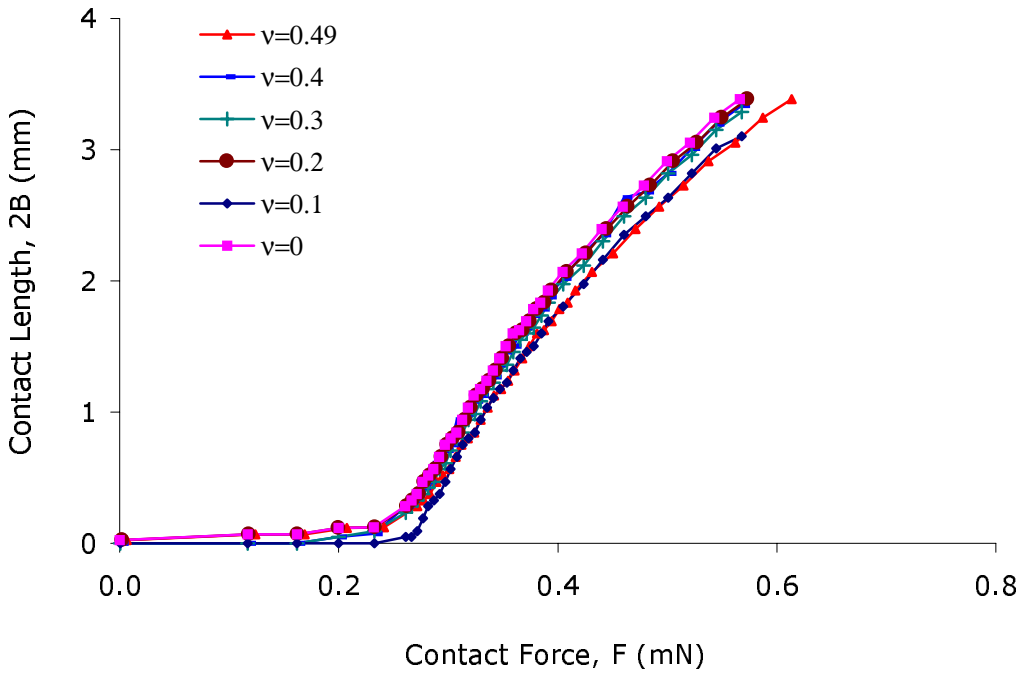

Figure 3.17 The relationship between contact length and the contact force. The contact length was taken as the point with maximum pressure.

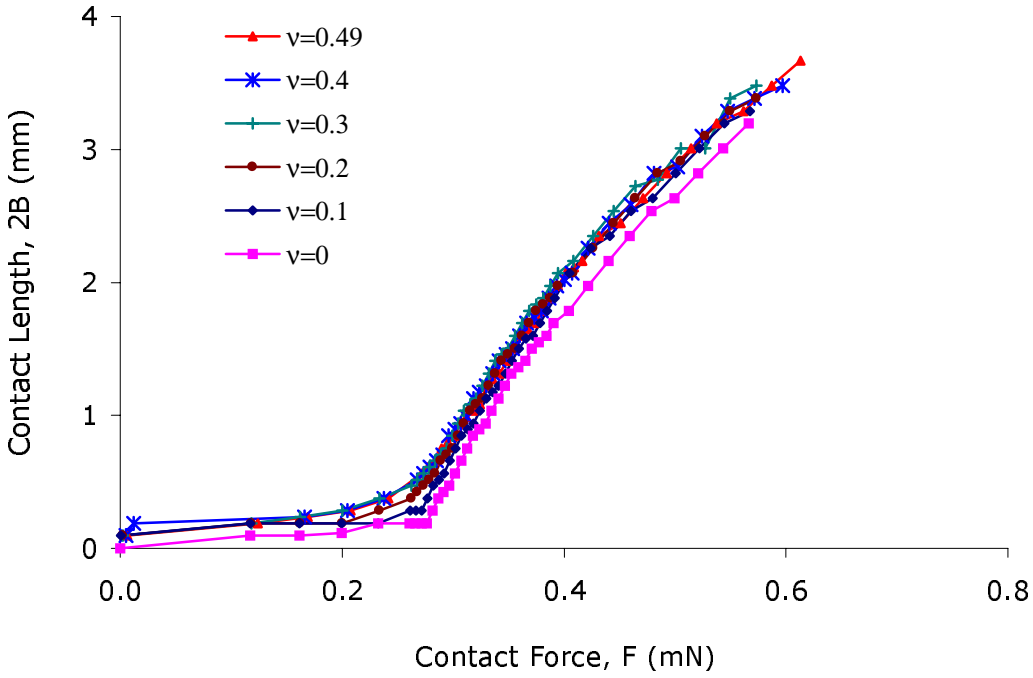

Figure 3.18 The relationship between contact length and contact force. The contact length was taken as the outer edge of the contact front.

CHAPTER 4 Comparison of Experimental, Numerical, and Analytical Results

4.1 Analytical solution

Analytical studies of an elastica loop in contact with a flat surface have been conducted by Dalrymple [46]. In her analysis, the elastica strip was assumed to be a thin, uniform, inextensible beam, which was very flexible in bending. To form the loop, both of the ends were lifted to an equal height, rotated, and clamped vertically at a specified distance apart. The loop was then moved downward and brought into contact with a flat, rigid, horizontal surface as shown in Figure 4.1. The friction between the strip and the flat surface was neglected, and attractive interfacial forces existed within the region of contact between the elastica and the rigid substrate. As the load applied on the loop continued to increase, the contact area increased and the strip flattened onto the substrate. Due to the interfacial energy between the two surfaces, the attractive forces acting in the region of contact caused additional loop deformation and extra contact area. By comparing the differences of the contact length before and after the interfacial energy was considered in the analysis, the adhesion effect can be determined.

The nondimensional length of the elastica was defined as $2l=2L/L=2$. Based on the length L and flexible rigidity, all other parameters in the analysis were nondimensionalized such as the work of adhesion, w_{adh}, contact length, b, contact forces, q, displacement, δ, and the separation distance between the clamped ends, 2c, as listed in Table 4.1, in which the value for W_{adh}, E, I, L, and C used were all taken directly from the experiments. According to Figure 4.2, where the definitions of all the variables are shown, the governing equations for an elastica in contact with a flat surface are given by

$$\frac{dx}{ds} = \cos\theta\,,\ \frac{dy}{ds} = \sin\theta\,,\ EI\frac{d\theta}{ds} = m\,,\ \text{and}\ \frac{dm}{ds} = -p\sin\theta + q\cos\theta$$

where s is the arc length, θ is the angle of the tangent of the curve with respect to the horizontal direction, p and q are the forces parallel to the x and y directions, respectively, m is the moment, and EI is the flexural rigidity of the elastica. The appropriate end conditions were then applied to solve for the desired parameters. For the no contact or single-point contact cases, x = y =0 at s = 0, and x = c, $\theta = \pi/2$ at s = 1. When a finite contact area existed, the boundary conditions were x = y = θ =0 at s = 0 and x = c-b, $\theta = \pi/2$ at s=1-b, with s=0 at the lift-off point.

A shooting method was used to solve the governing nonlinear equilibrium equations numerically in Mathematica. To use this method, initial values of p and m(0) at s=0 were guessed, then the elastica equations were numerically integrated until s = 1 for the no contact and single-point contact cases, and s=1-b for the finite contact cases. Once p and m(0) were determined to the desired precision, the shapes for the loop were otained using the equations for x and y. To consider the effect of the interfacial attraction, a moment, m_b, as shown in Figure 4.3 was allowed to assume a non-zero value at the point of the contact separation between the elastica and the substrate. The moment m_b was determined in the process of minimizing the total energy of the system with respect to the contact length b.

Due to the lack of the surface energy term in the governing equations for an elastica in contact with a flat surface, an energy minimization method was used to account for its presence and to obtain the equilibrium position. The nondimensionalized total energy of the system u_T consisted of the strain energy, u_E, mechanical potential energy, u_M, and adhesion energies, u_A, as $u_T = u_E + u_M + u_A$. To determine the equilibrium solution, the total energy u_T was calculated for a variety of equilibrium loop shapes obtained using the shooting method with constant end separation distance, c, and vertical force, q, but varying contact length, b. The equilibrium shape with a minimum

total energy was determined as the equilibrium solution. Once the equilibrium solution was obtained, the values m_b and b were also determined. Obviously, the total calculation process requires a series of iterations before a convergent solution can be obtained.

In addition, differences in the results caused by different loading cycles or different control methods were also modeled in the analyses. The vertical forces and displacements experienced by the elastica as the loop traveled through the no contact, point contact, and line contact regions were dependent upon whether the elastica was being pushed onto or pulled off of the substrate, or whether the vertical displacement or the vertical force was being controlled during the contact sequence. When the vertical displacement was controlled, the vertical force experienced a sudden jump in value. When the vertical force was controlled, the vertical displacement experienced a sudden jump in value. Similar findings are well known for JKR tests [22].

4.2 Comparison of numerical and analytical results

A comparison between the numerical results and the analytical results was made through examining the contact length versus contact force curves obtained numerically and analytically. To accomplish this, the geometry and material properties of the samples were first nondimensionalized according to Table 4.1. Then the nondimensionalized variables were input into the analytical solution program discussed earlier to calculate the contact length versus contact force curve. The curve was then converted back to quantities with units in order to compare with the numerical results. Since the effect of interfacial energy was not present in the finite element analysis, comparisons were made only between curves with no surface energy. Although the finite element model did not include the effect of adhesion forces, the analysis did take into account the anticlastic bending effect of the strip, a factor not included in the analytical solution.

Figure 4.4 shows the contact length versus contact force curves obtained both numerically and analytically. The dimensions of the loop used in the analyses were 14.7 mm in length, 0.96 mm in width, and 0.17 mm in thickness. The separation distance between the two ends was 6.38 mm, the modulus of the material was 1.81 MPa, and the Poisson's ratio was 0.49. Due to the curved contact front caused by the anticlastic bending of the strip, contact lengths were measured from the three different locations on the contact front, i.e., the outer edge point of the contact front, center point of the arched contact front, and the point with maximum contact pressure. Since beam theory was used in the analytical solution, the effect of anticlastic bending was not considered. The results show that the contact length predicted by the analytical solution is higher than the contact length measured at the center point of the contact front, but is slightly lower than the contact length measured at the point with maximum pressure. This difference in results is very well understood when anticlastic bending is considered. Overall, the analytical predictions agree with the numerical results. However, the analytical solution fails to predict the portion of the numerical curves corresponding to contact lengths less than half of the width of the loop. According to the numerical results, the contact length increases with contact force slowly as the contact starts until the contact length passes a certain value depending on the measuring position, where the contact starts to spread rapidly. According to the figure, the analytical solution did not predict this contact transition accurately.

Figure 4.5, Figure 4.6, and Figure 4.7 compare the analytical solution against numerical predictions with different Poisson's ratios and further demonstrate the effect of anticlastic bending. In these figures, the contact lengths obtained in the numerical analysis were taken from the three different locations discussed earlier, and each numerical curve corresponds to a different Poisson's ratio. If the contact length is measured either from the center of the contact front or from the outer edge of the contact front, Figure 4.6 and Figure 4.7 show that the analytical solution is relatively close to the numerical curves with relatively low Poisson's ratios. If the contact length is measured

from the point with maximum pressure, Figure 4.6 indicates that the analytical solution agrees relatively well with the numerical curve with Poisson's ratio of 0.49. These results can again be explained using the effect of anticlastic bending. In the analytical solution, the width effects of the loop were not modeled. As a result, the contact front in the analytical solution is a straight line, which is comparable to the case of $\nu = 0$ in the finite element analysis when the contact length is measured from either the center point of the contact front or from the outer edge. These results provide useful insights into the choice of the proper point for measuring the contact length in the experiments and also provide a possibility to estimate the error between the experiments and the analytical solution.

4.3 Comparison of experimental and analytical results

Similarly, a comparison between the experimental data and the analytical results was made by comparing the contact length versus contact force curves obtained experimentally and analytically. To accomplish this, the geometry and the material properties of the samples were first nondimensionalized according to Table 4.1. Then the nondimensionalized variables were input into the analytical solution program discussed earlier along with the interfacial energy measured in the JKR experiments to calculate the contact length versus contact force curve. After the analytical solution was obtained, the results were then converted back to quantities with units to compare with the experimental results.

For the case of the PDMS loop in contact with a PDMS substrate, the dimensions of the elastica loop were 14.7 mm in length, 0.96 mm in width, and 0.17 mm in thickness. The separation distance between the two ends was 6.38 mm, the modulus of the material was 1.81 MPa, and the Poisson's ratio was assumed to be 0.49. The work of adhesion measured between the two surfaces by the JKR technique was 43.6 mJ/m^2, which consequently leads to an interfacial energy value of 21.8 mJ/m^2. Figure 4.8 shows the analytical contact length versus contact force curve and the experimental data for

both the loading and unloading cycles. Due to the contact hysteresis discussed earlier, the unloading data are shifted to the left of the loading data.

Figure 4.8 shows that the analytical solution and the experimental data have very similar characteristics. Both results show that the contact length increases with the contact force once the contact spreading occurs. On the other hand, the figure shows that the portion of the experimental data corresponding to the contact lengths greater than half of the width of the loop agree closely with the analytical curve obtained by ignoring the surface energy. This result indicates that the effect of interfacial energy on the deformation of the loop becomes less significant as the contact area increases, which is possibly due to the decrease of the compliance of the loop when the contact length increases, and the interfacial attractive force is not large enough to produce measurable deformation. Moreover, the analytical solution fails to predict the portion of the experimental data corresponding to the contact lengths less than half of the width of the loop, which were obtained during the early stage of the contact procedure. Possible reasons for the inconsistency of the experimental data with the analytical solution are:

a) Transverse sliding at the interface might occur during the contact procedure as the load increased.

b) According to the analytical solution [45], when the loop is in contact with the substrate, the contact pressure in the contact region is zero. Since the surface attractive force only acts within a very small range near the surface and decreases rapidly with the distance from the surface (proportional to r^{-3} according to reference 3, where the r is the distance from the surface). Consequently, a small asperity on the surface of the loop or slight contamination on the substrate may decrease the degree of the intimate contact between the two surfaces in the center of the loop. However, this decrease in the degree of intimate contact may not be able to observe optically under the current macrolens system because the wavelengths used might be essentially larger than the distance between these two surfaces in the center of the loop. Although in the tests of this study, the PDMS

films were all carefully prepared and cured with little control of the surface smoothness, microscopic-scale asperity or blisters caused by a small amount of air trapped in the PDMS gel may still exist, which would certainly decrease the degree of intimate contact between the two surfaces.

c) The effect of the anticlastic bending was not fully understood.

Very similar results have been found for the cases of the PDMS loop in contact with a glass surface and the commercially available cellulose acetate substrate (3M ScotchTM Transparent Tape 600) as indicated in Figure 4.9 and Figure 4.10. In the test of the PDMS loop in contact with a glass surface, the dimension of this loop was 15.8 mm in length, 0.94 in width, and 0.17 mm in thickness. The separation distance between the two ends was 6.38 mm, the modulus of the material was 1.81 MPa, and the Poisson's ratio was estimated as 0.49. In the case of the PDMS loop in contact with the commercially available cellulose acetate substrate (3M Scotch^{TM} Transparent Tape 600), the dimensions of this loop were 15.8 mm in length, 0.84 in width, and 0.17 mm in thickness. The separation distance between the two ends was 6.38 mm, the modulus of the material was 1.81 MPa, and the Poisson's ratio was estimated as 0.49. Figure 2.9 and Figure 4.10 again show that the experimental data points corresponding to the contact lengths greater than half of the width of the loop fall near the analytical curve obtained by ignoring the presence of surface energy, and the analytical solution fails to predict the portion of the experimental curve corresponding to the contact lengths less than half of the width of the loop.

In summary, Figure 4.11 shows a comparison of the experimental, numerical, and analytical results for tests of the PDMS-PDMS system.

4.4 Sensitivity studies of errors

To investigate the effect of errors in measuring geometry and material properties on the predictions of the analytical solution, sensitivity studies were performed by

changing the sample geometry and material modulus in the analytical solution. The case of the PDMS loop in contact with PDMS substrate was chosen for this study. The actual dimensions of the elastica loop were 14.7 mm in length, 0.96 mm in width, and 0.17 mm in thickness. The actual separation distance between the two ends was 6.38 mm, the modulus of the material was 1.81 MPa, and the Poisson's ratio was 0.49. The work of adhesion measured between the two surfaces was 43.6 mJ/m^2, which consequently led to the interfacial energy value of 21.8 mJ/m^2.

Figure 4.12 shows the effect of reducing the length of the strip 2L by 5%, 10%, and 20% on the resultant contact length versus contact force curve. The figure shows that the analytical curve leaned toward the experimental results as the length of the strip decreased, and at the same time the overall curvature of the curve increased, which indicates that overestimating the length of the strip would cause the analytical solution to differ from the experimental results. On the other hand, underestimating the length of the strip would cause the analytical solution to be closer to the experimental results.

Similarly, the effect of changing the width of the loop W was studied and the results are shown in Figure 4.13. The effect of varying the thickness of the loop t is shown in Figure 4.14, and the effect of reducing the separation distance 2C between the two clamped ends is shown in Figure 4.15. All the figures indicate that increasing W or t and reducing C would make the analytical solution closer to the experimental data, which can help us identify possible sources of measurement errors.

Young's modulus was also considered as a possible source of errors. Therefore, the effect of changing the modulus of the loop was studied by increasing the modulus by 10%, 20%, and 30% in the analysis, and the results are shown in Figure 4.16. The figure shows that the analytical contact length versus contact force curve has a trend moving closer to the experimental data as the modulus increases. On the other hand, reducing the

modulus of the loop will cause the analytical solution to differ more from the experimental data.

4.5 PDMS loop in contact with various substrates

Because all the experimental results are close to the analytical solution with γ=0, experiments of PDMS loop in contact with four different substrates were performed to study the sensitivity of this technology with respect to various interfacial interactions. The four substrates were a glass plate treated with chemical Au etch, a glass plate deposited with a layer of Cu, acetone cleaned glass plate, and a glass plate with a 30 min treatment of vinylsilane. Following the testing procedure discussed in Chapter 2, the relationships of the contact length 2B versus contact force F were obtained for these four substrates as shown in Figure 4.17. The figure indicates that the differences between the loading curves for the four interfaces are relatively small. However, the unloading curves and the hysteresis loop for these four interfaces significantly differ from each other, which is possible due to the different interfacial interactions.

A possible explanation for the small differences between the loading curves is that intimate contact especially in the center of the loop as the contact increased was not achieved between the surfaces in contact, and experimental data differed from the analytical solution with $\gamma > 0$ significantly but agree with the analytical solution with $\gamma = 0$ more. As discussed earlier, according to the analytical solution [45], when the loop is in contact with the substrate, the contact pressure in the contact region is zero. Since the surface attractive force only acts within a very small range near the surface and decreases rapidly with the distance from the surface (proportional to r^{-3} according to reference 3, where the r is the distance from the surface). Consequently, a small asperity on the surface of the loop or slight contamination on the substrate may decrease the degree of the intimate contact between these two surfaces in the center of the loop. However, this decrease in the degree of intimate contact may not be able to observe optically under the current microscope system because the wavelengths used might be essentially larger than

the distance between these two surfaces in the center of the loop. Although in the tests of this study, the PDMS films were all carefully prepared and cured with little control of the surface smoothness, microscopic-scale asperity or blisters caused by a small amount of air trapped in the PDMS gel may still exist, which would certainly decrease the degree of intimate contact between the two surfaces.

The testing apparatus may also have possible sources of errors. In the analytical solution, the vertically symmetric line of the loop passing through the center of the loop and the middle point of the end separation distance were assumed to be perfectly perpendicular to the substrate. However, this perfect alignment was very difficult to accomplish during the tests, which may cause slight changes in the readings of the contact lengths. Additionally, in the analytical solution, the substrate was considered as a flat, rigid, and smooth surface. But in the experiments, the coatings with certain thickness were not perfectly rigid, which, although the effect was estimated to be small in this study, may still cause some errors for the tests. Knowing these possible sources of error will help us improve the accuracy of the analytical solution and the experimental measurements.

Table 4.1 Nondimensionalization process

Nondimensional Quantity	Definition
Arc length, s	S/L
Horizontal coordinate, x	X/L
Vertical coordinate, y	Y/L
Height of the loop, h	H/L
Contact length, b	B/L
Distance between the ends, c	C/L
Displacement, δ	Δ/L
Horizontal force, p	$FL^2/(EI)$
Contact force, q	$QL^2/(EI)$
Moment at clamped end, m_o	M_o L/(EI)
Moment at beginning of contact, m_b	M_b L/(EI)
Work of adhesion, w_{adh}	W_{adh} $L^2/(EI)$
Energy, $u_{(E, M, A, or T)}$	$U_{(E,M,A, or T)}$ L/(EI)

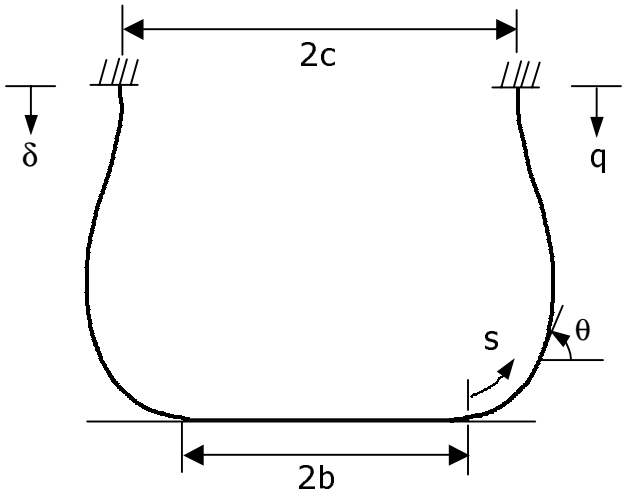

Figure 4.1 An elastica loop in contact with a flat, rigid, smooth, horizontal surface. After reference 46.

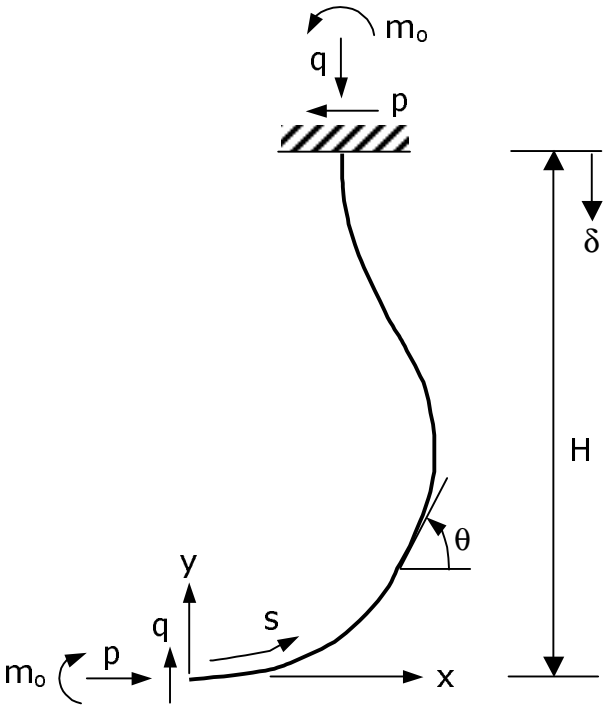

Figure 4.2 Definitions of variables. After reference 46.

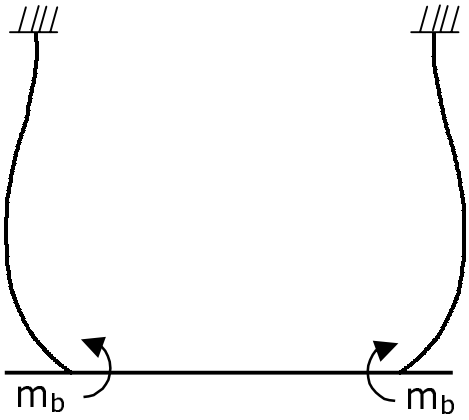

Figure 4.3 Model adhesion effects. After reference 46.

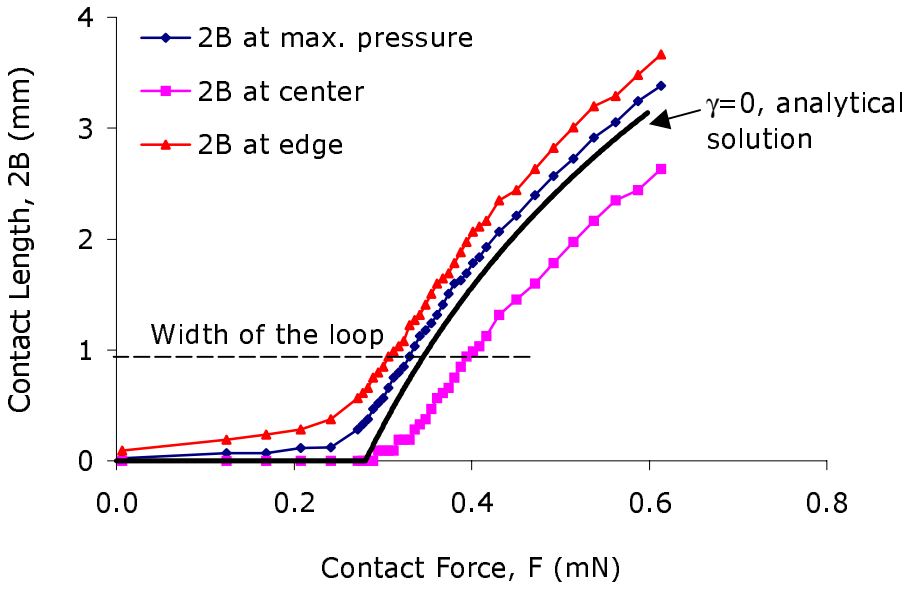

Figure 4.4 Comparison of numerical and analytical results: contact lengths were measured at different positions.

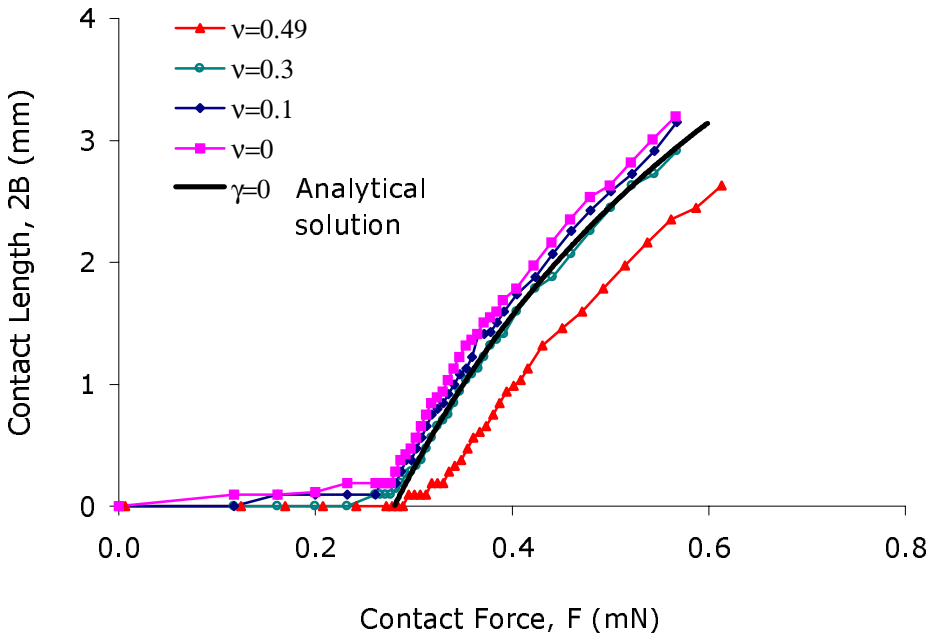

Figure 4.5 Comparison of numerical and analytical results: contact lengths were measured in the cases with different value of Poisson's ratio at the center of contact front.

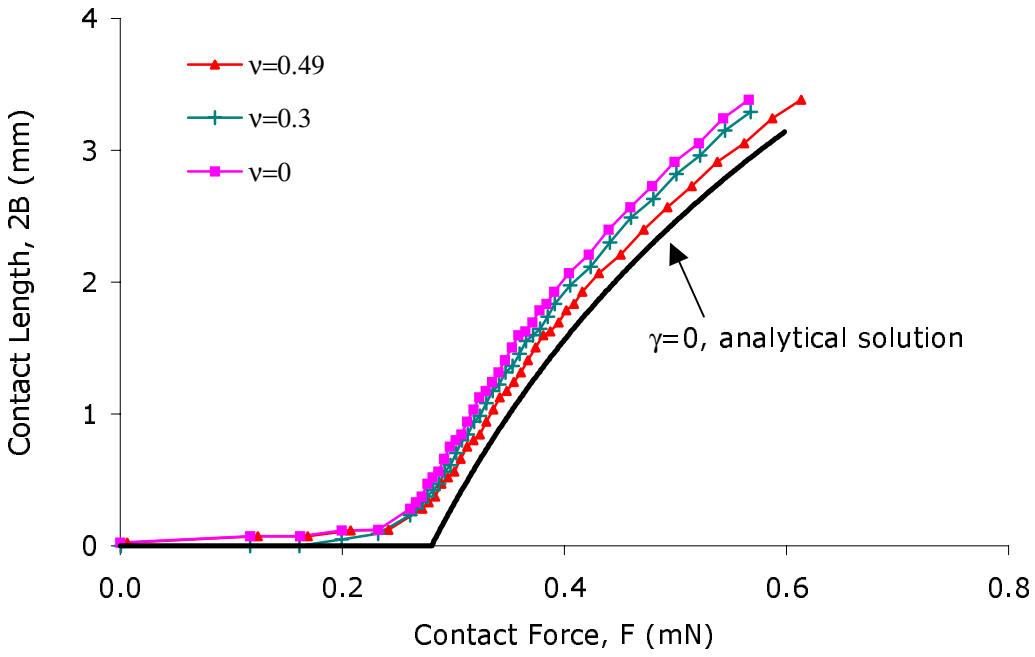

Figure 4.6 Comparison of numerical and analytical results: contact lengths were measured in the cases with different values of Poisson's ratio at the points of maximum pressure.

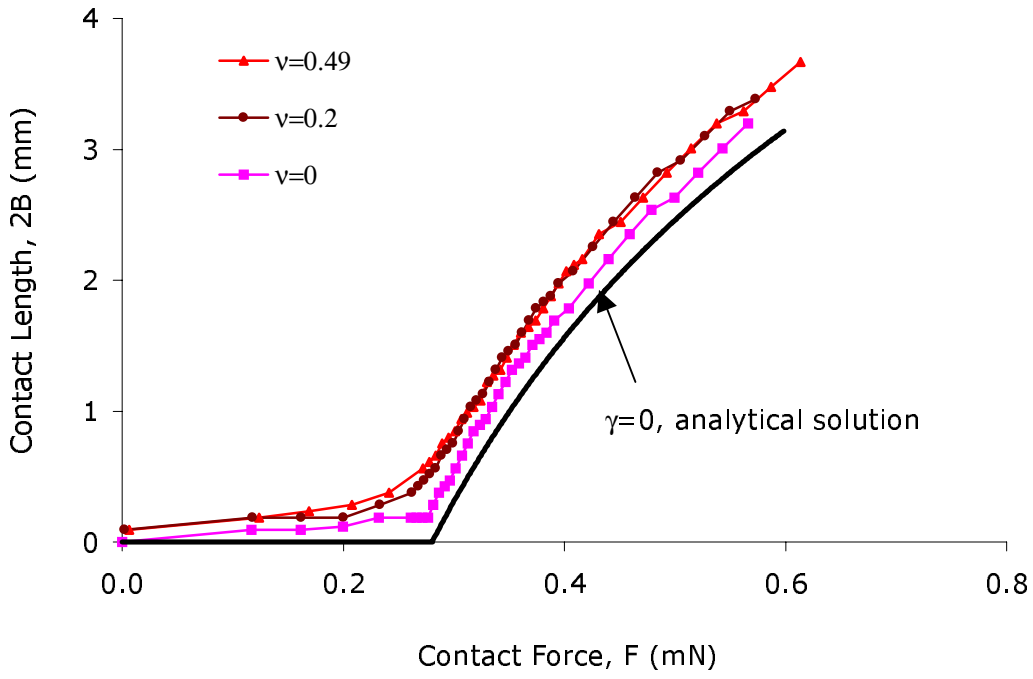

Figure 4.7 Comparison of numerical and analytical results: contact lengths were measured in the cases with different values of Poisson's ratio at the outer edge of contact front.

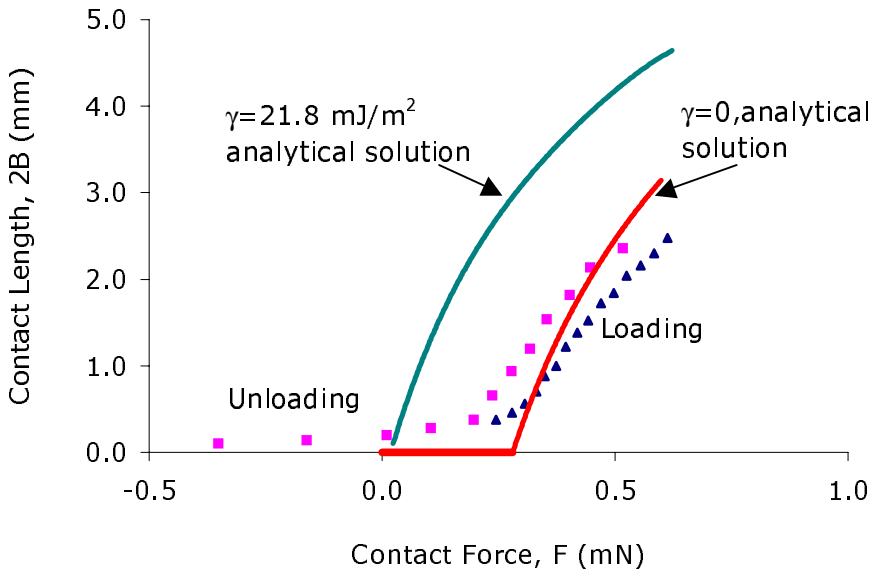

Figure 4.8 Comparison of the experimental and analytical results: PDMS loop in contact with PDMS film coated on glass plate.

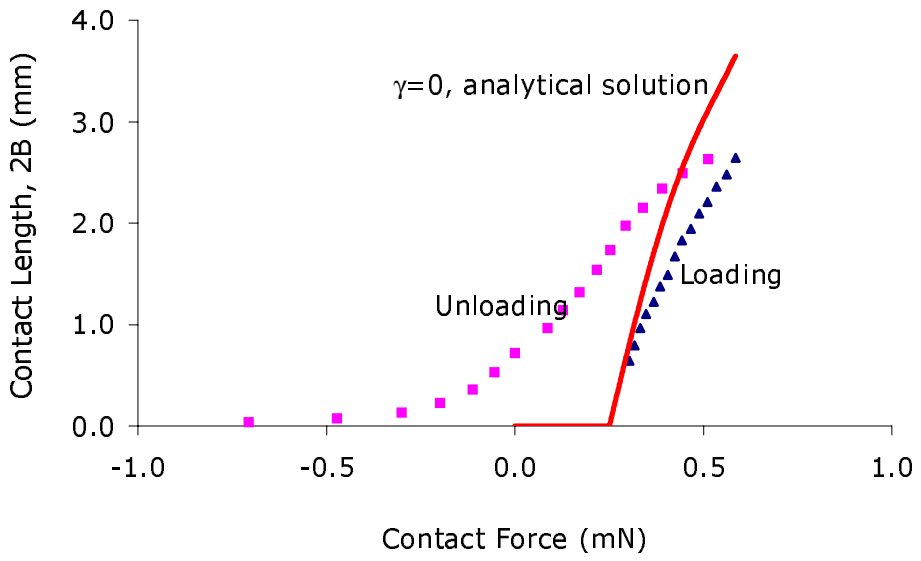

Figure 4.9 Comparison of the experimental and analytical results: PDMS loop in contact with a glass plate.

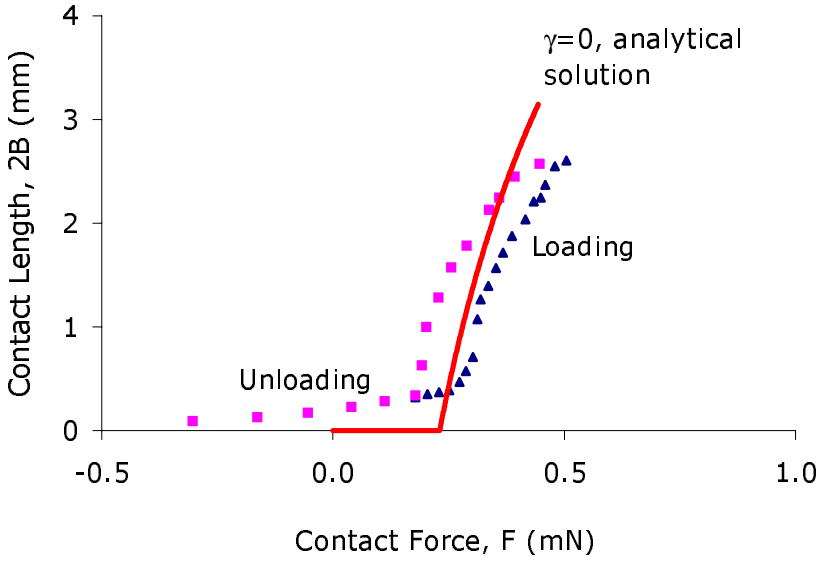

Figure 4.10 Comparison of the experimental and analytical results: the PDMS loop in contact with cellulose acetate substrate (3M Scotch™ Transparent Tape 600).

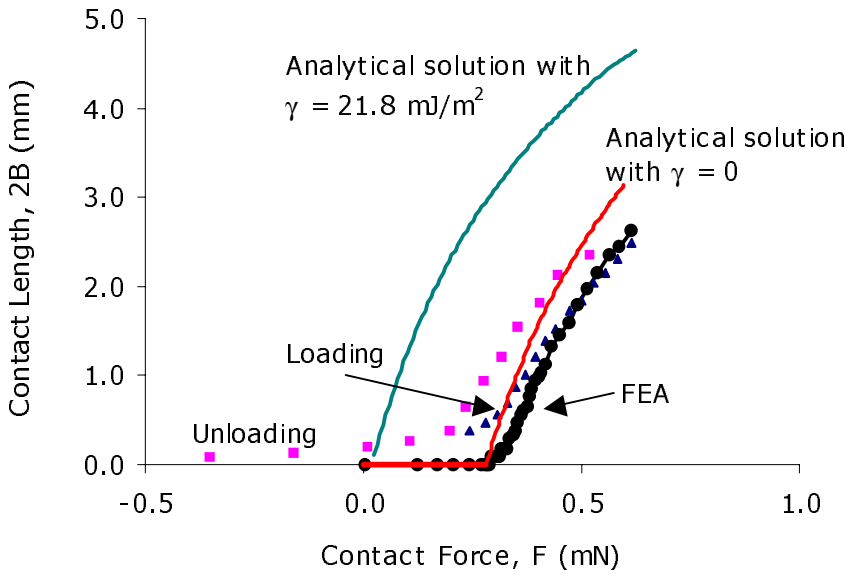

Figure 4.11 Comparison of analytical, experimental and numerical results: PDMS loop in contact with PDMS film coated on a glass plate, and the contact lengths were taken from the center of contact front.

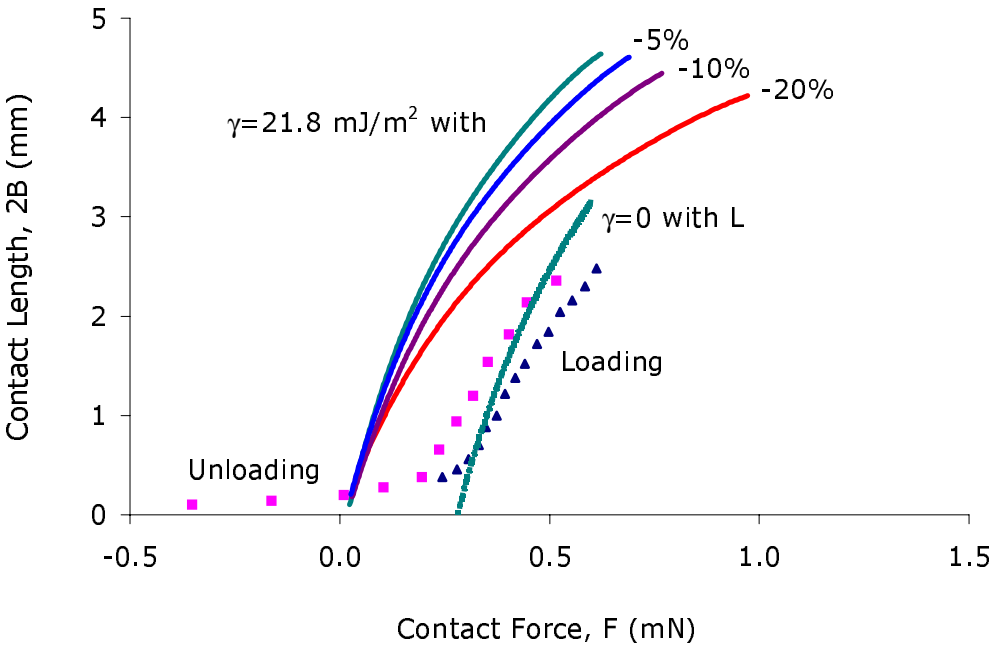

Figure 4.12 Effects of reducing length by 5%, 10%, 20%.

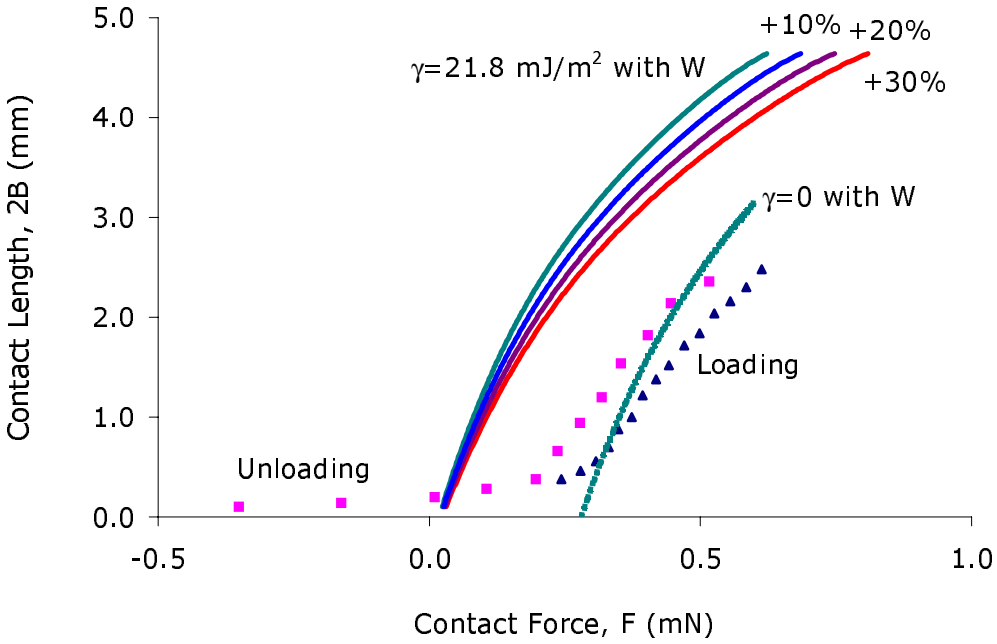

Figure 4.13 Effects of increasing width by 10%, 20%, and 30%.

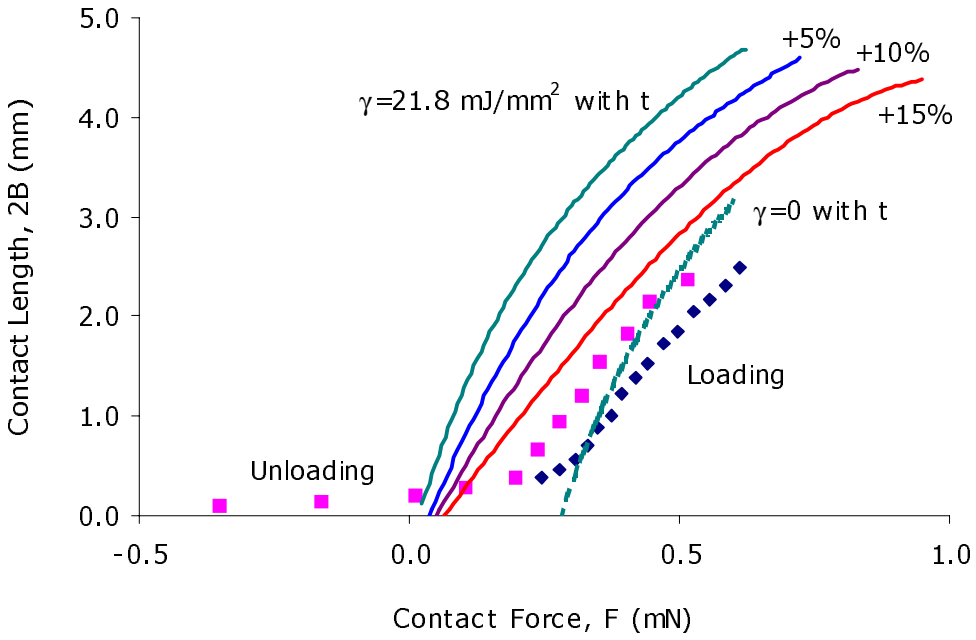

Figure 4.14 Effects of increasing thickness by 5%, 10%, and 15%.

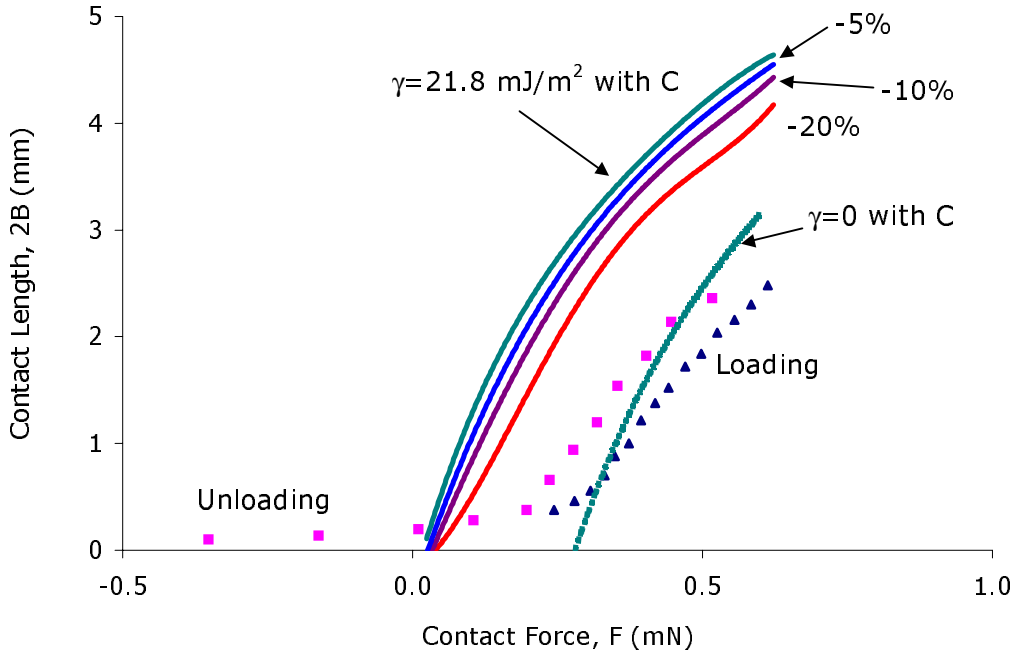

Figure 4.15 Effects of reducing the separation distance between the ends by 5%, 10%, and 20%.

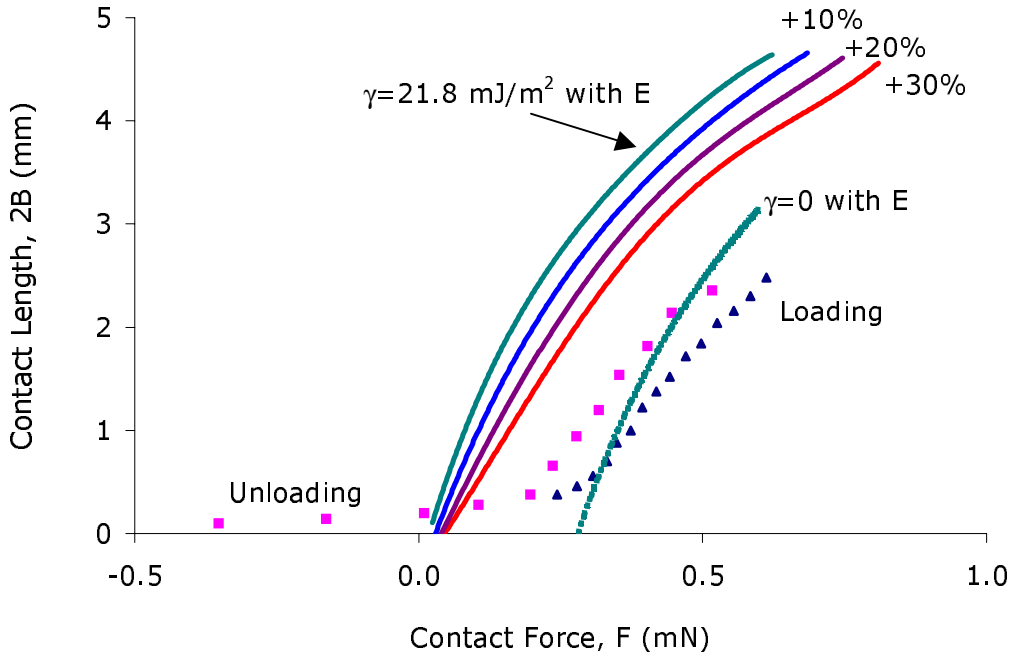

Figure 4.16 Effects of increasing Young's modulus by 10%, 20%, and 30%.

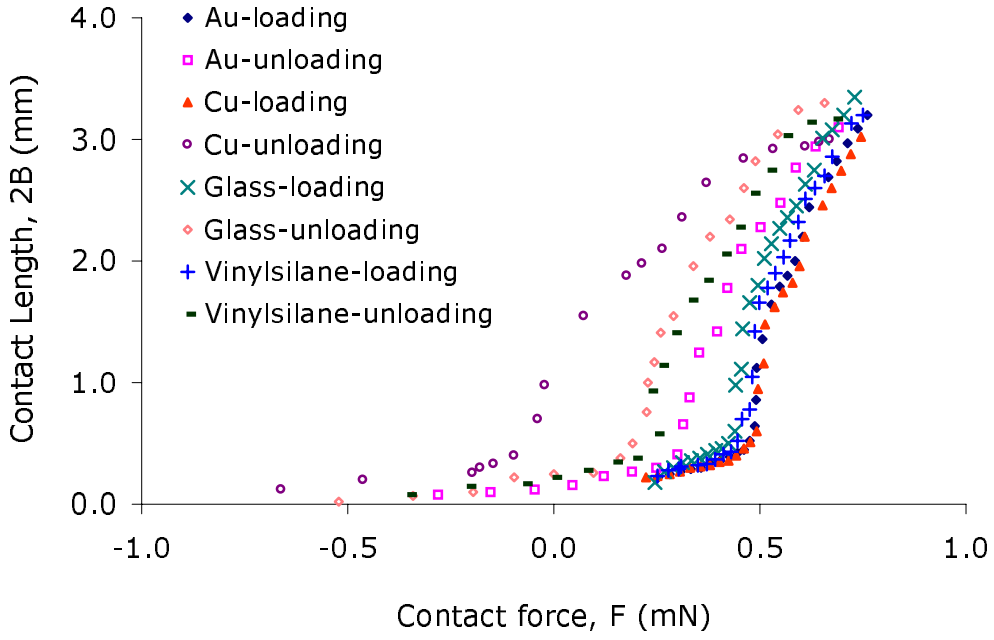

Figure 4.17 Plots of contact length, 2B vs. contact force, F: PDMS loop in contact with four different substrates.

CHAPTER 5 Conclusions and Recommendations for Future Work

5.1 Summary and conclusions

In this thesis, a novel technique has been developed to measure the surface and interfacial energies between solids using an elastica loop. The apparatus consists of a precise displacement control device, an accurate force measurement device, an optical system, and a computer control interface that has been built in order to perform the measurement in a well-controlled manner. Experiments of a PDMS elastica loop in contact with four different substrates have been conducted along with the conventional JKR tests. Through the investigations of the experimental procedure, experimental data, and comparisons between the experimental, numerical, and analytical results, the following conclusions are made:

1. Overall, the current apparatus is a successful design, upon which both the conventional JKR measurement and the elastica loop test can be conducted. For the PDMS-PDMS system tested, the JKR test results obtained using the apparatus were consistent with those reported in the literature.
2. For transparent materials, the contact patterns for both the JKR and elastica loop tests can be observed using the current optical system with about 50x magnification factor. Due to the compliant structure design, the contact length observed in the elastica loop test was in general larger than the contact diameter observed in the JKR test. However, due to anticlastic bending, the contact front observed in the elastica loop test was curved. Based on a variety of experimental observations and finite element analyses, the shape of the contact front remained relatively constant during the entire contact process.

3. The displacement control system provided very precise contact process control. Because of the precise displacement control, the events such as the initiation, spread, and separation of the contact were well controlled and the finite contact area at the moment of contact initiation and separation were clearly observed and were accurately measured.
4. With the force measurement device and the computer control interface, the contact force can be measured simultaneously with the displacement at a specified rate of data acquisition. As compared to the conventional JKR test, the contact force measured in the elastica loop test was in general smaller.
5. Through testing a PDMS elastica loop in contact with various substrates, the relationships between the contact lengths versus contact forces were obtained for each system. The results indicated that the contact length increased slowly with the contact force as the contact started until the contact length exceeded about half of the width of the loop, when the contact started to spread rapidly. The finite element analyses indicated that this contact rate transition was due to the combined effects of longitudinal main bending and anticlastic bending. The difference between the experimental data and FEA results should be the effect of the interfacial energies.
6. Large hysteresis has been observed in the contact length versus contact force curves for all the material systems tested. The hysteresis was primarily caused by interfacial interactions in the contact region and appeared to be rate dependent.
7. The FEA numerical analyses successfully simulated the contact procedure. Through the analyses, the relationship between the contact length and the contact force for the case with no interfacial energy was obtained, which was used to verify the analytical solution. The numerical analyses also helped to investigate the strain and stress states of the elastica loop, the contact pressure distribution, and the effect of the anticlastic bending.
8. The FEA numerical analyses successfully demonstrated the effect of anticlastic bending. Due to the effect of anticlastic bending, the contact front between the

loop and the flat surface was curved, and the curvature was larger than that of the contact front observed in the experiments, indicating the effect of the interfacial interaction. The results also showed that the anticlastic bending effect decreased as the Poisson's ratio decreased and vanished when the Poisson's ratio was zero.

9. Overall the analytical solution agreed with the numerical analyses results corresponding to $\nu = 0$ after the contact rate transition had occurred. However, since the anticlastic bending was not considered in the analytical solution, differences did exist, especially when the contact length is measured from the center of the contact front. In addition, for the same reason, the analytical solution did not predict the contact rate transition and the contact initiation.
10. The agreement between the analytical solution and the experimental data was relatively poor. Possible reasons for this poor agreement were discussed in the sensitivity studies through identifying possible sources of errors in the tests. These possible sources of errors include the measurement errors of the geometry and modulus of the loop and testing misalignment. In addition, transverse sliding at the interface might occur during the contact procedure as the load increased; intimate contact in the center of the loop might not achieved; and the effect of the anticlastic bending might not fully understood.

5.2 Limitations

Despite the poor agreement with the analytical solution, this elastica loop test still remains a novel technique with potential for measuring interfacial energies between solids. However, there are still limitations with the current apparatus and technique.

First of all, this technique requires very careful sample preparation. The elastica strips need to be very thin to achieve desirable loop compliance, which, especially for materials with high modulus, sometimes may be very difficult. In order to use this technique, the surfaces of the loop and the substrate need to be very smooth because the

interfacial attraction only acts within a very small range, and surface asperities will significantly decrease the effect of surface energy on the deformation of the elastica loop.

The settings of the optical system in the current apparatus can only work with transparent substrate in order to observe the contact area from the top of the interface. To work with non-transparent material as the substrate, a new optical system which would allow observation of the contact from the side of the interface would be necessary to overcome the limitation.

In all the tests conducted in this study, low modulus PDMS loops were used. However, this technique possibly can be used to measure the interfacial energies between materials with high modulus. If one of the materials of interest is transparent, this material has to be used as the substrate with the current setup. On the other hand, if none of the materials of interest is transparent, then the new optical systems mentioned earlier are needed. However, for the loops made of high modulus materials, the thickness of the loop needs to be very thin to achieve a desirable structural compliance. Some trial experiments also showed that contact buckling occurred easily in testing a loop with high modulus, which greatly increases the difficulty of the test. In addition, intimate contact between the loop and the substrate may also be very difficult to achieve. Consequently, the test should also be focused on achieving contact initiation and spread curves in order to obtain information on interfacial interactions.

5.3 Future work

For the future work, the most important experimental issue needs to be addressed is to detect the intimate contact level because the interfacial interactions are not able to detect if intimate contact is not achieved between the surfaces in contact. To this end, experimental devices can be further improved. For example, special filters can be added to the light source of the microscope system to achieve a light with single short wave length, which can help us to detect the contact level more clearly. The measuring device

for contact length can also be redesigned so that measurements can be taken either from the top or from the side of the interface. More experiments involving stiffer materials can be investigated. To perform the tests, substrates narrower than the elastica loop can possibly be used and contact can be controlled to only occur in the center of the width of the loop since the effect of anticlastic bending has been thoroughly investigated and understood. In this way, a relatively uniform contact length will result, and the possibility of contact buckling will also be reduced. In addition, investigations to take the adhesion forces into account in the numerical analysis can be conducted, and the rigid substrate can be modeled as a high modulus material with a coating on the surface in order to simulate the contact behavior more accurately.

References

[1]. A. J. Kinloch, *Adhesion and Adhesives: Science and Technology*, Chapman & Hall, 1994.

[2]. V. S. Mangipudi and M. Tirrell, Contact-mechanics-based studies of adhesion between polymers, *Rubber Chemistry and Technology*, **71**, 407-447, 1998.

[3]. A. W. Adamson and A. P. Gast, *Physical Chemistry of Surfaces*, Wiley-Interscience, New York, 1997.

[4]. A. N. Gent and J. Schultz, Effect of wetting liquids on the strength of adhesion of viscoelastic materials, *Journal of Adhesion*, **3**, 281, 1972.

[5]. E. H. Andrews and A. J. Kinloch, Mechanics of Adhesive, *Proc. R. Soc. London*, Ser. **A 332**, 385-389, 1973.

[6]. J. P. Wightman, T.D. Lin, and H. F. Webster, Surface chemical aspects of polymer/metal adhesion, *International Journal of Adhesion and Adhesives,* **12**, 133-137, 1992.

[7]. J. N. Israelachvili, *Intermolecular and Surface Forces: with Application to Colloidal and Biological Systems*, Academic Press, London, 1985.

[8]. K. L. Johnson, *Contact mechanics*, Cambridge University Press, Cambridge, England, 1985.

[9]. E. H. Lee and J. R. M. Radok, The contact problem for viscoelastic bodies, *J. Appl. Mech.*, **27**, 438-444, 1960.

[10]. G. A. C. Graham, The contact problem in the linear theory of viscoelasticity when the time dependent contact area has any number of maximum and minimum, *Int. J. Engng. Sci.,* **5**, 495-514, 1967.

[11]. W. H. Yang, The contact problem for viscoelastic bodies, *J. Appl. Mech.*, **33**, 359-401, 1966.

[12]. K. L. Johnson, K. Kendall, and A. D. Roberts, Surface energy and the contact of elastic solids, *Proc. R. Soc. London*, **A 324**, 301-313, 1971.

[13]. D. Tabor, Surface forces and surface interactions, *Journal of Colloid and Interface Science*, **58**, 2-13, 1977.

[14]. M. K. Chaudhury, and G. M. Whitesides, Direct measurement of interfacial interactions between semispherical lenses and flat sheets of poly(dimethlysiloxane) and their chemical derivatives, *Langmuir*, **7**, 1013-1025, 1991.

[15]. V. S. Mangipudi, M. Tirrell and A. V. Pocius, Direct measurement of molecular level adhesion between poly(ethylene terephthalate) and polyethylene films: determination of surface and interfacial energies, *Journal of Adhesion Science and Technology*, **8**, 1251-1270, 1994.

[16]. V. S. Mangipudi, M. Tirrell, and A. V. Pocius, Direct measurement of the surface energy of Corona-treated polyethylene using the surface forces apparatus, *Langmuir*, **11**, 19-23, 1995.

[17]. M. Tirrell, Measurement of interfacial energy at solid polymer surfaces, *Langmuir*, **12**, 4548-4551, 1996.

[18]. V. S. Mangipudi, E. Huang, M. Tirrell, and A. V. Pocius, Measurement of interfacial adhesion between glassy polymers and using JKR method, *Macromol. Symp.*, **102**, 131-143, 1996.

[19]. D. Ahn and K. R. Shull, JKR studies of acrylic elastomer adhesion to glassy polymer substrate, *Macromolecules,* **29**, 4381-4390, 1996.

[20]. K. R. Shull, D. Ahn, and C. L. Mowery, Finite-size correction to the JKR technique for measuring adhesion: soft spherical caps adhering to flat, rigid surface, *Langmuir,* **13**, 1799-1804, 1997.

[21]. R. G. Horn, J. N. Israelachvili, and F. Pribac, Measurement of the deformation and adhesion of solids in contact, *Journal of Colloid and Interface Science*, **115**, 480-492, 1987.

[22]. I. Sridhar, K. L. Johnson and N. A. Fleck, Adhesion mechanics of the surface force apparatus, *Journal of Physics, D: Applied Physics*, **30**, 1710-1719, 1997.

[23]. B. V. Derjaguin, V. M. Muller and Y. P. Toporov, Effect of contact deformations on the adhesion of particles, *Journal of Colloid and Interface Science*, **53**, 314-326, 1975.

[24]. V. M. Muller, V. S. Yushchenko and B. V. Derjaguin, On the influence of molecular forces on the deformation of an elastic sphere and its sticking to a rigid plane, *Journal of Colloid and Interface Science,* **77**, 91-101, 1980.

[25]. V. M. Muller, V. S. Yushchenko and B. V. Derjaguin, General theoretical consideration of the influence of surface forces on contact deformations and the reciprocal adhesion of elastic spherical particles, *Journal of Colloid and Interface Science,* **92**, 92-101, 1983.

[26]. M. D. Pashley, Further consideration of the DMT model for elastic contact, *Colloids and Surfaces*, **12**, 69-77, 1984.

[27]. D. J. Tabor, Role of molecular forces in contact deformations, *Journal of Colloid and Interface Science,* **73**, 294, 1980.

[28]. D. J. Tabor, Surface forces and surface interactions, *Journal of Colloid and Interface Science,* **58**, 2-13, 1977.

[29]. D. Maugis, Adhesion of spheres: the JKR-DMT transition using the Dugdale model, *Journal of Colloid and Interface Science*, **150**, 243-269, 1992.

[30]. D. Maugis and M. B. Gauthier, JKR-DMT transition in the presence of a liquid meniscus, *Journal of Adhesion Science and Technology,* **8**, 1311-1322, 1994.

[31]. J. M. Baney and C. Y. Hui, A cohesive zone model for the adhesion of cylinders, *Journal of Adhesion Science and Technology*, **11**, 393-406, 1997.

[32]. P. Silberzan, S. Perutz, E. J. Kramer and M. K. Chaudhury, Study of the self-adhesion hysteresis of a siloxane elastomer using the JKR method, *Langmuir*, **10**, 2466-2470, 1994.

[33]. G. Y. Choi, S. Kim, and A. Ulman, Adhesion hysteresis studies of extracted poly(dimethylsiloxane) using contact mechanics, *Langmuir*, **13**, 6333-6338, 1997.

[34]. S. Kim, G. Y. Choi, A. Ulman and C. Fleischer, Effect of chemical functionality on adhesion hysteresis, *Langmuir*, **13**, 6850-6856, 1997.

[35]. H. She, D. Malotky, M. K. Chaudhury, Estimation of adhesion hysteresis at polymer/oxide interfaces using rolling contact mechanics, *Langmuir*, **14**, 3090-3100, 1998.

[36]. L. Li and M. Tirrell, Adhesion studies on acrylic pressure sensitive adhesives: temperature and composition effect, *Proceedings of the 23rd Annual Meeting of the Adhesion Society*, Myrtle Beach, SC, USA, 31-35, 2000.

[37]. R. W. Carpick, N. Agrait, D. F. Ogletree, and M. Salmeron, Variation of the interfacial shear strength and adhesion of a nanometer sized contact, *Langmuir*, **12**, 3334-3340, 1996.

[38]. D. H. Gracias and G. A. Somorjai, Continuum forces microscopy study of the elastic modulus, hardness and friction of polyethylene and polypropylene surfaces, *Macromolecules*, **31**, 1269-1276, 1998.

[39]. K. Takahashi, N. A. Burnham, H. M. Pollock, and T. Onzawa, Stiffness of measurement system and significant figures of displacement which are required to interpret adhesional force curves, *IEICE Transaction on Electronics*, **E80-C**, 255-262, 1997.

[40]. D. S. Rimai, L. P. Demejo, and W. B. Vreeland, Effect of thin semi-rigid coatings on the adhesion-induced deformations between rigid particles and soft substrates, *Journal of Applied Physics*, **73**, 668-672, 1993.

[41]. M. Soltani, G. Ahmadi, R. G. Bayer, and M. A. Gaynes, Particle detachment mechanisms from rough surfaces under substrate acceleration, *Journal of Adhesion Science and Technology*, **9**, 453-473, 1995.

[42]. B. Gady, R. Reifenberger, and D. M. Schaefer, R. C. Bowen, D. S. Dimai, L. P. Demejo, and W. Vreeland, Particle adhesion to elastomeric substrates and elastomeric substrates with semi-rigid coatings, *Journal of Adhesion*, **67**, 19-36, 1998.

[43]. K. M. Liechti, S. T. Schnapp and J. G. Swadener, Contact angle and contact mechanics of a glass/epoxy interface, *International Journal of Fracture*, **86,** 361-374, 1997.

[44]. M. E. R. Shanahan, A novel test for the appraisal of solid/solid interfacial interactions, *Journal of Adhesion*, **63**, 15-29, 1997.

[45]. R. H. Plaut, S. Suherman, D. A. Dillard, B. E. Williams, and L. T. Watson, Deflections and buckling of a bent elastica in contact with a flat surface, *International Journal of Solids and Structures*, **36,** 1209-1229, 1999.

[46]. A. J. Dalrymple, The effect of adhesion on the contact of an elastica with a rigid surface, MS thesis, Virginia Tech, 1999.

[47]. *ABAQUS 5.8*, Hibbitt, Karlsson & Sorensen, Inc., Pawtucket, Rhode Island, 1998.

[48]. *LabVIEW 5.0*, National Instruments Corporation, Austin, Texas, 1999.

Appendix A. Mathematica file for fitting the work of adhesion using traditional JKR testing technique.

```
<< Statistics`NonlinearFit`
R0 = 0.0023318;
data1 = {{0.002980, 0.000217^3}, {0.008915, 0.000267^3},
   {0.015245, 0.000302^3}, {0.026509, 0.000351^3},
   {0.048629, 0.000431^3}, {0.066152, 0.000487^3},
   {0.077636, 0.000493^3}, {0.102743, 0.000538^3}};
data2 = {{0.065517, 0.00051^3}, {0.053308, 0.000481^3},
   {0.036618, 0.000431^3}, {0.029166, 0.000405^3},
   {0.016446, 0.000343^3}, {0.006808, 0.000287^3},
   {0.003135, 0.000251^3}, {0.002278, 0.000163^3}};
NonlinearFit[data1,
 R0/K1 (p1 + 3 γ1 π R0 + Sqrt[p1 6 γ1 π R0 + (3 γ1 π R0)^2]), {p1},
 {K1, γ1}]

BestFitParameters /. NonlinearRegress[data1,
R0/K1 (p1 + 3 γ1 π R0 + Sqrt[p1 6 γ1 π R0 + (3 γ1 π R0)^2]), {p1},
  {γ1, K1},
RegressionReport -> BestFitParameters]

NonlinearFit[data2,
 R0/K2 (p2 + 3 γ2 π R0 + Sqrt[p 6 γ2 π R0 + (3 γ2 π R0)^2]), {p2},
 {K2, γ2}]

BestFitParameters /. NonlinearRegress[data2,
R0/K2 (p2 + 3 γ2 π R0 + Sqrt[p2 6 γ2 π R0 + (3 γ2 π R0)^2]), {p2},
  {γ2, K2},
RegressionReport -> BestFitParameters]
```

Appendix B. ABAQUS input file for contact simulation

```
**********************************************************************
**   14.712 mm * 0.956 mm * 0.165 mm (7.356,0.0.956,0.165 half sample)
**   GEOMETRIC NON-LINEAR SHELL ELEMENT: S4R
**   20*50 & 20*30 NODE 21 * 36
**   BOUNDARY CONDITION: BUILD IN
**   CONSTRAINS : ROTATE 90 DEGREE, AND MOVE INSIDE
**   OUTPUT: REACTION FORCES
**   c=6.375 mm
**********************************************************************
*HEADING
CONTACT PROBLEM USING SHELL ELEMENT
**********************************************************
**   DEFINE NODES: X 81; Y 21
**********************************************************
*NODE
1,0.0,0.0,0.0
21,0.0,0.956,0.0
1051,2.356,0.0,0.0
1071,2.356,0.956,0.0
1072,2.406,0.0,0.0
1092,2.406,0.956,0.0
1660,6.99495,0.0,0.0
1680,6.99495,0.956,0.0
1681,7.356,0.0,0.0
1701,7.356,0.956,0.0
2000,0.0,0.0,6.5
*NGEN,NSET=SIDE1
1,21,1
*NGEN,NSET=SIDE2
1051,1071,1
*NGEN,NSET=SIDE3
1681,1701,1
*NGEN,NSET=SIDE4
1072,1092,1
*NGEN,NSET=SIDE5
1660,1680,1
*NFILL,NSET=ALL
SIDE1,SIDE2,50,21
*NFILL,NSET=ALL,BIAS=0.931828
SIDE2,SIDE3,30,21
```

```
SIDE4,SIDE5,28,21
**********
**  DEFINE ELEMENTS : X 40; Y 10
**********
*ELEMENT,TYPE=S4R,ELSET=RUBBER
1,1,22,23,2
*ELGEN,ELSET=RUBBER
1,20,1,1,80,21,20
**********
**  DEFINE MATERIAL: RUBBER: E=1.81 MPA, V=0.49
**********
*MATERIAL,NAME=RUBBER
*ELASTIC, TYPE=ISOTROPIC
1.81,0.49
**********
**  THICKNESS=0.165 mm **
**********
*SHELL GENERAL SECTION,ELSET=RUBBER,MATERIAL=RUBBER
0.165
**********
** SURFACE DEFINITION       **
**********
*RIGID SURFACE,NAME=RIGID,TYPE=CYLINDER,REF NODE=2000
5.0,0.0,6.5,5.0,0.1,6.5
6.0,0.0,6.5
START,-1.0,0.0
LINE,2.0,0.0
*SURFACE DEFINITION,NAME=SURF
RUBBER,SPOS
**********
**      TYPE OF CONTACT      **
**********
*CONTACT PAIR,INTERACTION=HERTZ
SURF,RIGID
*SURFACE INTERACTION,NAME=HERTZ
**********
**  DEFINE BOUNDARY: END IS BUILD IN
**********
*NSET,NSET=END,GEN
1681,1701,1
*NSET,NSET=XMID,GEN
1,21,1
**NSET,NSET=YMID,GEN
```

```
**1,1660,21
*BOUNDARY
END,1,5
XMID,1
XMID,5
2000,1,6
**********
**  STEP PROCEDURE   **
**********
**********
** STEP 1, APPLY LOAD
*STEP,NLGEOM,INC=1000
*STATIC
1.0,1.0,0.001
*CLOAD
XMID,3,1.0E-6
*RESTART,WRITE,OVERLAY
*EL PRINT,FREQUENCY=0
S
*NODE PRINT,FREQUENCY=0
U
*END STEP
**********
**2
*STEP,NLGEOM,INC=1000
*STATIC
1.0,1.0,0.001
*BOUNDARY
end,1,1,-0.25
*RESTART,WRITE,OVERLAY
*EL PRINT,FREQUENCY=0
S
*NODE PRINT,FREQUENCY=0
U
*END STEP
**STEP 3
*STEP,NLGEOM, INC=1000
*STATIC
1.0,1.0,0.01
*BOUNDARY
end,5,5,0.1
*RESTART,WRITE,OVERLAY
*EL PRINT,FREQUENCY=0
```

```
S
*NODE PRINT,FREQUENCY=0
U
*END STEP
**4
*STEP,NLGEOM,INC=1000
*STATIC
0.002,10.0,0.00001
*BOUNDARY
end,5,5,0.2
*RESTART,WRITE,OVERLAY
*EL PRINT,FREQUENCY=0
S
*NODE PRINT,FREQUENCY=0
U
*END STEP
**5
*STEP,NLGEOM,INC=1000
*STATIC
0.002,10.0,0.00001
*BOUNDARY
end,5,5,0.3
*RESTART,WRITE,OVERLAY
*EL PRINT,FREQUENCY=0
S
*NODE PRINT,FREQUENCY=0
U
*END STEP
**6
*STEP,NLGEOM,INC=1000
*STATIC
0.002,10.0,0.00001
*BOUNDARY
end,1,1,-0.5
*RESTART,WRITE,OVERLAY
*EL PRINT,FREQUENCY=0
S
*NODE PRINT,FREQUENCY=0
U
*END STEP
**7
*STEP,NLGEOM,INC=1000
*STATIC
```

0.002,10.0,0.00001
*BOUNDARY
end,5,5,0.522
*RESTART,WRITE,OVERLAY
*EL PRINT,FREQUENCY=0
S
*NODE PRINT,FREQUENCY=0
U
*END STEP
**8
*STEP,NLGEOM,INC=1000
*STATIC
0.002,10.0,0.00001
*BOUNDARY
end,1,1,-0.7
*RESTART,WRITE,OVERLAY
*EL PRINT,FREQUENCY=0
S
*NODE PRINT,FREQUENCY=0
U
*END STEP
**9
*STEP,NLGEOM,INC=1000
*STATIC
0.02,10.0,0.00001
*BOUNDARY
end,1,1,-1.0
*RESTART,WRITE,OVERLAY
*EL PRINT,FREQUENCY=0
S
*NODE PRINT,FREQUENCY=0
U
*END STEP
**10
*STEP,NLGEOM,INC=1000
*STATIC
0.02,10.0,0.00001
*BOUNDARY
end,5,5,0.698
*RESTART,WRITE,OVERLAY
*EL PRINT,FREQUENCY=0
S
*NODE PRINT,FREQUENCY=0

U
*END STEP
**11
*STEP,NLGEOM,INC=1000
*STATIC
0.02,10.0,0.000011
*BOUNDARY
end,1,1,-1.5
*RESTART,WRITE,OVERLAY
*EL PRINT,FREQUENCY=0
S
*NODE PRINT,FREQUENCY=0
U
*END STEP
**12
*STEP,NLGEOM,INC=1000
*STATIC
0.02,10.0,0.00001
*BOUNDARY
end,1,1,-2.1685
*RESTART,WRITE,OVERLAY
*END STEP
**13
*STEP,NLGEOM,INC=1000
*STATIC
0.02,10.0,0.00001
*BOUNDARY
end,1,1,-3.1685
*RESTART,WRITE,OVERLAY
*EL PRINT,FREQUENCY=0
S
*NODE PRINT,FREQUENCY=0
U
*END STEP
**14
*STEP,NLGEOM,INC=1000
*STATIC
0.02,10.0,0.00001
*BOUNDARY
end,1,1,-4.1685
*RESTART,WRITE,OVERLAY
*EL PRINT,FREQUENCY=0
S

```
*NODE PRINT,FREQUENCY=0
U
*END STEP
**********************************************
**15  UNLOADING
*STEP,INC=1000
*STATIC
0.02,10.0,0.00001
*CLOAD,OP=NEW
*RESTART,WRITE,OVERLAY
*EL PRINT,FREQUENCY=0
S
*NODE PRINT,FREQUENCY=0
U
*END STEP
**********************************************
**16
*STEP,NLGEOM,INC=1000
*STATIC
0.02,10.0,0.00001
*BOUNDARY
end,5,5,0.872
*RESTART,WRITE,OVERLAY
*EL PRINT,FREQUENCY=0
S
*NODE PRINT,FREQUENCY=0
U
*END STEP
**17
*STEP,NLGEOM,INC=1000
*STATIC
0.02,10.0,0.00001
*BOUNDARY
end,5,5,0.96
*RESTART,WRITE,OVERLAY
*EL PRINT,FREQUENCY=0
S
*NODE PRINT,FREQUENCY=0
U
*END STEP
**18
*STEP,NLGEOM,INC=1000
*STATIC
```

```
0.02,10.0,0.00001
*BOUNDARY
end,5,5,1.04
*RESTART,WRITE,OVERLAY
*EL PRINT,FREQUENCY=0
S
*NODE PRINT,FREQUENCY=0
U
*END STEP
**19
*STEP,NLGEOM,INC=1000
*STATIC
0.02,10.0,0.00001
*BOUNDARY
end,5,5,1.13
*RESTART,WRITE,OVERLAY
*EL PRINT,FREQUENCY=0
S
*NODE PRINT,FREQUENCY=0
U
*END STEP
**20
*STEP,NLGEOM,INC=1000
*STATIC
0.02,10.0,0.00001
*BOUNDARY
end,5,5,1.22
*RESTART,WRITE,OVERLAY
*EL PRINT,FREQUENCY=0
S
*NODE PRINT,FREQUENCY=0
U
*END STEP
**21
*STEP,NLGEOM,INC=1000
*STATIC
0.02,10.0,0.00001
*BOUNDARY
end,5,5,1.31
*RESTART,WRITE,OVERLAY
*EL PRINT,FREQUENCY=0
S
*NODE PRINT,FREQUENCY=0
```

```
U
*END STEP
**22
*STEP,NLGEOM,INC=1000
*STATIC
0.02,10.0,0.00001
*BOUNDARY
end,5,5,1.40
*RESTART,WRITE,OVERLAY
*EL PRINT,FREQUENCY=0
S
*NODE PRINT,FREQUENCY=0
U
*END STEP
**23
*STEP,NLGEOM,INC=1000
*STATIC
0.02,10.0,0.00001
*BOUNDARY
end,5,5,1.48
*RESTART,WRITE,OVERLAY
*EL PRINT,FREQUENCY=0
S
*NODE PRINT,FREQUENCY=0
U
*END STEP
**24
*STEP,NLGEOM,INC=1000
*STATIC
0.02,10.0,0.00001
*BOUNDARY
end,5,5,1.57
*RESTART,WRITE,OVERLAY
*EL PRINT,FREQUENCY=0
S,E
*NODE PRINT,FREQUENCY=0
U
*END STEP
**********************************************
**25 RIGID SURFACE MOVES DOWN          **
**********************************************
*STEP,NLGEOM,INC=1000
*STATIC
```

```
0.02,10.0,0.00001
*BOUNDARY
2000,3,3,-0.6
*RESTART,WRITE,OVERLAY
*EL PRINT,FREQUENCY=0
*NODE PRINT,FREQUENCY=0
*END STEP
**26
*STEP,NLGEOM,INC=1000
*STATIC
0.02,10.0,0.00001
*BOUNDARY
2000,3,3,-0.8
*RESTART,WRITE,OVERLAY
*EL PRINT,FREQUENCY=0
S,E
*NODE PRINT,FREQUENCY=0
U
*CONTACT
PRINT,TOTAL=YES,SLAVE=SURF,MASTER=RIGID,FREQUENCY=15
carea,cfn,cft
*CONTACT FILE,SLAVE=SURF,MASTER=RIGID,FREQUENCY=15
carea,cfn,cft
*NODE PRINT,TOTAL=YES,NSET=END,FREQUENCY=15
RF
*END STEP
**27
*STEP,NLGEOM,INC=1000
*STATIC
0.02,10.0,0.00001
*BOUNDARY
2000,3,3,-1.0
*RESTART,WRITE,OVERLAY
*EL PRINT,FREQUENCY=0
S,E
*NODE PRINT,FREQUENCY=0
U
*CONTACT
PRINT,TOTAL=YES,SLAVE=SURF,MASTER=RIGID,FREQUENCY=15
carea,cfn,cft
*CONTACT FILE,SLAVE=SURF,MASTER=RIGID,FREQUENCY=15
carea,cfn,cft
*NODE PRINT,TOTAL=YES,NSET=END,FREQUENCY=15
```

RF
*END STEP
**28
*STEP,NLGEOM,INC=1000
*STATIC
0.02,10.0,0.00001
*BOUNDARY
2000,3,3,-1.1
*RESTART,WRITE,OVERLAY
*EL PRINT,FREQUENCY=0
S
*NODE PRINT,FREQUENCY=0
U
*CONTACT
PRINT,TOTAL=YES,SLAVE=SURF,MASTER=RIGID,FREQUENCY=15
carea,cfn,cft
*CONTACT FILE,SLAVE=SURF,MASTER=RIGID,FREQUENCY=15
carea,cfn,cft
*NODE PRINT,TOTAL=YES,NSET=END,FREQUENCY=15
RF
*END STEP
**29
*STEP,NLGEOM,INC=1000
*STATIC
0.02,10.0,0.00001
*BOUNDARY
2000,3,3,-1.2
*RESTART,WRITE,OVERLAY
*EL PRINT,FREQUENCY=0
S
*NODE PRINT,FREQUENCY=0
U
*CONTACT
PRINT,TOTAL=YES,SLAVE=SURF,MASTER=RIGID,FREQUENCY=15
carea,cfn,cft
*CONTACT FILE,SLAVE=SURF,MASTER=RIGID,FREQUENCY=15
carea,cfn,cft
*NODE PRINT,TOTAL=YES,NSET=END,FREQUENCY=15
RF
*END STEP
**30
*STEP,NLGEOM,INC=1000
*STATIC

```
0.02,10.0,0.00001
*BOUNDARY
2000,3,3,-1.3
*RESTART,WRITE,OVERLAY
*EL PRINT,FREQUENCY=0
S
*NODE PRINT,FREQUENCY=0
U
*CONTACT
PRINT,TOTAL=YES,SLAVE=SURF,MASTER=RIGID,FREQUENCY=15
carea,cfn,cft
*CONTACT FILE,SLAVE=SURF,MASTER=RIGID,FREQUENCY=15
carea,cfn,cft
*NODE PRINT,TOTAL=YES,NSET=END,FREQUENCY=15
RF
*END STEP
**31
*STEP,NLGEOM,INC=1000
*STATIC
0.02,10.0,0.00001
*BOUNDARY
2000,3,3,-1.4
*RESTART,WRITE,OVERLAY
*EL PRINT,FREQUENCY=0
S
*NODE PRINT,FREQUENCY=0
U
*CONTACT
PRINT,TOTAL=YES,SLAVE=SURF,MASTER=RIGID,FREQUENCY=15
carea,cfn,cft
*CONTACT FILE,SLAVE=SURF,MASTER=RIGID,FREQUENCY=15
carea,cfn,cft
*NODE PRINT,TOTAL=YES,NSET=END,FREQUENCY=15
RF
*END STEP
**32
*STEP,NLGEOM,INC=1000
*STATIC
0.02,10.0,0.00001
*BOUNDARY
2000,3,3,-1.42
*RESTART,WRITE,OVERLAY
*EL PRINT,FREQUENCY=0
```

```
S
*NODE PRINT,FREQUENCY=0
U
*CONTACT
PRINT,TOTAL=YES,SLAVE=SURF,MASTER=RIGID,FREQUENCY=15
carea,cfn,cft
*CONTACT FILE,SLAVE=SURF,MASTER=RIGID,FREQUENCY=15
carea,cfn,cft
*NODE PRINT,TOTAL=YES,NSET=END,FREQUENCY=15
RF
*END STEP
**33
*STEP,NLGEOM,INC=1000
*STATIC
0.02,10.0,0.00001
*BOUNDARY
2000,3,3,-1.44
*RESTART,WRITE,OVERLAY
*EL PRINT,FREQUENCY=0
S
*NODE PRINT,FREQUENCY=0
U
*CONTACT
PRINT,TOTAL=YES,SLAVE=SURF,MASTER=RIGID,FREQUENCY=15
carea,cfn,cft
*CONTACT FILE,SLAVE=SURF,MASTER=RIGID,FREQUENCY=15
carea,cfn,cft
*NODE PRINT,TOTAL=YES,NSET=END,FREQUENCY=15
RF
*END STEP
**34
*STEP,NLGEOM,INC=1000
*STATIC
0.02,10.0,0.00001
*BOUNDARY
2000,3,3,-1.46
*RESTART,WRITE,OVERLAY
*EL PRINT,FREQUENCY=0
S
*NODE PRINT,FREQUENCY=0
U
*CONTACT
PRINT,TOTAL=YES,SLAVE=SURF,MASTER=RIGID,FREQUENCY=15
```

carea,cfn,cft
*CONTACT FILE,SLAVE=SURF,MASTER=RIGID,FREQUENCY=15
carea,cfn,cft
*NODE PRINT,TOTAL=YES,NSET=END,FREQUENCY=15
RF
*END STEP
**35
*STEP,NLGEOM,INC=1000
*STATIC
0.02,10.0,0.00001
*BOUNDARY
2000,3,3,-1.48
*RESTART,WRITE,OVERLAY
*EL PRINT,FREQUENCY=0
S
*NODE PRINT,FREQUENCY=0
U
*CONTACT
PRINT,TOTAL=YES,SLAVE=SURF,MASTER=RIGID,FREQUENCY=15
carea,cfn,cft
*CONTACT FILE,SLAVE=SURF,MASTER=RIGID,FREQUENCY=15
carea,cfn,cft
*NODE PRINT,TOTAL=YES,NSET=END,FREQUENCY=15
RF
*END STEP
**36
*STEP,NLGEOM,INC=1000
*STATIC
0.02,10.0,0.00001
*BOUNDARY
2000,3,3,-1.50
*RESTART,WRITE,OVERLAY
*EL PRINT,FREQUENCY=0
S
*NODE PRINT,FREQUENCY=0
U
*CONTACT
PRINT,TOTAL=YES,SLAVE=SURF,MASTER=RIGID,FREQUENCY=15
carea,cfn,cft
*CONTACT FILE,SLAVE=SURF,MASTER=RIGID,FREQUENCY=15
carea,cfn,cft
*NODE PRINT,TOTAL=YES,NSET=END,FREQUENCY=15
RF

```
*END STEP
**37
*STEP,NLGEOM,INC=1000
*STATIC
0.02,10.0,0.00001
*BOUNDARY
2000,3,3,-1.52
*RESTART,WRITE,OVERLAY
*EL PRINT,FREQUENCY=0
S
*NODE PRINT,FREQUENCY=0
U
*CONTACT
PRINT,TOTAL=YES,SLAVE=SURF,MASTER=RIGID,FREQUENCY=15
carea,cfn,cft
*CONTACT FILE,SLAVE=SURF,MASTER=RIGID,FREQUENCY=15
carea,cfn,cft
*NODE PRINT,TOTAL=YES,NSET=END,FREQUENCY=15
RF
*END STEP
**38
*STEP,NLGEOM,INC=1000
*STATIC
0.02,10.0,0.00001
*BOUNDARY
2000,3,3,-1.54
*RESTART,WRITE,OVERLAY
*EL PRINT,FREQUENCY=0
S
*NODE PRINT,FREQUENCY=0
U
*CONTACT
PRINT,TOTAL=YES,SLAVE=SURF,MASTER=RIGID,FREQUENCY=15
carea,cfn,cft
*CONTACT FILE,SLAVE=SURF,MASTER=RIGID,FREQUENCY=15
carea,cfn,cft
*NODE PRINT,TOTAL=YES,NSET=END,FREQUENCY=15
RF
*END STEP
**39
*STEP,NLGEOM,INC=1000
*STATIC
0.02,10.0,0.00001
```

```
*BOUNDARY
2000,3,3,-1.56
*RESTART,WRITE,OVERLAY
*EL PRINT,FREQUENCY=0
S
*NODE PRINT,FREQUENCY=0
U
*CONTACT
PRINT,TOTAL=YES,SLAVE=SURF,MASTER=RIGID,FREQUENCY=15
carea,cfn,cft
*CONTACT FILE,SLAVE=SURF,MASTER=RIGID,FREQUENCY=15
carea,cfn,cft
*NODE PRINT,TOTAL=YES,NSET=END,FREQUENCY=15
RF
*END STEP
**40
*STEP,NLGEOM,INC=1000
*STATIC
0.02,10.0,0.00001
*BOUNDARY
2000,3,3,-1.58
*RESTART,WRITE,OVERLAY
*EL PRINT,FREQUENCY=0
S
*NODE PRINT,FREQUENCY=0
U
*CONTACT
PRINT,TOTAL=YES,SLAVE=SURF,MASTER=RIGID,FREQUENCY=15
carea,cfn,cft
*CONTACT FILE,SLAVE=SURF,MASTER=RIGID,FREQUENCY=15
carea,cfn,cft
*NODE PRINT,TOTAL=YES,NSET=END,FREQUENCY=15
RF
*END STEP
**41
*STEP,NLGEOM,INC=1000
*STATIC
0.02,10.0,0.00001
*BOUNDARY
2000,3,3,-1.60
*RESTART,WRITE,OVERLAY
*EL PRINT,FREQUENCY=0
S
```

```
*NODE PRINT,FREQUENCY=0
U
*CONTACT
PRINT,TOTAL=YES,SLAVE=SURF,MASTER=RIGID,FREQUENCY=15
carea,cfn,cft
*CONTACT FILE,SLAVE=SURF,MASTER=RIGID,FREQUENCY=15
carea,cfn,cft
*NODE PRINT,TOTAL=YES,NSET=END,FREQUENCY=15
RF
*END STEP
**42
*STEP,NLGEOM,INC=1000
*STATIC
0.02,10.0,0.00001
*BOUNDARY
2000,3,3,-1.62
*RESTART,WRITE,OVERLAY
*EL PRINT,FREQUENCY=0
S
*NODE PRINT,FREQUENCY=0
U
*CONTACT
PRINT,TOTAL=YES,SLAVE=SURF,MASTER=RIGID,FREQUENCY=15
carea,cfn,cft
*CONTACT FILE,SLAVE=SURF,MASTER=RIGID,FREQUENCY=15
carea,cfn,cft
*NODE PRINT,TOTAL=YES,NSET=END,FREQUENCY=15
RF
*END STEP
**43
*STEP,NLGEOM,INC=1000
*STATIC
0.02,10.0,0.00001
*BOUNDARY
2000,3,3,-1.64
*RESTART,WRITE,OVERLAY
*EL PRINT,FREQUENCY=0
S
*NODE PRINT,FREQUENCY=0
U
*CONTACT
PRINT,TOTAL=YES,SLAVE=SURF,MASTER=RIGID,FREQUENCY=15
carea,cfn,cft
```

```
*CONTACT FILE,SLAVE=SURF,MASTER=RIGID,FREQUENCY=15
carea,cfn,cft
*NODE PRINT,TOTAL=YES,NSET=END,FREQUENCY=15
RF
*END STEP
**44
*STEP,NLGEOM,INC=1000
*STATIC
0.02,10.0,0.00001
*BOUNDARY
2000,3,3,-1.66
*RESTART,WRITE,OVERLAY
*EL PRINT,FREQUENCY=0
S
*NODE PRINT,FREQUENCY=0
U
*CONTACT
PRINT,TOTAL=YES,SLAVE=SURF,MASTER=RIGID,FREQUENCY=15
carea,cfn,cft
*CONTACT FILE,SLAVE=SURF,MASTER=RIGID,FREQUENCY=15
carea,cfn,cft
*NODE PRINT,TOTAL=YES,NSET=END,FREQUENCY=15
RF
*END STEP
**45
*STEP,NLGEOM,INC=1000
*STATIC
0.02,10.0,0.00001
*BOUNDARY
2000,3,3,-1.68
*RESTART,WRITE,OVERLAY
*EL PRINT,FREQUENCY=0
S
*NODE PRINT,FREQUENCY=0
U
*CONTACT
PRINT,TOTAL=YES,SLAVE=SURF,MASTER=RIGID,FREQUENCY=15
carea,cfn,cft
*CONTACT FILE,SLAVE=SURF,MASTER=RIGID,FREQUENCY=15
carea,cfn,cft
*NODE PRINT,TOTAL=YES,NSET=END,FREQUENCY=15
RF
*END STEP
```

```
**46
*STEP,NLGEOM,INC=1000
*STATIC
0.02,10.0,0.00001
*BOUNDARY
2000,3,3,-1.7
*RESTART,WRITE,OVERLAY
*EL PRINT,FREQUENCY=0
S
*NODE PRINT,FREQUENCY=0
U
*CONTACT
PRINT,TOTAL=YES,SLAVE=SURF,MASTER=RIGID,FREQUENCY=15
carea,cfn,cft
*CONTACT FILE,SLAVE=SURF,MASTER=RIGID,FREQUENCY=15
carea,cfn,cft
*NODE PRINT,TOTAL=YES,NSET=END,FREQUENCY=15
RF
*END STEP
**47
*STEP,NLGEOM,INC=1000
*STATIC
0.02,10.0,0.00001
*BOUNDARY
2000,3,3,-1.72
*RESTART,WRITE,OVERLAY
*EL PRINT,FREQUENCY=0
S
*NODE PRINT,FREQUENCY=0
U
*CONTACT
PRINT,TOTAL=YES,SLAVE=SURF,MASTER=RIGID,FREQUENCY=15
carea,cfn,cft
*CONTACT FILE,SLAVE=SURF,MASTER=RIGID,FREQUENCY=15
carea,cfn,cft
*NODE PRINT,TOTAL=YES,NSET=END,FREQUENCY=15
RF
*END STEP
**48
*STEP,NLGEOM,INC=1000
*STATIC
0.02,10.0,0.00001
*BOUNDARY
```

```
2000,3,3,-1.74
*RESTART,WRITE,OVERLAY
*EL PRINT,FREQUENCY=0
S
*NODE PRINT,FREQUENCY=0
U
*CONTACT
PRINT,TOTAL=YES,SLAVE=SURF,MASTER=RIGID,FREQUENCY=15
carea,cfn,cft
*CONTACT FILE,SLAVE=SURF,MASTER=RIGID,FREQUENCY=15
carea,cfn,cft
*NODE PRINT,TOTAL=YES,NSET=END,FREQUENCY=15
RF
*END STEP
**49
*STEP,NLGEOM,INC=1000
*STATIC
0.02,10.0,0.00001
*BOUNDARY
2000,3,3,-1.76
*RESTART,WRITE,OVERLAY
*EL PRINT,FREQUENCY=0
S
*NODE PRINT,FREQUENCY=0
U
*CONTACT
PRINT,TOTAL=YES,SLAVE=SURF,MASTER=RIGID,FREQUENCY=15
carea,cfn,cft
*CONTACT FILE,SLAVE=SURF,MASTER=RIGID,FREQUENCY=15
carea,cfn,cft
*NODE PRINT,TOTAL=YES,NSET=END,FREQUENCY=15
RF
*END STEP
**50
*STEP,NLGEOM,INC=1000
*STATIC
0.02,10.0,0.00001
*BOUNDARY
2000,3,3,-1.78
*RESTART,WRITE,OVERLAY
*EL PRINT,FREQUENCY=0
S
*NODE PRINT,FREQUENCY=0
```

U
*CONTACT
PRINT,TOTAL=YES,SLAVE=SURF,MASTER=RIGID,FREQUENCY=15
carea,cfn,cft
*CONTACT FILE,SLAVE=SURF,MASTER=RIGID,FREQUENCY=15
carea,cfn,cft
*NODE PRINT,TOTAL=YES,NSET=END,FREQUENCY=15
RF
*END STEP
**51
*STEP,NLGEOM,INC=1000
*STATIC
0.02,10.0,0.00001
*BOUNDARY
2000,3,3,-1.8
*RESTART,WRITE,OVERLAY
*EL PRINT,FREQUENCY=0
S
*NODE PRINT,FREQUENCY=0
U
*CONTACT
PRINT,TOTAL=YES,SLAVE=SURF,MASTER=RIGID,FREQUENCY=15
carea,cfn,cft
*CONTACT FILE,SLAVE=SURF,MASTER=RIGID,FREQUENCY=15
carea,cfn,cft
*NODE PRINT,TOTAL=YES,NSET=END,FREQUENCY=15
RF
*END STEP
**52
*STEP,NLGEOM,INC=1000
*STATIC
0.02,10.0,0.00001
*BOUNDARY
2000,3,3,-1.82
*RESTART,WRITE,OVERLAY
*EL PRINT,FREQUENCY=0
S
*NODE PRINT,FREQUENCY=0
U
*CONTACT
PRINT,TOTAL=YES,SLAVE=SURF,MASTER=RIGID,FREQUENCY=15
carea,cfn,cft
*CONTACT FILE,SLAVE=SURF,MASTER=RIGID,FREQUENCY=15

carea,cfn,cft
*NODE PRINT,TOTAL=YES,NSET=END,FREQUENCY=15
RF
*END STEP
**53
*STEP,NLGEOM,INC=1000
*STATIC
0.02,10.0,0.00001
*BOUNDARY
2000,3,3,-1.84
*RESTART,WRITE,OVERLAY
*EL PRINT,FREQUENCY=0
S
*NODE PRINT,FREQUENCY=0
U
*CONTACT
PRINT,TOTAL=YES,SLAVE=SURF,MASTER=RIGID,FREQUENCY=15
carea,cfn,cft
*CONTACT FILE,SLAVE=SURF,MASTER=RIGID,FREQUENCY=15
carea,cfn,cft
*NODE PRINT,TOTAL=YES,NSET=END,FREQUENCY=15
RF
*END STEP
**54
*STEP,NLGEOM,INC=1000
*STATIC
0.02,10.0,0.00001
*BOUNDARY
2000,3,3,-1.86
*RESTART,WRITE,OVERLAY
*EL PRINT,FREQUENCY=0
S
*NODE PRINT,FREQUENCY=0
U
*CONTACT
PRINT,TOTAL=YES,SLAVE=SURF,MASTER=RIGID,FREQUENCY=15
carea,cfn,cft
*CONTACT FILE,SLAVE=SURF,MASTER=RIGID,FREQUENCY=15
carea,cfn,cft
*NODE PRINT,TOTAL=YES,NSET=END,FREQUENCY=15
RF
*END STEP
**55

```
*STEP,NLGEOM,INC=1000
*STATIC
0.02,10.0,0.00001
*BOUNDARY
2000,3,3,-1.90
*RESTART,WRITE,OVERLAY
*EL PRINT,FREQUENCY=0
S
*NODE PRINT,FREQUENCY=0
U
*CONTACT
PRINT,TOTAL=YES,SLAVE=SURF,MASTER=RIGID,FREQUENCY=15
carea,cfn,cft
*CONTACT FILE,SLAVE=SURF,MASTER=RIGID,FREQUENCY=15
carea,cfn,cft
*NODE PRINT,TOTAL=YES,NSET=END,FREQUENCY=15
RF
*END STEP
**56
*STEP,NLGEOM,INC=1000
*STATIC
0.02,10.0,0.00001
*BOUNDARY
2000,3,3,-1.95
*RESTART,WRITE,OVERLAY
*EL PRINT,FREQUENCY=0
S
*NODE PRINT,FREQUENCY=0
U
*CONTACT
PRINT,TOTAL=YES,SLAVE=SURF,MASTER=RIGID,FREQUENCY=15
carea,cfn,cft
*CONTACT FILE,SLAVE=SURF,MASTER=RIGID,FREQUENCY=15
carea,cfn,cft
*NODE PRINT,TOTAL=YES,NSET=END,FREQUENCY=15
RF
*END STEP
**57
*STEP,NLGEOM,INC=1000
*STATIC
0.02,10.0,0.00001
*BOUNDARY
2000,3,3,-2.0
```

```
*RESTART,WRITE,OVERLAY
*EL PRINT,FREQUENCY=0
S
*NODE PRINT,FREQUENCY=0
U
*CONTACT
PRINT,TOTAL=YES,SLAVE=SURF,MASTER=RIGID,FREQUENCY=15
carea,cfn,cft
*CONTACT FILE,SLAVE=SURF,MASTER=RIGID,FREQUENCY=15
carea,cfn,cft
*NODE PRINT,TOTAL=YES,NSET=END,FREQUENCY=15
RF
*END STEP
**58
*STEP,NLGEOM,INC=1000
*STATIC
0.02,10.0,0.00001
*BOUNDARY
2000,3,3,-2.05
*RESTART,WRITE,OVERLAY
*EL PRINT,FREQUENCY=0
S
*NODE PRINT,FREQUENCY=0
U
*CONTACT
PRINT,TOTAL=YES,SLAVE=SURF,MASTER=RIGID,FREQUENCY=15
carea,cfn,cft
*CONTACT FILE,SLAVE=SURF,MASTER=RIGID,FREQUENCY=15
carea,cfn,cft
*NODE PRINT,TOTAL=YES,NSET=END,FREQUENCY=15
RF
*END STEP
**59
*STEP,NLGEOM,INC=1000
*STATIC
0.02,10.0,0.00001
*BOUNDARY
2000,3,3,-2.1
*RESTART,WRITE,OVERLAY
*EL PRINT,FREQUENCY=0
S
*NODE PRINT,FREQUENCY=0
U
```

```
*CONTACT
PRINT,TOTAL=YES,SLAVE=SURF,MASTER=RIGID,FREQUENCY=15
carea,cfn,cft
*CONTACT FILE,SLAVE=SURF,MASTER=RIGID,FREQUENCY=15
carea,cfn,cft
*NODE PRINT,TOTAL=YES,NSET=END,FREQUENCY=15
RF
*END STEP
**60
*STEP,NLGEOM,INC=1000
*STATIC
0.02,10.0,0.00001
*BOUNDARY
2000,3,3,-2.15
*RESTART,WRITE,OVERLAY
*EL PRINT,FREQUENCY=0
S
*NODE PRINT,FREQUENCY=0
U
*CONTACT
PRINT,TOTAL=YES,SLAVE=SURF,MASTER=RIGID,FREQUENCY=15
carea,cfn,cft
*CONTACT FILE,SLAVE=SURF,MASTER=RIGID,FREQUENCY=15
carea,cfn,cft
*NODE PRINT,TOTAL=YES,NSET=END,FREQUENCY=15
RF
*END STEP
**61
*STEP,NLGEOM,INC=1000
*STATIC
0.02,10.0,0.00001
*BOUNDARY
2000,3,3,-2.20
*RESTART,WRITE,OVERLAY
*EL PRINT,FREQUENCY=0
S
*NODE PRINT,FREQUENCY=0
U
*CONTACT
PRINT,TOTAL=YES,SLAVE=SURF,MASTER=RIGID,FREQUENCY=15
carea,cfn,cft
*CONTACT FILE,SLAVE=SURF,MASTER=RIGID,FREQUENCY=15
carea,cfn,cft
```

```
*NODE PRINT,TOTAL=YES,NSET=END,FREQUENCY=15
RF
*END STEP
**62
*STEP,NLGEOM,INC=1000
*STATIC
0.02,10.0,0.00001
*BOUNDARY
2000,3,3,-2.25
*RESTART,WRITE,OVERLAY
*EL PRINT,FREQUENCY=0
S
*NODE PRINT,FREQUENCY=0
U
*CONTACT
PRINT,TOTAL=YES,SLAVE=SURF,MASTER=RIGID,FREQUENCY=15
carea,cfn,cft
*CONTACT FILE,SLAVE=SURF,MASTER=RIGID,FREQUENCY=15
carea,cfn,cft
*NODE PRINT,TOTAL=YES,NSET=END,FREQUENCY=15
RF
*END STEP
**63
*STEP,NLGEOM,INC=1000
*STATIC
0.02,10.0,0.00001
*BOUNDARY
2000,3,3,-2.3
*RESTART,WRITE,OVERLAY
*EL PRINT,FREQUENCY=0
S
*NODE PRINT,FREQUENCY=0
U
*CONTACT
PRINT,TOTAL=YES,SLAVE=SURF,MASTER=RIGID,FREQUENCY=15
carea,cfn,cft
*CONTACT FILE,SLAVE=SURF,MASTER=RIGID,FREQUENCY=15
carea,cfn,cft
*NODE PRINT,TOTAL=YES,NSET=END,FREQUENCY=15
RF
*END STEP
**********************************************
```

Vita

Jia Qi was born on June 16, 1970 in Shijiazhuang, China. She graduated from Chengdu University of Science and Technology in July of 1992. In July of 1995, she completed her Master of Science in Mechanics from Peking University in Beijing, China. Following graduation, she worked at the Research and Development Center of Beijing Urban Construction Incorporation. In 1998, the author began to pursue her Master of Science in Engineering Mechanics at Virginia Tech.